

**CORROSION OF AUSTENITIC STAINLESS STEELS IN NITRIC ACID
AT TRANSPASSIVE POTENTIALS: EFFECT OF MATERIAL AND
PROCESS PARAMETERS**

By

SHAGUFTA

CHEM01200904018

Bhabha Atomic Research Centre, Mumbai

*A thesis submitted to the Board of Studies in
Chemical Sciences*

In partial fulfillment of requirements

For the Degree of

DOCTOR OF PHILOSOPHY

OF

HOMI BHABHA NATIONAL INSTITUTE



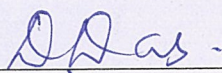
March, 2015

Homi Bhabha National Institute

Recommendations of the Viva Voce Committee

As members of the Viva Voce Committee, we certify that we have read the dissertation prepared by **Mrs. Shagufta** entitled “**Corrosion of austenitic stainless steels in nitric acid at transpassive potentials: effect of material and process parameters**” and recommend that it may be accepted as fulfilling the thesis requirement for the award of Degree of Doctor of Philosophy.

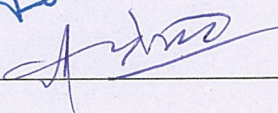
Chairman – Dr. D. Das



Date: 07-12-2015

External Examiner –

PROF. V.S. RAJA



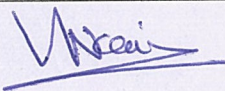
Date: 07/12/15

Guide/Convener – Dr. A. V. R. Reddy

Date:

07-12-15

Co-Guide – Dr. Vivekanand Kain



Date:

Dec. 7, 2015

Member – Dr. P. K. Pujari

Date:

Final approval and acceptance of this thesis is contingent upon the candidate's submission of the final copies of the thesis to HBNI.

I/We hereby certify that I/we have read this thesis prepared under my/our direction and recommend that it may be accepted as fulfilling the thesis requirement.

Date: 07.12.2015



Dr. A. V. R. Reddy
(Guide)

STATEMENT BY AUTHOR

This dissertation has been submitted in partial fulfillment of requirements for an advanced degree at Homi Bhabha National Institute (HBNI) and is deposited in the Library to be made available to borrowers under rules of the HBNI.

Brief quotations from this dissertation are allowable without special permission, provided that accurate acknowledgement of the source is made. Requests for permission for extended quotation from or reproduction of this manuscript in whole or in part may be granted by the Competent Authority of HBNI when in his or her judgment the proposed use of the material is in the interests of scholarship. In all other instances, however, permission must be obtained from the author.

SHAGUFTA

DECLARATION

I, hereby declare that the investigations presented in the thesis have been carried out by me. The work is original and has not been submitted earlier as a whole or in part for a degree / diploma to this or any other Institution / University.

SHAGUFTA

List of Publications arising from the thesis

Journals

1. Shagufta Khan, Vivekanand Kain, A.V. R. Reddy, Corrosion in Transpassive Potential Regime: Effect of Composition and Microstructure of Austenitic Stainless Steel, **Corrosion**, 2013, 70 (2014) 19.
2. Shagufta Khan, K. Chandra, V. Kain, A.V.R. Reddy, “End Grain Corrosion: Establishing Microstructural Causes And Preventive Steps”, **Materials Science forum**, 702-703 (2012) 693.
3. Vivekanand Kain, Shagufta Khan, A.V. R. Reddy and P. K. Wattal, Corrosion of non-sensitized austenitic stainless steels in nitric acid environment: An electrochemical approach, **Advanced Materials Research**, 794 (2013) 517-529.

Chapters in books and lectures notes

1. Nil

Conferences

1. Shagufta Khan, Vivekanand Kain, “Measurement and Prediction of Corrosion Damage in Stainless Steels in Nitric Acid Containing Oxidizing Ions”, **Corrosion 2012- NACE International, March 11-15, 2012, Salt Lake City, Utah , USA.**
2. Shagufta Khan, Vivekanand Kain, A.V.R Reddy, “Effect of Microstructure and Grain Size on Corrosion in Transpassive potential Regime”, **CICI 2012** (International Conference Corrosion In Infrasructure And Chemical Industries), December 6-8, 2012, Vadodara, Gujarat, India.
3. Shagufta Khan, Vivekanand Kain, A.V.R Reddy, “End Grain Corrosion of SS 304L (NAG): Effect of Sulfur Segregation and Cr (VI) Concentration”, **World Corcon 2012 NACE International**, 26-29 september 2012, Goa. India.

4. Shagufta Khan, Vivekanand Kain, A.V.R Reddy, Corrosion Behavior of Stainless Steel 304L at Transpassive Potentials in Nitric Acid, **World Corcon 2013 NACE International**, 2013, New Delhi India.
5. Shagufta Khan, Vivekanand Kain, A.V.R Reddy, Electrochemical Approach to Assess Corrosion of Stainless Steel used in PUREX Process, Fifth symposium on Nuclear Analytical Chemistry (**NAC V**), 20- 24 jan, 2014, BARC, Mumbai, India.

Others

1. Nil

SHAGUFTA

DEDICATION

To my parents

Mrs. Samiun Nesa

Mr. Magbool Ahmad Khan

and my son

Aaam

ACKNOWLEDGEMENTS

I would like to take this opportunity to first of all thank Bhabha Atomic Research Centre for the Senior Research Fellowship grant. The author wishes to express sincere respect and gratitude to Dr. A. V. R. Reddy, Head, Analytical Chemistry Division, Bhabha Atomic Research Centre, for his wholehearted support, encouragement and guidance during the whole research work. Thanks are due to his constant inspiration and keen interest in the subject. I wish to express my sincere gratitude to Dr. Vivekanand Kain, Head Corrosion Section, Bhabha Atomic Research Centre. I am deeply grateful to his constructive suggestions, thorough planning, and effective analytical approach. I sincerely thank my Doctoral Committee chairman Dr. D. Das, Head, Chemistry Division, and member Dr. P. K. Pujari, Head, Nuclear Chemistry Section, RCD for time to time evaluation of the research work, and useful suggestions which definitely improved the dissertation. I would also like to express my heartfelt thanks to Dr. Kamlesh Chandra for technical advice. I take this opportunity to thank with great pleasure for strong support from the officers working in Corrosion Science Section, Dr. Parag Ahamdabadi, Dr. M. Kiran, Dr. Supratik Roy Chaudhary, Dr Geogy Abraham, Mr. Vivekanand Dube and Mr. Sunil Kumar. I am thankful to Mr. Vivek Chaudhari and Mr. Thomas Abraham of corrosion section for their help during the lab experiments of this work. Nevertheless, nor the least, I am thankful, and indebted to all the research scholars working in the centre for their help and kind cooperation in every possible way. I am thankful to my parents and husband for their support. Finally, I thank Almighty for providing me the opportunity to step into the exciting world of science, enabling me to write the thesis.

March , 2015

Shagufta

CONTENTS

	Page
	No
Synopsis	i
List of figures	xiii
List of tables	xx
List of abbreviation	xxi
Chapter 1	1
Introduction	1
1.1 Background	1
1.2 Objectives and Scope	4
1.3 Problem Definition	5
1.4 Framework of the Thesis	5
Chapter 2	7
Literature review	
2.1 Spent nuclear fuel reprocessing	7
2.1.1 Problems encountered in fuel reprocessing plants	8
2.1.2 Material selection for nuclear spent fuel reprocessing plants	9
2.2 An overview of stainless steels	13
2.2.1 Types of stainless steels	14
2.2.2. Phase equilibrium diagram and stainless steel	15
2.2.3 Austenitic stainless steels	19
2.2.3.1 Passivity of austenitic stainless steel	24
2.3 Corrosion problems associated with reprocessing plants	28

2.3.1 Intergranular corrosion	28
2.3.1.1 Theories of intergranular corrosion	33
2.3.1.2 Factors affecting intergranular corrosion	35
2.3.2 End grain corrosion	41
2.3.3 Transpassive corrosion	44
2.3.4 Pitting corrosion	44
2.3.5 Crevice corrosion	46
2.4 General electrochemical behavior of austenitic SS in nitric media	46
2.4.1. Pure HNO ₃ solutions	47
2.4.2. HNO ₃ media containing oxidizing species	50
2.4.3. HNO ₃ media containing metallic elements	52
2.5 Techniques for measuring the tendency to IGC in austenitic stainless steel	53
2.5.1 Acid tests	53
2.6 Grain boundary engineering	59
2.6.1 Grain boundaries and its classification	59
2.6.2 Methods of grain boundary engineering	61
2.7 Scope of the present study	62
Chapter 3	64
Materials and experimental methodology	
3.1 Materials and processing	64
3.2 Microstructural characterization	65
3.3 Electrochemical techniques	67
3.3.1 Double loop electrochemical potentiokinetic reactivation test	67
3.3.2 potentiodynamic polarization	69
3.3.3 Potentiostatic tests	72

3.4. Study of “End Grain Corrosion” by weight loss techniques	74
3.4.1 Practice C, A262, ASTM	75
3.4.2 “End Grain Corrosion” test	76
3.5 Surface morphological characterization techniques	77
3.5.1 Optical microscopy	77
3.5.2 Scanning electron microscopy	77
3.6 Electron backscattered diffraction examination	78
Chapter 4	79
Alloy composition and microstructure	
4.1 Results and discussion	80
4.1.1 Degree of sensitization	80
4.1.2 Potentiodynamic polarization behavior	84
4.1.3 Corrosion behavior of austenitic stainless steel in near boiling 6M HNO ₃	87
4.2 Summary	100
Chapter 5	102
Grain size and grain boundary engineering	
5.1 Background	102
5.2 Results and discussion	105
5.2.1 Influence of grain size	105
5.2.2 Influence of grain boundary engineering	112
5.3 Summary	115
Chapter 6	117
Acid concentration and temperature	
6.1 Background	117

6.2 Results and discussion	118
6.2.1 Effect of acid concentration	118
6.2.2 Effect of test temperature on corrosion of Type 304 L NAG1	122
6.3 Summary	124
Chapter 7	125
End grain corrosion	
7.1 Background	126
7.2 Results and discussion	127
7.2.1 “End Grain Corrosion” at different concentrations of Cr ⁶⁺	127
7.2.2 Influence of intergranular elemental segregation on “End Grain Corrosion”	130
7.2.2.1 Degree of sensitization	130
7.2.2.2 Results of “End Grain Corrosion” tests.	132
7.3 Summary	138
Chapter 8	140
Conclusions	
Chapter 9	143
Scope for future work	
References	145

SYNOPSIS

Corrosion of Austenitic Stainless Steels in Nitric Acid at Transpassive Potentials: Effect of Material and Process Parameters.

Nuclear spent fuel reprocessing and waste management plants use austenitic stainless steel (SS) as material of construction and the process fluid is nitric acid (HNO_3) of concentrations up to 9 M and at temperatures up to its boiling point. In nuclear spent fuel reprocessing, the process fluid, HNO_3 , contains oxidizing fission product (Ce^{4+}) and corrosion products (Cr^{6+} and Fe^{3+}). In some components, a number of cycles of reduction in volume of the process fluid is done by evaporation. It leads to a gradual increase in concentration of these oxidizing ions. Austenitic SS in sensitized condition are prone to intergranular corrosion (IGC) in boiling HNO_3 environment [1-5]. However, even non-sensitized SS are susceptible to IGC and “End Grain Corrosion” in boiling HNO_3 containing oxidizing ions. Components made from tubular/bar products are especially prone to “End Grain Corrosion” [6, 7]. However, there is little information about IGC of nonsensitized SS in oxidizing HNO_3 especially on its online monitoring. The primary aim in this project, therefore, is (a) to develop an in-depth understanding of IGC and “End Grain Corrosion” of non sensitized SS in the transpassive potential regime in near boiling HNO_3 , and (b) Develop a technique to monitor electrochemical potential and correlate to the extent of IGC.

In view of industrial importance, continuous efforts are focused to address these issues and available relevant literature is briefly summarized. It is followed by description of the salient features of the investigations carried out under this thesis work. Conclusions drawn from the work are added after that.

Exposure of SS to a temperature range of 450-850°C leads to the formation of chromium carbides at the grain boundaries with concomitant formation of chromium depletion regions immediately adjacent to the carbides at the grain boundaries [1-3, 5]. It is also known that in highly oxidizing HNO₃, segregation of silicon or phosphorus at the grain boundaries is known to cause IGC in non-sensitized SS [1, 3]. All the austenitic SS in HNO₃ medium exhibit passive to transpassive transition behavior. The SS develop a passive film (chromium rich oxide) and current densities in the domain of passive potentials are very low (μAcm^{-2}). At sufficiently high potentials, SS enters the transpassive state in which the current density begins to increase exponentially with the applied voltage. This dissolution behavior in the transpassive potential regime is similar to that exhibited during active dissolution. The main reason for the increased current density at the onset of transpassivity for SS is conversion of Cr³⁺ to Cr⁶⁺ in the passive film itself. It has been shown that the form of corrosion of austenitic SS at transpassive potentials, even in non-sensitized condition, is IGC [8]. Increase in concentration and/or operating temperature of the nitric acid coupled with increase in concentration of oxidizing ions in the nitric acid increases the operating potential [8-10]. Therefore, for a given SS (even in a non-sensitized condition), there is a definite limit on concentration of nitric acid, temperature of nitric acid and concentration of oxidizing ions in the HNO₃ that can be allowed to avoid severe IGC [8-10]. It was reported [8] that for Type 304L NAG (nitric acid grade), there is a threshold potential below which only uniform corrosion occurs and above which IGC occurs in near boiling 6 M nitric acid. This was established in an earlier study by applying a potential on a specimen of SS that was immersed in a near boiling 6 M nitric acid for a period of 48 h. The data were validated by experiments in which specimen were exposed for 48 h in near boiling 6 M nitric acid in which different concentrations of oxidizing ions (1.5 g L⁻¹ Ce⁴⁺ + 1.5 g L⁻¹ V⁵⁺, 0.64 g L⁻¹ Ce⁴⁺+ 0.95 g L⁻¹ V⁵⁺ and 0.95 g L⁻¹ V⁵⁺ + 0.171 g L⁻¹ Cr⁶⁺) were added to vary potentials. These studies had also shown that a chemical potentiostat and an electronic potentiostat gave the same rates of corrosion. Though findings of this study are very useful for prediction of corrosion rate of SS in 6M nitric acid, a more extensive study is required to understand corrosion behavior of austenitic SS in nitric acid medium with respect to various materials and process parameters. This was the motivation for the present research work. Using the same methodology [8], potential corrosion rate relationship could be

established for austenitic SS at varying material and process parameters. Potential-corrosion rate relationship is useful for prediction of corrosion rate. Prediction of corrosion rate with accuracy is necessary to keep a structural material safe from corrosion degradation in plants. The broad objective of the present work is to study corrosion behavior of austenitic SS in nitric acid environment. The specific objectives include study of the effects of following parameters on corrosion behavior of austenitic SS in HNO₃ at transpassive potential regime: (a) material parameters - composition, microstructure, grain size and grain boundary character and (b) process parameters - nitric acid concentration and temperature. The present study also aims to study the mechanism of “End Grain Corrosion” in Type 304L NAG in HNO₃.

Three grade of austenitic SS Types 310L (chemical composition in wt % is: 24.31 Cr, 1.63 Mn, 20.17 Ni, 0.011 C, 0.022 N, 0.0005 S, 0.019 P, 0.09 Si and balance Fe), 304L NAG1 (chemical composition in wt % is: 18.72 Cr, 1.58 Mn, 10.19 Ni, 0.014 C, 0.018 N, 0.004 S, 0.024 P, 0.31 and balance Fe) and 304L1 (chemical composition in wt % is: 18.05 Cr, 1.47 Mn, 7.95 Ni, 0.024 C, 0.04 N, 0.003 S, 0.034 P, 0.49 Si balance Fe) were used to study the effects of chemical composition on corrosion behavior in 6M HNO₃ in transpassive potential regime. The reason for using these grades in the present study is their extensive use in spent fuel reprocessing plants and difference in their chemical composition especially with respect to C and Cr. Types 310L, 304L NAG1 and 304L1 were subjected to a heat treatment at 675 °C for 1 h to simulate the worst microstructure in weldments. Heat treated specimens were exposed to near boiling 6M HNO₃ for 48 h in a set of potentiostatic tests. The experimental set up used in these potentiostatic tests was the same as was used by Bhise and kain in a study carried out earlier [8] and details are available in the same reference. In these tests potentials (in transpassive regime) were applied to SS specimens for the entire period of exposure. Corrosion rate was calculated from the weight loss of the specimen after 48 h of exposure to near boiling 6M HNO₃ using equation 1:

$$r = \frac{87480 \times W}{A \times d \times t} \quad (1)$$

where r is corrosion rate in millimeters per year, W is weight loss in grams, A is total exposed surface area (cm^2), d is density of sample (gcm^{-3}) and t is time of exposure (h).

Corrosion rates obtained in these tests were plotted against applied potential (Fig.1). Potential at which a corrosion rate of 0.61 mmy^{-1} (24 mpy) was observed which was taken as the threshold potential in a previously reported study [8] as it is known that severe IGC (grain dropping) takes place when corrosion rates are above 0.61 mmy^{-1} [6]. Threshold potential was established with the help of corrosion rate vs potential plots (Fig.1). An equation derived from the curve fitting of these data is proposed to be used for predicting the corrosion rates of a specific stainless steel at any given operating potential.

$$r = ae^{V/b} \quad (2)$$

where r is the corrosion rate (mmy^{-1}) of SS upon exposure to near boiling 6M nitric acid for a period of 48 h, V is the applied potential (V_{SCE}) and, a and b are constants at that potential.

The threshold potentials for SS Types 304L1, 304L NAG1 and 310L (each after heat treatment at $675 \text{ }^\circ\text{C}$ for 1 h resulting in a “dual” microstructure) were 0.960, 0.965 and $0.966 V_{\text{SCE}}$ respectively. Corrosion rates measured in potentiostatic tests were in the order of Types $310L < 304L \text{ NAG1} < 304L1$ (Fig.1). The least corrosion rate shown by Type 310L is attributed to the fact that it contains the least content of C and Si, and the highest content of Cr among all the three grades.

To assess the effect of microstructure on corrosion behavior, specimens from Type 304L1 and Type 304L NAG1 were heat treated at $675 \text{ }^\circ\text{C}$ for different durations (1 to 171 h) to produce “dual” (discontinuous attack on chromium-depleted regions at the grain boundaries but no single grain completely encircled) [12] and “ditch” (continuous attack on chromium-depleted regions at the grain boundaries for at least one grain) [12] microstructures. In as-received condition Type 304L1 and Type 304L NAG1 had “step” (no precipitation of chromium carbides at grain boundaries) [12] microstructure. Heat treatment for 1h produced “dual” microstructure in Type 304L1 and Type 304L NAG1. Type 304L1 showed “ditch” microstructure after heat treatment for 142 h. No “ditch” microstructure was obtained for Type 304L NAG1 by the chosen heat treatments. As-received and heat treated specimens of Type 304L1 and Type 304L NAG1 were exposed to near boiling 6 M

HNO₃ for 48 h in a set of potentiostatic tests [8]. Results of these potentiostatic tests for Type 304L1 are shown in Fig. 2. The threshold potentials for Type 304L1 having “Step”, “Dual” and “Ditch” microstructure were 0.959, 0.960 and 0.952 V_{SCE} respectively. Corrosion rate at an applied potential of 0.97 V_{SCE} increased for the Type 304L1 SS with “step”/“dual” microstructure from 1.12 mmy⁻¹ (44 mpy) to 1.64 mmy⁻¹ (64.5 mpy) for the “ditch” microstructure. Specimens having “ditch” microstructure showed higher corrosion rates compared to specimens having “step” and “dual” microstructure at all applied transpassive potentials. The threshold potential for Type 304L NAG1 was 0.967 V_{SCE} for “step microstructure”, and 0.966 V_{SCE} for “Dual microstructure”. Specimens having “step” and “dual” microstructure showed comparable corrosion rates for both Type 304L1 and Type 304L NAG1 at all applied transpassive potentials. This is due to the fact that threshold potentials for “step” and “dual” microstructure are very close for both Type 304L1 and Type 304L NAG1.

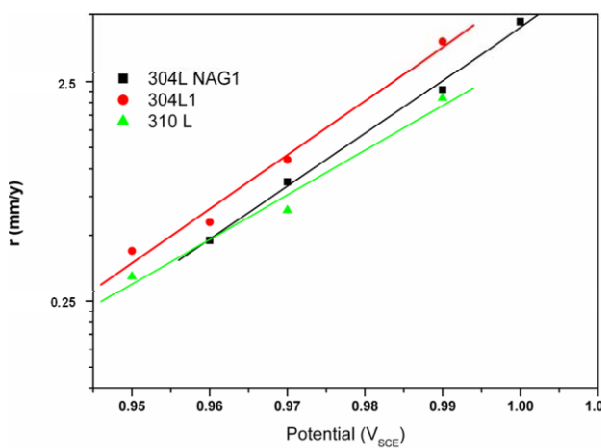


Fig.1 Correlation between corrosion rate (r) and applied potential (V) for three Types of austenitic SS heat-treated at 675 °C for 1 h exposed to near boiling 6 M nitric acid for 48 h.

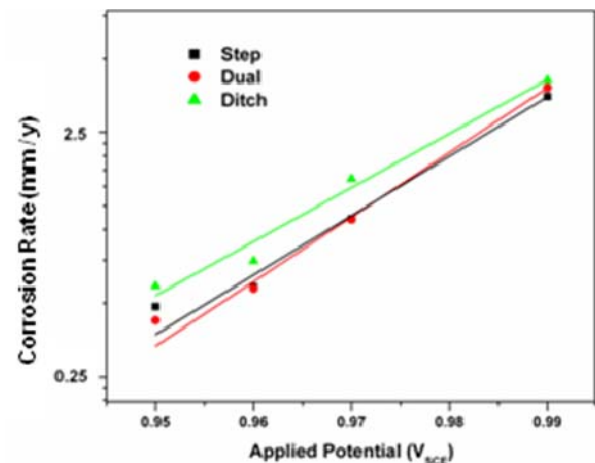


Fig.2 Correlation between corrosion rate (r) and applied potential (V) for "step", “dual” and “ditch” microstructures of Type304 L1, exposed to near boiling 6 M nitric acid for 48 h.

Type 304L2 (chemical composition in wt % is: 18.1 Cr, 1.54 Mn, 8.0 Ni, 0.023 C, 0.007 S, 0.04 P, 0.04 Si and balance Fe) was used to study the effects of grain size on corrosion behavior. Its grain size was varied by annealing heat treatments. In as-received condition Type 304L2 had “step” microstructure and its grain size was ASTM grain size number 8 (average intercept length of 22.4 μm). Solution annealing of as-received Type 304L2 specimens at 1050 °C for 45 min and 2 h increased the grain size to ASTM grain size no 6 (average intercept length of 45 μm) and ASTM grain

size number 4 (average intercept length of 90 μm) respectively. “Step” microstructure present in as-received Type 304L2 was retained after these solution-annealing treatments. As-received and solution-annealed specimens of Type 304L2 were subjected to heat treatment at 675 °C for 1 h. This heat treatment converted “step” microstructure to a light “dual” microstructure in all the specimens. Type 304L2 specimens with varying grain size (in light dual microstructure) were subjected to potentiostatic tests [8] in near boiling 6M HNO_3 . Results of these tests are shown in Fig.3. Corrosion rates of Type 304L2 specimens (in a light “dual” microstructure) having ASTM grain size numbers 8, 6 and 4 were 5.4 mmy^{-1} (216 mpy) , 3.8 mmy^{-1} (152 mpy) and 2.5 mmy^{-1} (102 mpy) respectively at 0.99 V_{SCE} . Increasing grain size of Type 304L2 (in a light “dual” microstructure) from ASTM grain size number 8 to 4 resulted in a decrease in the corrosion rate in potentiostatic tests in near boiling 6 M HNO_3 at all transpassive potentials . While discussing effects of microstructure on corrosion behavior of Type 304L1 and Type 304L NAG1, it was seen that for constant grain size corrosion rate was not much affected if microstructure changes from “step” to “dual”. A drastic change in corrosion rate was observed only if the microstructure becomes “ditch”. Microstructures of Type 304L2 specimens of various grain sizes changed from “step” to “dual” after sensitization heat treatment. Therefore if specimens were exposed to potentiostatic tests without sensitization, similar corrosion rates would be obtained. Specimens with smallest grain size possess largest grain boundary area. Grain boundaries possess excess free energy due to the presence of disorder. Therefore surface reactivity of specimen with least grain size was the highest and thus its tendency to IGC would be more compared to other two specimens.

To study the effect of grain boundary character, Type 304L1 was strain-annealed using previously reported [13] optimized parameters (5 % reduction in specimen thickness by cold rolling followed by annealing at 927°C for 72 h) for thermomechanical processing. During electron backscattered diffraction (EBSD) examination grain boundaries are classified as either special or general. Grain boundaries containing a high density of coincidence sites are called coincidence site lattice (CSL) boundaries or special boundaries. EBSD examination revealed that strain-annealing increased CSL frequency from 43.8 % to 52.9 % in Type 304L1. Shimada et al. [13] have reported 86.5 % frequency of CSL boundaries using the same parameters for thermomechanical treatment on

as- received Type 304 specimen having CSL frequency 63 %. The increase in CSL frequency in Type 304L1 was less compared to increase in CSL frequency using the same thermomechanical process for SS 304 used by Shimada et al. [13]. As-received and strain-annealed Type 304L1 specimens were exposed to potentiostatic tests [8] in near boiling 6M HNO₃ at 0.99 V_{SCE}. Strain-annealing decreased corrosion rate from 3.5 mmy⁻¹ (140 mpy) to 2.2 mmy⁻¹ (88 mpy) at 0.99 V_{SCE}. However, strain annealing could not decrease corrosion rate to a safe limit (0.61 mmy⁻¹ (24 mpy) or below) below which IGC resistance was achieved. Therefore IGC resistance achieved through strain-annealing was not sufficient to prevent IGC in near boiling 6M HNO₃ at transpassive potentials. Since increase in CSL frequency was marginal, decrease in corrosion rate after strain-annealing on Type 304L1 in potentiostatic test might be due to grain growth from ASTM grain size number 7 (average intercept length of 32 μm) to ASTM grain size number 4 (average intercept length of 90 μm).

Type 304L1 (heat treated at 675 °C for 1h) specimens were subjected to potentiostatic tests [8] in near boiling HNO₃ of concentrations 3M, 6M and 9M to assess influence of HNO₃ concentration on corrosion behavior. The results of these potentiostatic tests are shown in Fig. 4. Corrosion rate increased at each potential with decreasing concentration of HNO₃. For instance at 0.99 V_{SCE} corrosion rates were 7.3 mmy⁻¹ (289 mpy), 3.8 mmy⁻¹ (152 mpy) and 1.85 mmy⁻¹ (73 mpy) in 3M, 6M and 9M HNO₃ respectively. The threshold potentials [8] for Type 304L1 in 3M, 6M and 9M HNO₃ were 0.92 V_{SCE}, 0.96 V_{SCE} and 0.98 V_{SCE} respectively. Since threshold potential for Type 304L1 was lower in lower concentration of HNO₃, Type 304L1 would undergo IGC earlier in lower concentration HNO₃ than in higher concentration HNO₃. It is confirmed from morphology of corrosion attack that Type 304L1 showed IGC in HNO₃ of all the three concentrations (3M, 6M and 9M) at transpassive potentials.

Type 304L NAG1 (heat treated at 675 °C for 1 h) specimens were subjected to potentiostatic tests [8] in 6M HNO₃ at various temperatures (55, 75, 85 and 95 °C) to assess influence of acid temperature on corrosion behavior. The corrosion rates obtained in these tests increased from 0.11mmy⁻¹ (4.5 mpy) to 2.11 mmy⁻¹ (83 mpy) on increasing the solution temperature from 55 to 95 °C. The logarithm of corrosion rates measured in such experiments was plotted as a function of

inverse of temperature (Fig. 5). The activation energy for corrosion of Type 304L NAG1 in 6M HNO₃ at 0.99 V_{SCE} for the temperature range 55 to 95 °C was calculated using this plot as 72.56 kJmol⁻¹.

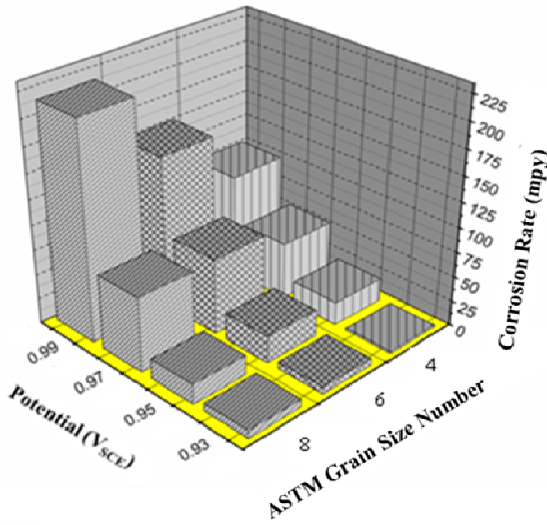


Fig. 3 Results of potentiostatic tests conducted on Type 304L2 specimens of different grain size in near boiling 6M HNO₃ for 48 h.

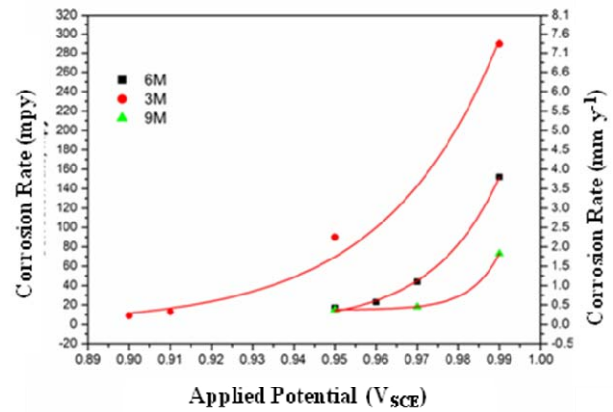


Fig. 4 Corrosion rate of Type 304L1 as a function of applied potential at different concentrations of near boiling HNO₃.

Type 304L NAG2 tube (chemical composition in wt % is: 18.1Cr, 1.54 Mn, 8.0 Ni, 0.023 C, 0.12 N, 0.007 S, 0.04 P, 0.04 Si and balance Fe) was used to study “End Grain Corrosion” in boiling 9M HNO₃ containing Cr⁶⁺. In order to study effect of Cr⁶⁺ concentration on “End Grain Corrosion” as-received Type 304L NAG2 specimens were exposed to: (1) boiling 9M HNO₃ + 1.5 g L⁻¹ Cr⁶⁺ for 19 periods, each of 3 h duration (2) boiling 9M HNO₃ + 1.25 g L⁻¹ Cr⁶⁺ for 20 periods, each of 3 h duration and (3) boiling 9M HNO₃ + 1 g L⁻¹ Cr⁶⁺ for 4 periods, each of 24 h duration. The corrosion rate for as-received Type 304L NAG2 specimens exposed to boiling 9M HNO₃ containing 1.5, 1.25 and 1 g L⁻¹ Cr⁶⁺ after 57 h of exposure was 23 mmy⁻¹ (909 mpy), 17.4 mmy⁻¹ (688 mpy) and 8.4 mmy⁻¹ (332 mpy) respectively. Increase in Cr⁶⁺ concentration in boiling 9M HNO₃ increased the susceptibility of as-received Type 304L NAG2 to “End Grain Corrosion”. This increase in susceptibility of Type 304L NAG2 to “End Grain Corrosion” was attributed to increase in attained potential with increase in Cr⁶⁺ concentrations (Fig.6).

A few as-received specimens of Type 304L NAG2 were subjected to heat treatment at 650 °C/100 h, 650 °C/ 3 h, 990 °C/ 5 min to induce elemental segregation [14, 15]. Specimen previously heat treated at 650 °C for 100 h was annealed at 950 °C for 90 min. The heat treatment at 950 °C for 90 min is shown to equilibrate segregation without sensitization or grain growth of the material [7].

None of the above heat treatments caused extensive sensitization and Type 304L NAG2 remained resistant to IGC in practice A and C, A 262, ASTM. Heat-treated and as-received specimens of Type 304L NAG2 were subjected to “End Grain Corrosion” test. In this test specimens were exposed to boiling 9M HNO₃ containing 1g L⁻¹ Cr⁶⁺ for 4 periods of 24 h each. Results obtained from this test are summarized in Fig.7.

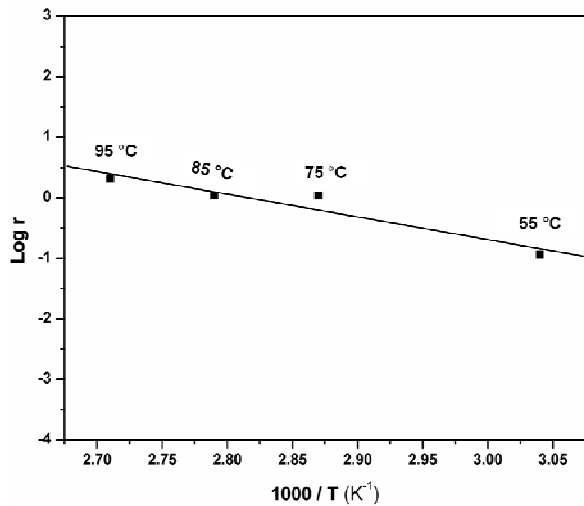


Fig.5 Arrhenius plot of log r vs. 1 / T to obtain activation energy for corrosion in nitric acid.

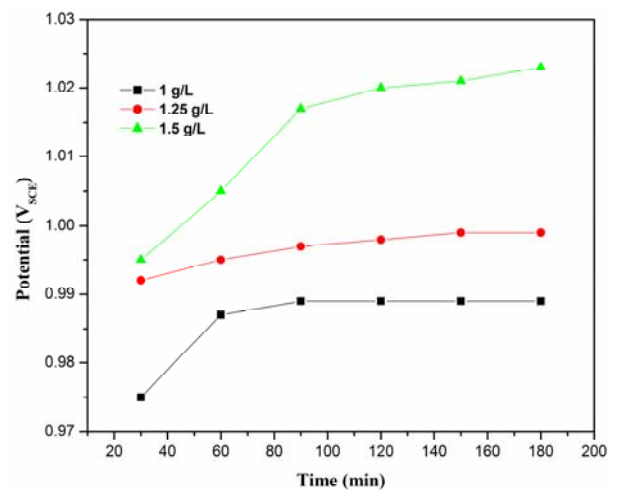


Fig.6 Potential variation with time in boiling 9 M HNO₃ containing different concentrations of Cr⁶⁺.

Specimen heat treated at 650 °C for 100 h exhibited corrosion rate of 11.09 mmy⁻¹ (437 mpy) in the first period which increased to 27.5 mmy⁻¹ (1083 mpy) in the second period. Because of such a high corrosion rate, specimen heat treated at 650 °C for 100 h was not subjected to “End Grain Corrosion” test beyond second period. It is reported that heat treatment at 650 °C for 100h induces maximum segregation of phosphorus at the grain boundary in austenitic SS [14]. This might be the reason for significant increase in “End Grain Corrosion” in specimen with heat treatment at 650 °C for 100 h. When specimen previously heat treated at 650 °C for 100 h was annealed at 950 °C for 90 min and subjected to “End Grain Corrosion” test, the average corrosion rate decreased from 19.3 mmy⁻¹ (760 mpy) to 3.2 mmy⁻¹ (126 mpy)). The morphology of corrosion attack starting from the cross section of the tube, examined after the “End Grain Corrosion” test showed very deep “End Grain Corrosion” in specimen heat treated at 990 °C for 5 min (Fig.8). It is shown that heat treatment at 990 °C for 5 min results in intergranular segregation of S in austenitic stainless steel [15]. Very severe “End Grain Corrosion” in specimen heat treated at 990 °C for 5 min might be due to segregation of sulfur along the grain boundaries. In “End Grain Corrosion” tests average corrosion

rate for specimen heat treated at 990 °C for 5 min was 5.6 mmy⁻¹ (221.2 mpy) while average corrosion rate for as-received specimen was 8.3 mmy⁻¹ (328.2 mpy). In specimen heat treated at 990 °C for 5 min morphological study showed deep IGC starting from cross-section of the tube and propagating along longitudinal direction of the tube (“End Grain Corrosion”) and nominal IGC from ID (inner diameter) and OD (outer diameter) side of the tube. In as-received specimen morphological study showed (a) IGC starting from cross-section of the tube and propagating along longitudinal direction of the tube (“End Grain Corrosion”), (b) IGC starting from ID side of the tube and (c) IGC starting from OD side of the tube. IGC starting from ID and OD side of the tube was much severe in as-received specimen compared to specimen heat treated at 990 °C for 5. This might be the reason for higher corrosion rate shown by as-received specimen compared to specimen heat treated at 990 °C for 5 min (Fig. 7).

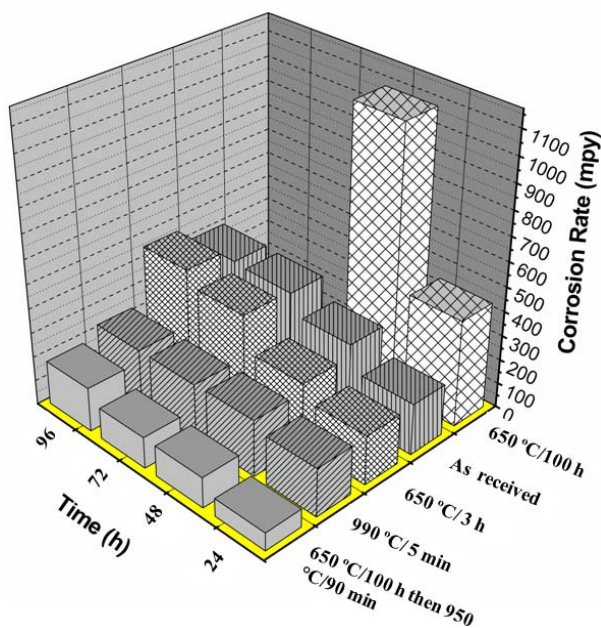


Fig.7 Corrosion rate measured in different 24 h periods of the “End Grain Corrosion” test in boiling 9 M HNO₃ + 1 g L⁻¹ Cr⁶⁺ solution.

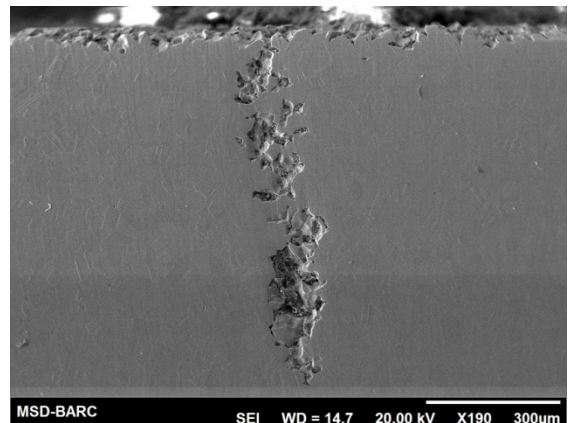


Fig.8 Morphology of “End Grain Corrosion” after specimen heat treated at 990 C for 5 min was exposed to 9 M HNO₃ containing 1g Cr⁶⁺ for 4 periods of 24 h each.

With respect to the objectives of this project to develop an in-depth understanding of IGC and “End Grain Corrosion” in oxidizing HNO₃ (in transpassive potential regime) and to develop a methodology to monitor electrochemical potential to access the extent of IGC, the key conclusions from this work are provided below:

1. In near boiling 6M HNO₃ in transpassive potential regime:

- a. IGC starts even in solution annealed Type 304L1 and Type 304L NAG1.
 - b. Type 304L1 having “ditch” microstructure is more susceptible to IGC compared to same alloy having “step”/ “dual” microstructure.
 - c. Rate of IGC remains comparable when microstructure changes from “Step” to “Dual” for both Type 304L1 and Type 304L NAG1.
 - d. Type 304L2 with coarser grains is less susceptible to IGC compared to same material with finer grains. (This is applicable to ASTM grain size number 8 (average intercept length of 22.4 μm), 6 (average intercept length of 45 μm) and 4 (average intercept length of 90 μm)).
2. In near boiling HNO_3 of concentrations 3M, 6M and 9M Type 304L1 showed IGC rate in the order of $3\text{M} > 6\text{M} > 9\text{M}$ in transpassive potential range.
 3. The activation energy for corrosion of Type 304L NAG1 in 6M HNO_3 for temperature range 55 to 95 $^\circ\text{C}$ at 0.99 V_{SCE} is 72.56 kJ M^{-1} .
 4. Increase in Cr^{6+} concentration (from 1g to 1.5 g L^{-1}) in boiling 9M HNO_3 increased susceptibility of Type 304L NAG2 to “End Grain Corrosion”.
 5. The heat treatments known to induce intergranular segregation of phosphorus or sulfur caused significant increase in the severity of “End Grain Corrosion” in Type 304L NAG2 in boiling 9M HNO_3 .

REFERENCES:

- [1] M. G. Fontana, Corrosion Engineering, third ed., Tata McGraw-Hill Publishing Company Limited, New York, 2005.
- [2] D.A. Jones, Principles and Prevention of Corrosion, second ed., MacMillan Publishing Co., 1992.
- [3] A. J. Sedriks, Corrosion of stainless steels, second ed., John Wiley and Sons, New York, NY, 1996.
- [4] V. Cihal, Intergranular Corrosion of Stainless Steels and Alloys, Materials Science Monograph No. 18, Elsevier, New York, 1984, p.196.
- [5] V. Kain, Corrosion Resistant Materials, in: S. Banerjee and A. K. Tyagi (Eds), Functional Materials: Preparation, Processing and Applications, Elsevier, 2011. ISBN: 9780123851420.
- [6] V. Kain, P. Sengupta, P. K. De, S. Banerjee, Metall. Mater. Trans. A., 36 (2005)1075-1084.

- [7] K. Chandra, V. Kain, P. Ganesh, *ASM J. Mater. Eng. Perform.*, 17 (2008) 115-122.
- [8] S. Bhise, V. Kain, *Corros. Eng. Sci. Techn.*, 47(2011) 61- 69.
- [9] P. Fauvet, F. Balbaud, R. Robin, Q. -T. Tran, A. Mugnier, D. Espinoux, *J. Nucl. Mater.*, 375 (2008) 52- 64.
- [10] M. A. Striecher, *J. Electrochem. Soc.*, 106 (1959)161-180.
- [11] ASTM A240/A240M-11a, “Standard Specification for Chromium and Chromium Nickel Stainless Steel Plate, Sheet and Strip for Pressure Vessels and for General Applications” (West Conshohocken, PA: ASTM International, 2011).
- [12] “ASTM Designation A 262 – 02a”: Standard practice for detecting susceptibility to intergranular attack in austenitic stainless steels, *Annual book of ASTM standards*, ASTM International, West Conshohocken, PA 19428-2959, United States, 2002.
- [13] M. Shimada, H. Kokawa, Z.J. Wang, Y.S. Sato, I. Karibe, *Acta Mater.*, 50 (2002) 2331–2341.
- [14] C. L. Briant and E. L. Hall, *Corrosion*, 43 (1987) 525-533.
- [15] H. Tvrdy, R. Setdl, L. Hyspecka, K. Razanec, *Scr. metal.*, 19 (1985) 51-55.

LIST OF FIGURES

S. No.	Figure No.	Title of the figure	Page No.
1	2.1	Purex process flow sheet	8
2	2.2	Schaeffler diagram	15
3	2.3	Compositional and property linkages in the stainless steel family of alloys	16
4	2.4	Fe-C equilibrium phase diagram	17
5	2.5	Fe-Cr equilibrium phase diagram	18
6	2.6	Fe-Cr-Ni ternary phase diagram	18
7	2.7	Intergranular corrosion exhibited by an austenitic stainless steel (a) surface of the specimen, (b) cross-sectional view shows the depth of penetration of the attack along the grain boundaries	29-30
8	2.8	Preferential attack in low-temperature heat affected zones (A) of Type 302 stainless steel welded strip	31
9	2.9	Chromium distribution profile at grain boundary	33
10	2.10	Effect of the chromium content on the corrosion behavior of austenitic stainless steels in nitric acid (65 wt%, boiling temperature)	35
11	2.11	Effect of the carbon content on the behavior of 304 stainless steel in nitric acid, as revealed by the double loop EPR technique	37
12	2.12	Effect of the silicon content on the behavior of austenitic stainless steels in boiling 5 M L ⁻¹ nitric acid + 1 g L ⁻¹ Cr ⁶⁺	38
13	2.13	Effect of phosphorus concentration on corrosion rate	38

14	2.14	Reduction in solution potential	40
15	2.15	Corrosion rate variation with exposure for 4M nitric acid	41
16	2.16.	(a) Schematic of end grain corrosion and (b) a typical end grain attack in austenitic stainless steel	43
18	2.17	Pitting corrosion of austenitic stainless steel in nitric acid medium containing chloride ions	45
19	2.18.	General electrochemical behavior of austenitic SS in acidic media as a function of the potential	47
20	2.19	Pictorial representation of the mechanism of reduction of nitric acid. (a) Low to moderate concentrations ($<6 \text{ M L}^{-1}$) and (b) high concentrations ($>8 \text{ M L}^{-1}$).	49
21	2.20	(a) “step” microstructure (500 X) (b) “dual” microstructure (250X) and (c) “ditch” microstructure (500 X)	56-57
22	3.1	Type 304L NAG 1 specimen mounted in cold setting resin for microstructure evolution.	67
23	3.2	Cross sectional view an electrochemical cell for corrosion study	68
24	3.3	Photograph of the specimen for DL- EPR test.	69
25	3.4	Schematic diagram of the DL- EPR test	69
26	3.5	Experimental set-up used for measurement or application of potential at 95 °C (a) schematic of set-up (b) photograph of the actual set-up	71
27	3.6.	Photograph of the set up used for Practice C, A262, ASTM.	76
28	4.1	Microstructural characterization of Type 304L1 by optical microscope (a) as-received condition, (b) after heat-treatment at 675 °C for 1 h and (c) after heat-treatment at 675 °C for 142 h.	81

29	4.2	Microstructural characterization of Type 304L NAG1 by optical microscope (a) as-received condition, (b) after heat treatment at 675 °C for 1 h, (c) after heat treatment at 675 °C for 142 h and (d) after heat treatment at 675 °C for 171 h.	82
30	4.3	Microstructural characterization of Type 310 L observed by optical microscope (a) as-received condition and (b) after heat treatment at 675 °C for 1 h.	83
31	4.4.	Polarization curves of SS heat treated at 675 °C for 1 h in near boiling 6M HNO ₃ .	85
32	4.5	Polarization curves of Type 304L1 for “step” and “ditch” microstructure in near boiling 6M HNO ₃ .	86
33	4.6.	Polarization curves of Type 304L NAG1 in near boiling 6M HNO ₃ .	87
34	4.7	Correlation between corrosion rate (r) and applied potential (V) for three Types of austenitic stainless steels heat-treated at 675 °C for 1 h exposed to near boiling 6M HNO ₃ for 48 h	89
35	4.8	IGC observed by SEM for (a) Type 304L1, (b) Type 304L NAG1 and (c) Type 310L each heat-treated at 675 °C for 1 h and exposed to near boiling 6M HNO ₃ at 0.99 V _{SCE} for 48 h.	91
36	4.9	IGC observed by optical microscope for Type 304L1 heat-treated at 675 °C for 1 h exposed to near boiling 6M HNO ₃ for 48 h at (a) 0.95 V _{SCE} and (b) 0.99 V _{SCE} .	91
37	4.10	IGC observed after Type 310L heat-treated at 675 °C for 1 h and exposed to near boiling 6M HNO ₃ for 48 h at (a) 0.96 V _{SCE} under SEM, (b) 0.99 V _{SCE} under SEM and (c) 0.99 V _{SCE} under optical microscope.	93

- 38 4.11 IGC observed after Type 304L NAG1 heat-treated at 675 °C for 1 h 94
and exposed for 48 h to near boiling 6M HNO₃ at (a) 0.96 V_{SCE}
under optical microscope (b) 0.99 V_{SCE} under optical microscope
and (c) 0.99 V_{SCE} under SEM.
- 39 4.12 Correlation between corrosion rate (r) and applied potential (V) for 95
"step", "dual" and "ditch" microstructures of Type304 L1, exposed
to near boiling 6M HNO₃ for 48 h.
- 40 4.13 IGC observed observed by optical microscope after exposure in 96
HNO₃ 6M nitric acid for 48 h in Type 304L1, having "step"
microstructure at (a) 0.95 V_{SCE}, (b) 0.97 V_{SCE} and (c) 0.99 V_{SCE},
having "dual" microstructure at (d) 0.95 V_{SCE}, (e) 0.97 V_{SCE} and (f)
0.99 V_{SCE} and having "ditch" microstructure at (g) 0.95 V_{SCE}, (h)
0.97 V_{SCE} and (i) 0.99 V_{SCE}.
- 41 4.14 Correlation between corrosion rate (r) and applied potential (V) for 98
"step", and "dual" microstructures of Type 304L NAG1, exposed to
near boiling 6M nitric acid for 48 h.
- 50 5.1 Microstructures of longitudinal surface of Type 304L2 observed by 107
optical microscope (a) in as-received condition, (b) After heat
treatment at 1050 °C for 45 min and (c) After heat treatment at
1050 °C for 2 h.
- 51 5.2. Microstructures of longitudinal surface of Type 304L2 observed by 108
optical microscope after (a) heat treatment at 675 °C for 1 h on as-
received specimen, (b) heat treatment at 675 °C for 1 h on
specimen annealed at 1050 °C for 45 min and (c) heat treatment at
675 °C for 1 h on specimen annealed at 1050 °C for 2 h.

52	5.3	Results of potentiostatic tests conducted on Type 304L2 specimens of different grain size in 6M near boiling HNO ₃ for 48 h.	109
53	5.4	Morphology of corrosion (observed by optical microscope) attack on longitudinal surface of Type 304L2 (ASTM grain size no 4) exposed to near boiling 6M HNO ₃ at 0.93 V _{SCE} .	110
54	5.5	Morphology of corrosion attack (observed by optical microscope) on Type 304L2 specimens (having varying grain size) exposed to near boiling 6M HNO ₃ at 0.97 V _{SCE} and 0.99 V _{SCE} .	111
55	5.6	Microstructure of Type 304L1 (observed by optical microscope) after 5 % reduction in specimen thickness by cold rolling followed by annealing at 927 °C for 72 h	112
56	5.7	OIM images for (a) as-received Type 304 L1 specimen (b) strain-annealed (5 % reduction in specimen thickness followed by annealing at 927 °C for 72 h) Type 304 L1 specimen	114
57	5.8	Morphology of corrosion attack (observed by optical microscope) on strain-annealed Type 304L1 specimen exposed to 6M HNO ₃ at 0.99 V _{SCE} .	115
58	6.1	Polarization curves of Type 304L1 in near boiling HNO ₃ .	119
59	6.2	Corrosion rate of Type 304L1 as a function of applied potential at different concentrations of near boiling HNO ₃	120
60	6.3	Uniform corrosion of Type 304L1 (observed under optical microscope) exposed to near boiling 3M HNO ₃ at 0.90 V _{SCE} .	120
61	6.4	Morphology of corrosion attack (observed by optical microscope) of Type 304L1 at 0.95 V _{SCE} in (a) 9M (b) 3M and at 0.99 V _{SCE} (c) 9M and (d) near boiling 3M HNO ₃ .	121

62	6.5	Relationship between corrosion rate and solution temperature for Type 304L NAG1 at 0.99 V_{SCE} in 6M HNO_3 .	122
63	6.6	Arrhenius plot of $\log r$ vs. $1 / T$.	123
64	7.1	Microstructure of Type 304L NAG2 in as received condition	128
65	7.2.	Corrosion rate as a function of time at different concentrations of Cr^{6+} in boiling 9M HNO_3 .	128
66	7.3	Corrosion attack as seen in the longitudinal direction of specimen by optical microscope exposed to 9M HNO_3 containing (a) 1.25 g $L^{-1} Cr^{6+}$ and (b) 1.5 g $L^{-1} Cr^{6+}$.	129
67	7.4	Potential variation with time in boiling 9M HNO_3 containing different concentrations of Cr^{6+} .	129
68	7.5	Microstructures of the transverse section of the material observed by optical microscope after the following heat treatments (a) 650 °C for 3 h, (b) 650 °C for 100 h, (c) 650 °C for 100 h then 950 °C for 90 min and (d) 990 °C for 5 min.	131
69	7.6	Corrosion rate measured as a function of discrete periods using the “End Grain Corrosion” test in boiling 9M HNO_3 + 1 g $L^{-1} Cr^{6+}$ solution	132
70	7.7	Morphology of corrosion attack observed by optical microscope in (a) As received, (b) 650 °C for 3h, (c) 650 °C for 100h, (d) 650 °C for 100 h then annealed at 950 °C for 90 min and (e) 990 °C for 5 min.	134-135
71	7.8	IGC observed by optical microscope after modified practice C (a) in as-received specimen from OD side of the tube, (b) in as-received specimen from ID side of the tube and (c) in specimen	136

heat treated at 990 °C for 5 min from OD side of the tube.

- 72 7.9 Morphology of “End Grain Corrosion” observed by SEM after (a) 137
specimen heat treated at 650 °C for 100 h was exposed to 9M
HNO₃ containing 1 g L⁻¹ Cr⁶⁺ for four periods of 24 h and (b)
specimen heat treated at 990 °C for 5 min was exposed to 9 M
HNO₃ containing 1 g Cr⁶⁺ for four periods of 24 h.

List of Tables

S. No	Table No	Title	Page No.
1	2.1	Data on the ‘oxidizing’ ions susceptible to be present in spent fuel treatment media	51
2	2.2	Metallic elements susceptible to induce a galvanic corrosion of stainless steels in hot and concentrated nitric media	52
3	2.3	Standard IGC tests for austenitic SS	54
4.	3.1	Chemical composition of austenitic stainless steels used in the present study (wt %)	65
5	3.2	Heat treatments used in the present study	66
6	3.3	Heat treatment and its influence on the microstructure (wt %)	75
7	4.1	Extent of sensitization for three Types of stainless steels in different heat-treated condition	84
8	4.2	Constants calculated by fitting of equation 4.2 for the three stainless steels (Fig. 4.7)	88
9	4.3	Constants calculated by fitting of equation 4.2 for Type 304L1 having “step”, “dual” and “ditch” microstructure (Fig.4.12)	95
10	4.4	Constants calculated by fitting of equation 4.2 for Type 304L NAG1 having “step” and “dual” microstructure (Fig.4.14)	99
11	5.1	Corrosion rates of as-received Type 304L1 and strain-annealed Type 304L1 specimens after exposure to near boiling 6M HNO ₃ at 0.99 V _{SCE} for 48 h	115
12	7.1	Degree of sensitization evaluated from DL-EPR test of Type 304L NAG2 in as-received condition and after heat treatments	131

List of Abbreviation

AISI	American iron and steel institute
ASTM	American society for testing and materials
BEI	Backscattered electron imaging
CSL	Coincident site lattice
DL-EPR	Double loop electrochemical potentiokinetic reactivation
EBS	Electron backscattered diffraction
ECORR	Corrosion potential
ESR	Electro slag remelting
GBE	Grain boundary engineering
HAZ	Heat affected zone
I_{CORR}	Corrosion current density
ID	Inner diameter
IGC	Intergranular corrosion
NAG	Nitric acid grade
OCP	Open circuit potential
OD	Outer diameter
PUREX	Plutonium uranium reduction by extraction
SEI	Secondary electron imaging
SFE	Stacking fault energy
SPD	Severe plastic deformation
SS	Stainless steel
UNS	Unified numbering system

CHAPTER 1

INTRODUCTION

1.1 Background

Austenitic stainless steel (SS) alloys are used in a wide variety of industries including power, chemical and petrochemical processes. The austenitic SS alloys have an excellent combination of mechanical strength, corrosion resistance, fabricability and cost effectiveness. A passive, chromium rich oxide film on SS surfaces protects them from corrosion [1-6]. Austenitic SS alloys are passivated in nitric acid (HNO_3) [3, 7-9] before supply as plates/tubes/products. Passive film formed over Type 304 SS (UNS S30400) after exposure to 20 % HNO_3 at 50 °C for 30 minutes is shown to be 2.4 nm thick [10]. However, these steels are susceptible to localized corrosion, such as pitting corrosion, crevice corrosion and environment-induced cracking in chloride environment [1-6, 9]. The austenitic SS alloys are also prone to intergranular corrosion (IGC) in HNO_3 environment [1-2, 5-6, 11-14]. Austenitic SS alloys also show IGC in acetic acid, ammonium nitrate, calcium nitrate, chromic acid, formic acid, hydrocyanic acid, lactic acid, oxalic acid, seawater, phosphoric acid, phthalic acid, sulfamic acid and sulfuric acid [1].

Nuclear spent fuel reprocessing and waste management plants use austenitic stainless steel (SS) as material of construction and the process fluid is nitric acid (HNO_3) of concentrations up to 9M and at temperatures up to its boiling point. In nuclear spent fuel reprocessing, the process fluid, HNO_3 , contains oxidizing fission product (Ce^{4+}) and corrosion products (Cr^{6+} and Fe^{3+}). In some components, a number of cycles of reduction in volume of the process fluid is done by evaporation. It leads to a gradual increase in concentration of these oxidizing ions. Austenitic SS alloys in sensitized condition are prone

to intergranular corrosion (IGC) in boiling HNO_3 environment [1, 2, 5, 6, 9]. However, even non-sensitized SS alloys are susceptible to IGC and “End Grain Corrosion” in boiling HNO_3 containing oxidizing ions. However, there is little information about IGC of nonsensitized SS in oxidizing HNO_3 especially on its online monitoring. The primary aim in this work, therefore, is (a) to develop an in-depth understanding of IGC and “End Grain Corrosion” corrosion behavior of non sensitized SS in the transpassive potential regime in near boiling HNO_3 , and (b) Develop a technique to monitor electrochemical potential and correlate to the extent of IGC.

The basic cause of IGC is sensitization of SS [1-3, 5, 9, 15-18]. Exposure of SS to a temperature in the range of 450-850 °C leads to formation of chromium rich carbides (Cr_{23}C_6) at the grain boundaries with concomitant formation of chromium depletion regions immediately adjacent to the carbides at the grain boundaries [1-3, 5, 9, 19-20]. When the level of chromium in the depleted regions is less than 12 wt. %, the passive film formed over these chromium depleted regions is weak and prone to breakdown during service [1-2, 5, 15]. It has been shown clearly that mainly the carbon content (and indirectly chromium and nickel contents also) in Type 304/304L SS (UNS S30400/S30403) determines its resistance to sensitization [1-2, 4-5, 15, 21]. Welding of austenitic SS is the main fabrication process during which the heat affected zone (HAZ) is exposed to a temperature range in which chromium carbide formation takes place and sensitization occurs [1-6, 15, 20]. Such sensitized SS with “ditch” (at least one grain having complete encirclement with attacked chromium carbide/chromium depletion regions) microstructure may be prone to IGC in boiling HNO_3 [16-17, 22]. There are mechanisms other than carbide precipitation that make SS prone to IGC. In highly oxidizing HNO_3 , segregation of silicon or phosphorus at the grain boundaries is known to cause IGC in non-sensitized SS [1, 5, 23- 28]. Similarly, “End Grain Corrosion” is a form of corrosion that affects even non-sensitized austenitic SS components

that are in tubular or bar forms [23-25, 29-30]. The understanding developed over the last four decades on sensitization and IGC due to segregation of certain elements (for example Cr and Si) in oxidizing environments had lead to the development of a nitric acid grade (NAG) variety of Type 304L SS. Though a sub-set of Type 304L SS, Type 304L NAG has a tighter control over alloying elements, especially Cr, Ni and C as also over Si and P [23-25, 29-31]. Because of this tight chemical composition specification, Type 304L NAG does not get sensitized during welding. These NAG steels also have lower rates of uniform corrosion [25, 29].

All the austenitic SS in HNO₃ medium exhibit passive to transpassive transition behavior. The SS develop a passive film (chromium rich oxide) and current densities in the domain of passive potentials are very low (μAcm^{-2}). At sufficiently high potentials, many passive metals and alloys, including SS, enter the transpassive state in which the current density begins to increase exponentially with the applied voltage. This behavior in the transpassive potential regime is similar to that exhibited during active dissolution. At still higher potentials, oxygen evolution occurs and may mask the transpassive behavior. The main reason for increased current density at the onset of transpassivity for SS is conversion of Cr³⁺ to Cr⁶⁺ in the passive film itself. As potentials increase further in the transpassive potential regime, faster dissolution of chromium occurs through the oxide film. It has been shown clearly that thickness of oxide film increases over SS in the transpassive regime of potentials [32-34]. It has been shown that the form of corrosion of austenitic SS in transpassive potentials, even in non-sensitized condition, is IGC [35]. Increase in concentration and/or operating temperature of the HNO₃ coupled with increase in concentration of oxidising ions in the HNO₃ increases the operating potential [35-39]. Therefore, for a given SS (even in a non- sensitized condition), there is a definite limit on

concentration of HNO₃, temperature of HNO₃ and concentration of oxidizing ions in the HNO₃ that can be allowed to avoid heavy IGC [21, 35-38].

In an earlier study [35], it was shown that for Type 304L NAG, there was a threshold potential below which only uniform corrosion occurs and above which IGC occurs in near boiling 6M HNO₃. This was established by applying a given potential on a specimen of SS that was immersed in near boiling 6M HNO₃ for a period of 48 h. The data were validated by experiments in which specimen were exposed for 48 h in near boiling 6M HNO₃ in which different concentrations of oxidizing ions (1.5 g L⁻¹ Ce⁴⁺ + 1.5 g L⁻¹ V⁵⁺, 0.64 g L⁻¹ Ce⁴⁺ + 0.95 g L⁻¹V⁵⁺ and 0.95 g L⁻¹ V⁵⁺ + 0.171 g L⁻¹Cr⁶⁺) were added to attain different potentials. This study had also shown that a chemical potentiostat and an electronic potentiostat gave the same rates of corrosion. These experiments were done on Type 304L NAG that was in a lightly sensitized condition (“dual” microstructure) after a heat treatment at 675 °C for 1 h. This new methodology was proposed to be used for online measurement of corrosion in operating plants and for predicting corrosion rates of SS in HNO₃ service [35].

1.2 Objectives and Scope

The above discussion suggests that there is enough scope to investigate corrosion behavior of various austenitic SS alloys. Thus the broad objective of the present work is to study corrosion behavior of austenitic SS alloys in HNO₃ environment. Although the scope is large for this thesis work a few specific objectives were chosen and listed below:

1. Effect of microstructure on corrosion behavior of austenitic SS in transpassive potential regime.
2. Effect of alloy composition on corrosion behavior of austenitic SS in transpassive potential regime.
3. Effect of HNO₃ concentration and temperature on corrosion behavior of austenitic SS in transpassive potential regime.

4. Effect of grain size and grain boundary nature on corrosion behavior of austenitic SS in transpassive potential regime.

5. Understanding mechanism of “End Grain Corrosion” in Type 304L NAG.

In view of the above the problem and framework of thesis were defined as given in section 1.3 and 1.4 respectively.

1.3 Problem Definition

Present work aimed to establish potential-corrosion rate relationship of austenitic SS for various materials and process parameters. Material parameters include alloy chemical composition, microstructure, grain size and grain boundary character. Process parameters include acid concentration and temperature. Such a potential-corrosion rate relationship for a given system can be used as an online technique to predict corrosion rate. A “safe/limiting” electrochemical potential that develops in process fluid would be established that would keep the structural material safe from attack in plants. As mentioned in the previous section that high potential attained due to the presence of oxidizing ions/ high acid concentration/ high process temperature can lead to severe corrosion in structural material of plants, limiting potential can be used as a “control parameter” during plant operation. Present work also aimed to investigate mechanism of “End Grain Corrosion” of Type 304L NAG in HNO_3 medium containing oxidizing ions.

1.4 Framework of the Thesis

The thesis is divided into nine chapters. The first chapter is devoted to background of the present investigation, the problem definition, specific objectives, scope and framework of the thesis. A review of literature relevant to present investigation is given in chapter 2. Chapter 2 begins with an introduction to spent nuclear fuel reprocessing and problems encountered in reprocessing. The chapter focuses on material selection and their implementation for successful reprocessing in a plant. The subsequent section of chapter 2

gives an overview of austenitic SS. A separate section of chapter 2 has been devoted to corrosion problems associated with spent fuel reprocessing plants. General electrochemical behavior of austenitic SS in HNO₃ media is covered in another section. The last section of chapter 2 describes scope of the present investigation. Chapter 3 describes in detail materials, experimental tools and techniques used for the present investigation. The results and discussion part of the thesis is covered in chapters 4-7. The influence of alloy composition and microstructure on corrosion behavior of austenitic SS is described in chapter 4. Chapter 5 describes how grain size and grain boundary engineering could influence corrosion behavior of type 304L in HNO₃ medium at transpassive potentials. Chapter 6 describes influence of process parameters like acid concentration and temperature on corrosion behavior of SS in HNO₃ at transpassive potential regime. Chapter 7 is devoted to “End Grain Corrosion” of Type 304L NAG in highly oxidizing HNO₃. This chapter mainly incorporated whether intergranular segregation of P or S influences “End Grain Corrosion”. This chapter also describes influence of Cr⁶⁺ ion concentration present in HNO₃ solution on “End Grain Corrosion”. Chapter 8 describes the overall conclusions obtained from the present investigations. Scope for future work is described in chapter 9.

CHAPTER 2

LITERATURE REVIEW

The material requirement for spent nuclear fuel reprocessing, various associated problems and challenges in spent nuclear fuel reprocessing are briefly explained in this chapter. Out of several problems material selection, and their implementation for successful reprocessing plant application are described in detail. The chapter gives a brief introduction to the austenitic SS alloys with respect to their formation using Fe-C, Fe-Cr and Fe-Cr-Ni phase diagram and passivation properties. Apart from this, the chapter describes the process environment of nuclear fuel reprocessing, and the various corrosion problems of austenitic SS in the oxidizing environment of HNO_3 . The last section of this chapter briefly describes need for the present study.

2.1 Spent Nuclear Fuel Reprocessing

Nuclear fuel cycle is being practiced either in closed or open cycle option. In the closed fuel cycle options an important step is reprocessing of spent nuclear fuel and India's option is closed fuel cycle. Reprocessing involves a chemical separation process with the fractionation of useful radionuclides, and safe waste management [40, 41]. Over the last five decades the spent nuclear fuel reprocessing is being carried out with a prime objective to recover the plutonium, and unused uranium for resource conservation. The recovered materials can effectively close the fuel cycle and improve the energy security. Open cycle has the advantage that it avoids the difficulties of reprocessing. However it can only extract about half a percent of energy content of the uranium. The recovered material can directly be enriched reducing the demand for mining and milling of new uranium. The initiatives for nuclear fuel reprocessing in India started in 1964 as the available sources of uranium are

inadequate to meet the long-term nuclear power programme [41]. At present India is having three nuclear fuel reprocessing plants, one at Trombay of reprocessing capacity 60 tons per year, the second and third plants located at Tarapur and Kalpakkam, respectively with capacity of 100 tons of power reactor fuel per year. PUREX (Plutonium Uranium Reduction Extraction) is the main separation process in India for reprocessing of spent nuclear fuel. Thus reprocessing programme initiated with design, construction and commissioning of demonstration plant at Trombay using PUREX as the aqueous reprocessing process. The flow sheet of a typical PUREX process is shown in Fig.2.1 [42].

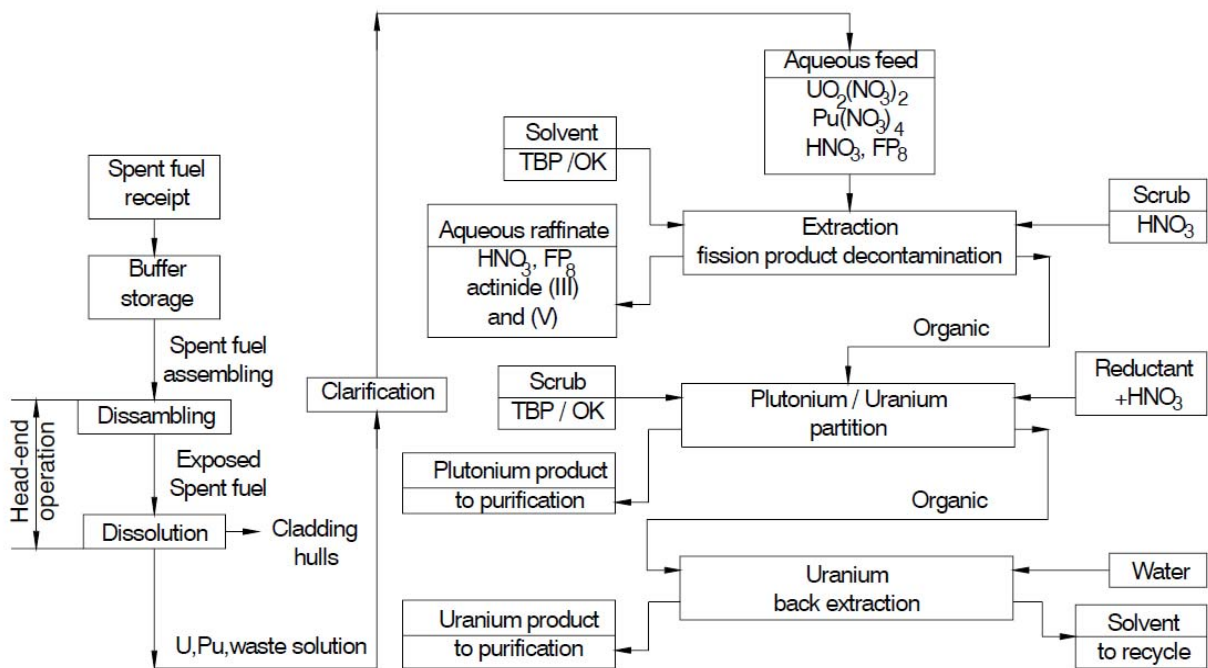


Fig.2.1 Purex process flow sheet [42].

2.1.1 Problems Encountered In Fuel Reprocessing Plants

Nuclear fuel reprocessing plant faces the same problems as associated with any other process industry. Moreover, the problems encountered in fuel reprocessing plant are more complex due to radiological considerations. Besides the presence of radioactivity, one has to deal with contaminated equipments. The major problems associated with reprocessing are safety concerns, problems in selection of materials of construction, cost of fuel reprocessing,

and radioactive disposal. Out of several critical issues, material challenges are of utmost importance for safe operation of fuel reprocessing plant as well as determining the overall plant life [43]. The selection criteria of materials of construction for nuclear fuel reprocessing plant is a complicated procedure involving various parameters such as their availability, cost, mechanical properties and corrosion resistance. The demanding criteria are the result of the presence of radiation and corrosive chemicals. Moreover, materials operating in these plants are difficult to access for maintenance. In these difficult conditions if the materials chosen perform for a prolonged periods then it would be ideal. Thus, development of high corrosion resistant materials with prolonged integrity is considered one of the challenging areas for ensuring the safety, and economical operation of commercial reprocessing plants.

2.1.2 Material Selection for Nuclear Spent Fuel Reprocessing

Plants

Nuclear fuel reprocessing plant uses a variety of materials in different environments depending upon the circumstances prevailing, such as presence of radioactivity, corrosive chemicals, high temperature and areas where maintenance is restricted. Thus material selection is dictated by requirement of avoidance to radiation damage, their corrosion resistance, ability to decontaminate, availability and cost effectiveness. Hence, selection of the proper material as well as effective shielding design are the most important in order to ensure adequate attenuation of the radiation. Corrosion is one of the most challenging issues, and a wide spread problem in spent nuclear fuel reprocessing plants. Corrosion problems arise at various stages of fuel reprocessing such as during dissolution of spent fuel, due to dissolver off gases, during solvent extraction, and during storage of waste generated from reprocessed spent fuel. Out of several materials, austenitic SS (300 series), titanium and its variants, and zirconium are used for construction of structural components of the spent nuclear fuel reprocessing plant which is summarized below.

I. Austenitic SS

Very low carbon austenitic SS alloys (Type AISI 304 L, 316 L and 310 Nb) are used for the construction of majority of the equipments [43, 36]. The corrosion resistance of austenitic SS depends on the concentration of HNO_3 . For lower concentration ($< 50\%$) corrosion susceptibility is determined by chromium content in the alloy, and for higher concentration containing Cr^{6+} ions it is determined by impurity elements in the alloy. Mainly, AISI Type 304L SS finds large scale application because of good passivity, corrosion resistance, and appropriate practical aspects such as working, welding and cost competitiveness. Despite many beneficial properties, Type 304L fails in the oxidizing environment of HNO_3 leading to intergranular corrosion, “End Grain Corrosion”, transpassivity etc [44]. To overcome these problems different grades of austenitic SS alloys have been evolved over the years. High level of silicon prevents attack in nonsensitized SS alloys by HNO_3 solutions containing the hexavalent chromium ions [5]. The addition of titanium and niobium to these alloys further improves this property. However due to high silicon and low carbon content, these materials tend to form crack in the welded region. Similarly, special NAG austenitic SS alloys such as URANS-16 and URANS-65 are designed with sharp control of carbon, silicon, sulphur and phosphorus. Because of high chromium content and stringent control of impurities, NAG SS performs satisfactorily up to 65 % concentration in boiling condition. Nevertheless, these materials fail in HNO_3 solution containing hexavalent chromium (Cr^{6+}) at elevated temperature due to transpassivity [45]. Thus, use of these materials in these extreme conditions is restricted. Moreover, large scale use is also not possible due to extra cost in the manufacturing process because of controlling the impurity level. Detailed discussion on property and uses of austenitic SS alloys is given in section 2.2.3.

II. Zirconium

Zirconium is chosen for the construction of the most of the critical equipments in term of corrosion, such as fuel dissolvers and HNO₃ recovery concentrators [36]. Choice of zirconium is due to its high corrosion resistance as compared to titanium and austenitic SS with or without the presence of oxidizing species. As compared to austenitic SS, zirconium does not undergo IGC, and compared to titanium it does not suffer from vapor and condensate phase corrosion problems in boiling HNO₃. Comparative analysis on the corrosion resistance of 20 Cr-20 Ni austenitic SS, Ti, and Zr in 17-70 % HNO₃ in boiling condition in the presence of hexavalent chromium (Cr⁶⁺) showed high corrosion resistance for zirconium compared to others [46]. The high corrosion resistance is attributed to natural formation of stable and self healing zirconium oxide (ZrO₂) film on the surface which protects the material from corrosive environment [43]. Moreover, it does not form non-adherent oxide with poor corrosion resistance under condensing condition as seen in the case of titanium. Recent corrosion study on zirconium, and its welds showed superior corrosion resistance as compared to other candidate materials like Ti, Ti-5% Ta, and Ti- 5% Ta-1.8 % Nb [47]. No corrosion attack was observed in liquid, vapor and condensate zones of boiling 11.5 M HNO₃. Due to high corrosion resistance, inspection, and maintenance are also a less concern for zirconium. Even though, zirconium shows outstanding corrosion resistance in HNO₃ medium, certain factors require thorough investigation, such as fluoride content in the process medium and stress corrosion cracking. Zirconium is not recommended for handling fluoride-containing acids, unless the fluoride ions are complexed [48]. Stress corrosion cracking (SCC), can occur in Zr exposed to hot boiling HNO₃ (> 70 %) [46]. Particularly, heat affected zones of zirconium welds are considered to be sensitive to SCC. However, unlike austenitic SS alloys, large scale application of zirconium is restricted to demanding conditions only, because it is seven times expensive and fabrication cost is five times more compared to

conventional 304L austenitic SS. The main limitations in using zirconium and its alloys for HNO₃ service include [43]: (i) it exhibits passive-transpassive transition unlike titanium, (ii) it exhibits high corrosion potential; as concentration increases corrosion potential and transpassive potential move closer to cause higher corrosion, (iii) need for Zr sponge addition for inhibiting corrosion of Zr vessels in fluoride containing environments, and (iv) the possibility of undergoing stress corrosion cracking, particularly in the heat affected zones (HAZ) of welds.

III. Titanium

Titanium is a unique material, as strong as SS with less than 60 % of its density, and possesses excellent corrosion resistance. Titanium is used in critical components such as spent nuclear fuel dissolvers for handling hot concentrated HNO₃ where austenitic SS experiences intergranular corrosion. Higher resistance of titanium to corrosion is due to the formation of titanium dioxide (TiO₂) film on the surface due to formation of Ti⁴⁺ ions [43]. However, the composition of oxide film depends upon the film formation conditions such as electrolyte composition, hydro-dynamic flow, and temperature. The oxide film formed on titanium is more protective than that of austenitic SS, and often performs better in oxidizing environment of HNO₃. In boiling condition titanium corrosion resistance depends on HNO₃ purity, and higher the metallic ion content in the acid, the better titanium performs. This is in contrast to austenitic SS which is often adversely affected by the acid contaminants. This is because, titanium corrosion product (Ti⁴⁺) is highly inhibitive, and titanium exhibits superb performance in recycled HNO₃ streams. Despite many advantages, the use of titanium in spent nuclear fuel reprocessing plant is limited. One of the factors to this is the high cost relative to austenitic SS. Moreover, even if titanium is having excellent corrosion resistance, use of it is not the solution for all the corrosion problems. Failures in acid condensers and evaporators have been observed in the spent nuclear fuel reprocessing plant [43]. Under these

vapor and condensate conditions semi-protective oxide films form on the surface which do not fully retard the oxidizing action of HNO_3 . The presence of iron greater than 0.05 % in titanium enhances the corrosion rate due to formation, and segregation of iron rich ilmenite (FeTiO_3) intermetallic particles. In such situations advanced alloys such as Ti-5 % Ta-1.8 % Nb were recommended. These are titanium alloyed with more noble metals like tantalum and niobium which have similar size to that of titanium. The oxide film formed on such alloys shows low solubility and high stability in HNO_3 .

2.2 An Overview of SS

SS constitute a group of high-alloy steels based on Fe-Cr, Fe-Cr-C, and Fe-Cr-Ni systems. These steels must contain a minimum of 11 wt% chromium for becoming stainless [5]. This level of chromium allows formation of a passive surface oxide that prevents the formation of rust in unpolluted atmosphere [5]. Increasing Cr content to 17 to 20 %, as typical of the austenitic SS alloys or to 26 to 29 %, as possible in newer ferritic SS alloys, greatly increases the stability of the passive film [3]. The corrosion resistance is developed due to formation of surface film (mainly Cr_2O_3) that is of 25 -50 Å thick when formed in air at room temperature [49, 50]. It should also be pointed out that many steels containing 12 wt% Cr, or even those with more Cr, will, in fact, exhibit rust when exposed to ambient conditions. This is because some of the Cr is tied up as carbides or other compounds, reducing the matrix Cr composition below the level that will support a continuous protective oxide film. SS alloys also have good resistance to oxidation, even at high temperatures, and they are often referred to as heat-resisting alloys. Resistance to elevated temperature primarily depends upon chromium concentration, and some high chromium alloys (25 to 30 wt %) can be used at temperatures as high as 1000 °C. The same resistance to carburization in SS alloys can be obtained by using higher concentration of the nickel (35%) with moderate concentration of chromium (16 %) [51]. The most widely used stainless grades are the

austenitic with 74% production of total world SS production. Specifically AISI 304 and 304L are most popular grade of austenitic SS. The next most widely used grades are the ferritic steels such as AISI 410, followed by the molybdenum-alloyed austenitic steels AISI 316/316L [51]. Since the structure has a decisive effect on properties, SS alloys have traditionally been divided into various categories depending on their structure at room temperature. This gives a rough division in terms of both composition and properties.

2.2.1 Types of SS

The way to relate metallurgical structure to composition is by means of Schaeffler diagram [5, 52]. The Schaeffler diagram is shown in Fig-2.2. This diagram indicates structure obtained for steel cooled rapidly from 1050 °C to room temperature. As can be seen, the diagram is divided with four major areas according to structure: martensite, austenite, ferrite and austenite plus ferrite. These four structures provide a convenient basis for classification. All other elements behave as either chromium or nickel in affecting structure, and these have to be taken into account when predicting structure for a given composition. The degree of effect relative to chromium or nickel varies and equivalence factors have been proposed for all the commonly used elements. The diagram is based on the fact that the alloying elements can be divided into ferrite stabilizers and austenite-stabilizers. This means that they favor the formation of either ferrite or austenite in the structure. If the austenite-stabilizers ability to promote the formation of austenite is related to that for nickel, and the ferrite-stabilizers likewise compared to chromium, it becomes possible to calculate the total ferrite and austenite stabilizing effect of the alloying elements in the steel. The nickel and chromium equivalents, which form the two axes of the Schaeffler diagram, can be calculated using the following equation [5].

$$\text{Nickel equivalent} = \% \text{ Ni} + \% \text{ Co} + 30 (\% \text{ C}) + 25 (\% \text{ N}) + 0.5 (\% \text{ Mn}) + 0.3 (\% \text{ Cu})$$

Chromium equivalent = % Cr + 2 (% Si) + 1.5 (% Mo) + 5 (% V) + 5.5 (% Al) + 1.75(% Nb)
+ 1.5 (% Ti) + 0.75 (% W)

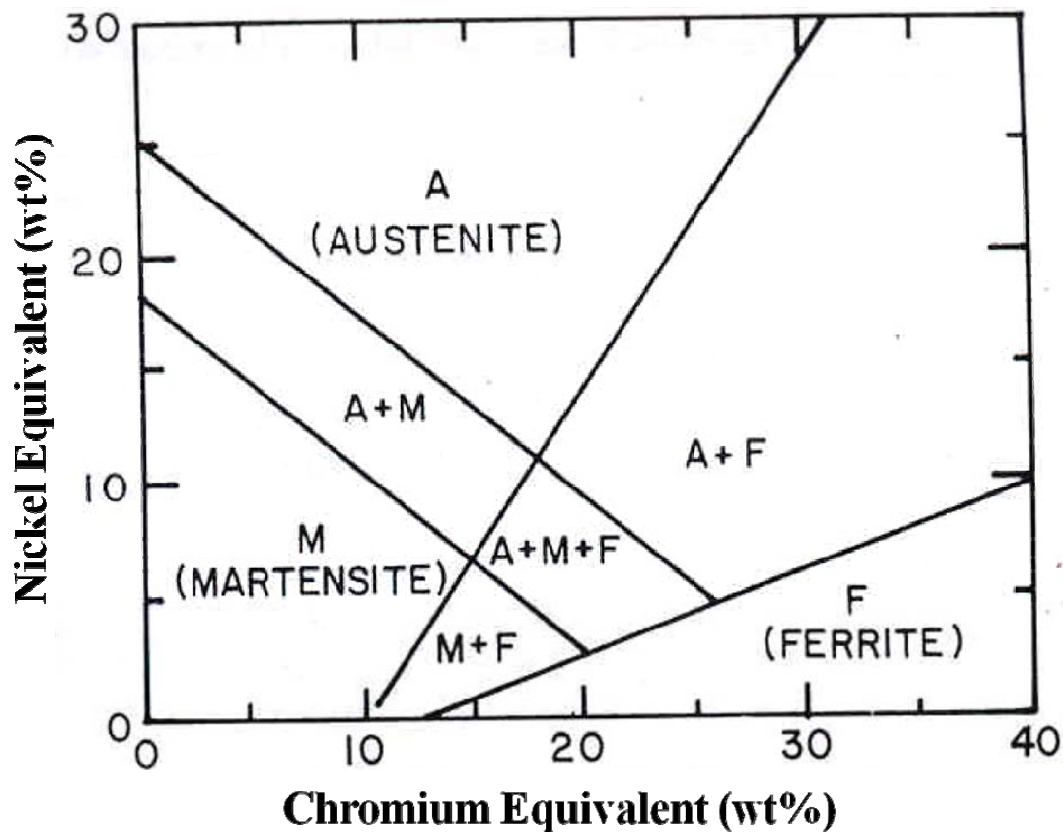


Fig. 2.2 Schaeffler diagram [5].

The family of austenitic and other SS alloys formed with addition of alloying elements starting from Fe- 19Cr-10Ni system is shown in Fig. 2.3[5].

2.2.2 Phase Equilibrium Diagram and SS

A study of the constitution and structure of all the steels starts from Fe-C equilibrium phase diagram. A portion of the Fe-C phase diagram is presented in Fig 2.4[53]. Pure iron upon heating experiences two changes in crystal structure before it melts. At room temperature the stable form called as ferrite (α -iron), has body centered cubic (bcc) crystal structure. Ferrite experiences a polymorphic phase transformation to austenite (γ -iron) at 912 °C which has a face centered cubic (fcc) crystal structure. The austenite phase persists up to 1394 °C, and at this temperature the austenite reverts back to the bcc phase known as δ -

ferrite. Carbon as an interstitial element forms solid solution with both α and δ ferrite, and also with γ -austenite as indicated by α , δ and γ phase fields in Fig. 2.4. Moreover, the much larger phase field of γ -iron compared to that of α -iron reflects the greater solubility of carbon in γ -iron, with a maximum value of 2.08 wt % at 1147 °C. Austenite is characterized as non-magnetic, high ductility, rapid work hardening rates, and excellent toughness. However, the iron-carbon equilibrium diagram as shown in Fig. 2.4 is modified by the addition of alloying elements such as chromium (Cr), Nickel (Ni), and other minor alloying elements, resulting in poly-component systems. Fig. 2.5 shows the Fe-Cr equilibrium phase diagram [5].

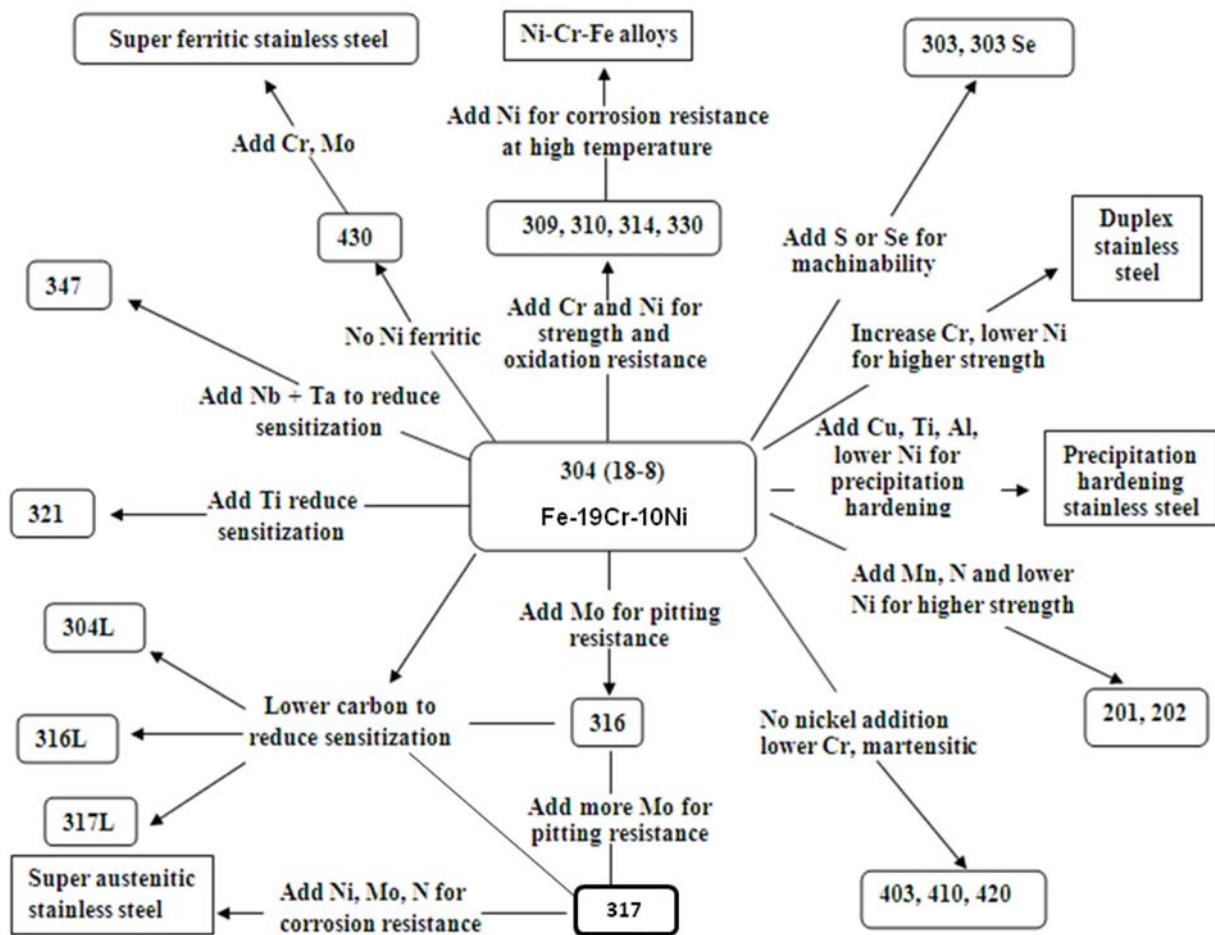


Fig. 2.3 Composition and property linkages in the SS family of alloys [5].

Chromium in excess of 12 wt % by weight is required to impart stainless characteristics of iron alloys. Thus, all SS alloys contain large amounts of chromium from 12

% to a maximum of 25 %. Chromium as a major alloying element stabilizes the body-centred cubic (bcc) phase of iron. Therefore with increasing chromium content the low temperature and high temperature α and δ ferrite fields expand. As the ferrite field expands the austenite field contracts, and produces what is often called as the gamma (γ) loop. However, the addition of carbon to the Fe-Cr binary alloy extends the gamma loop to higher chromium content, and also widens the (alpha plus gamma) phase field, and above 0.40 wt % C, the steel can be made fully austenitic if cooled directly from the gamma loop region. Moreover, nickel with a face-centred-cubic structure favours the formation of fcc austenite solid solution, and the stability range of austenite phase expands at the expense of bcc α -ferrite phase. The Fe-Cr-Ni ternary phase diagram is shown in Fig. 2.6 [52].

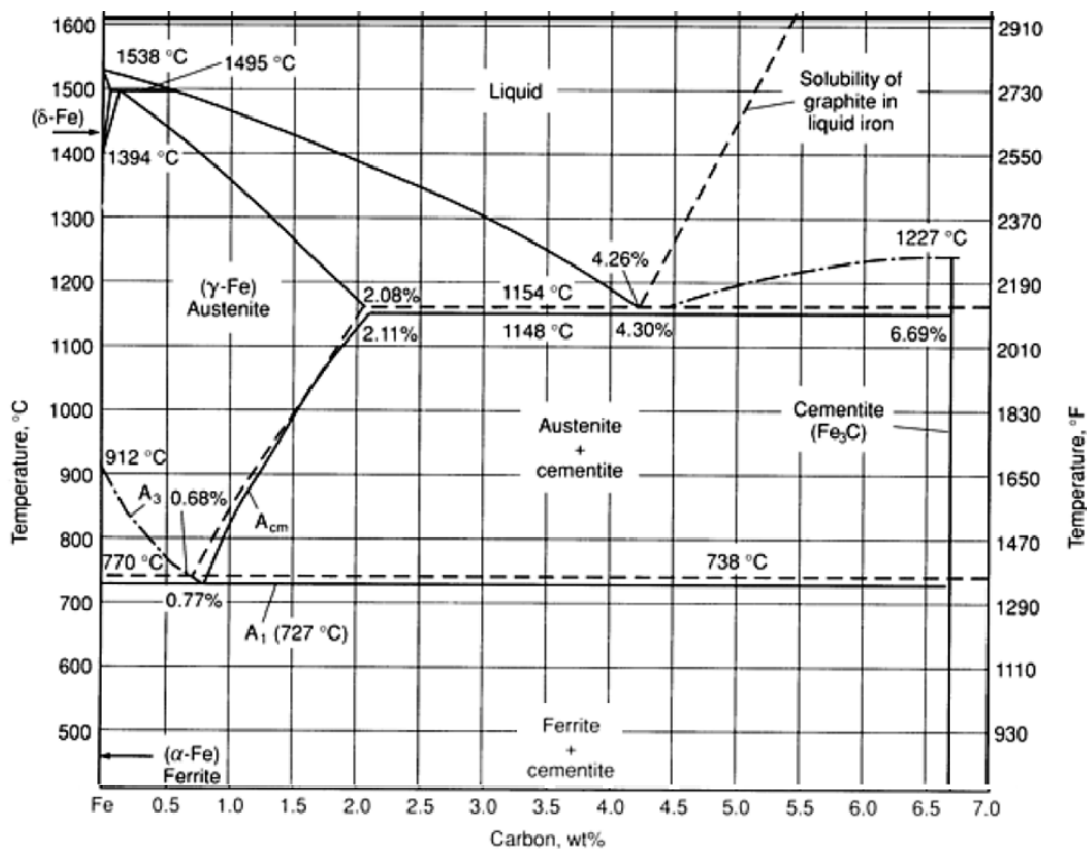


Fig. 2.4 Fe-C equilibrium phase diagram [54]

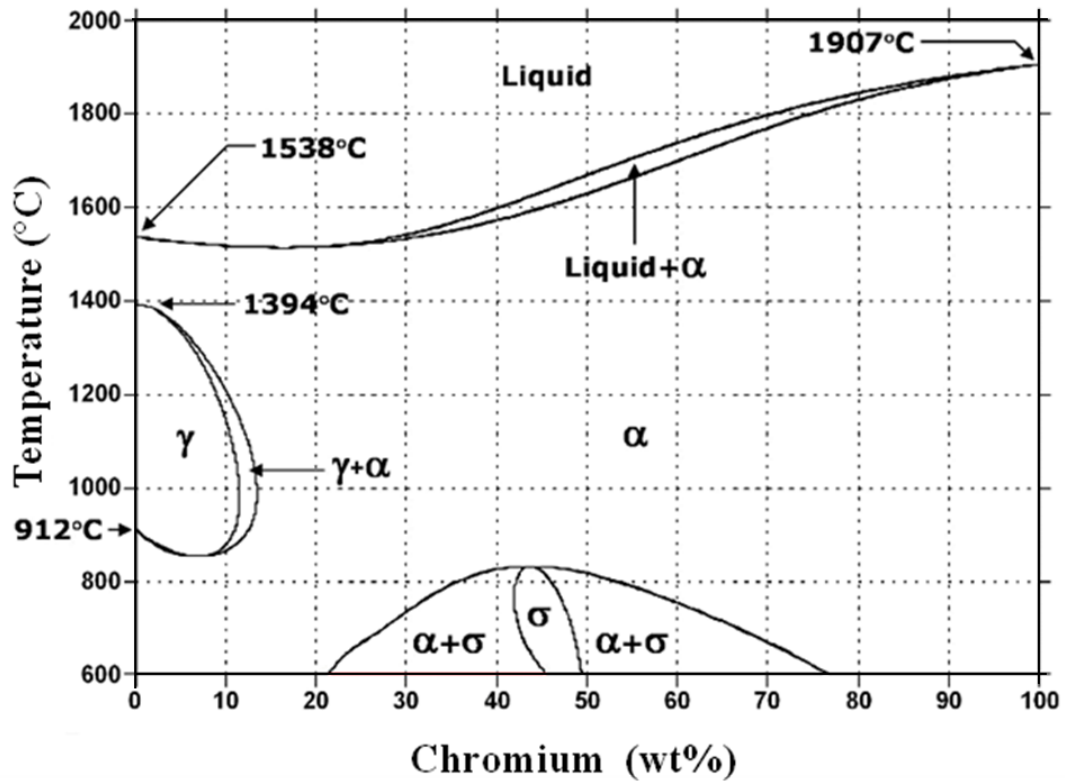


Fig. 2.5 Fe-Cr equilibrium phase diagram [5]

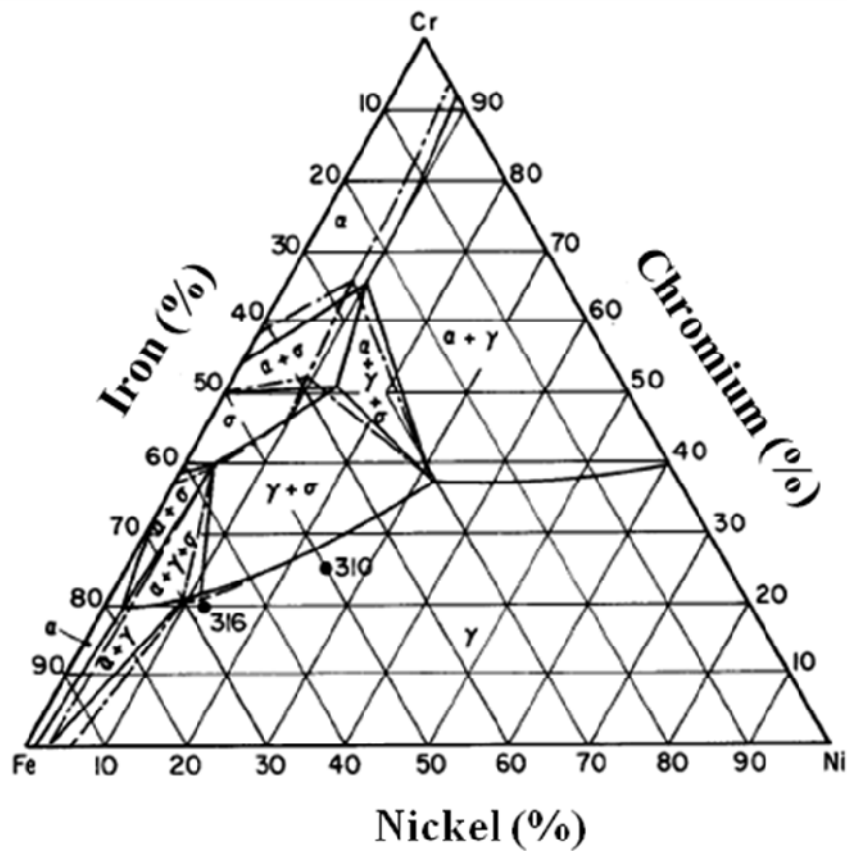


Fig. 2.6 Fe-Cr-Ni ternary phase diagram [52]

2.2.3 Austenitic SS

Austenitic SS alloys containing chromium and nickel are given a 300 Series classification and austenitic steels containing chromium, nickel and manganese are given a 200 series classification. It should be noted, however, that some austenitic SS alloys do not have these 200 and 300 series designations. The steels in this austenitic group have many compositions and properties, but they have many characteristics in common. They can be hardened by cold working but not by heat treatment. All are essentially nonmagnetic in the annealed condition, but some may become slightly magnetic by cold working. In the annealed condition they have excellent formability. The various grades of austenitic steels have excellent corrosion resistance in many environments, resisting attack by the atmosphere and by many industrial gases and chemicals. They have a resistance to scaling at temperatures as high as 2000 °F (1095°C). Many of these steels have good strength at high temperatures which accounts for their wide use at elevated temperatures. They are also among the primary materials selected for the use at extremely low temperatures since they do not become brittle as compared with other types of steel. All austenitic SS alloys are sensitive, to some degree, to chloride stress corrosion cracking and fully austenitic types may be sensitive to solidification cracking. Some types are susceptible to carbide precipitation or intermetallic phase under adverse conditions of fabrication and use. Type 304 SS is the most widely used steel of the austenitic group. It has a nominal composition of 18% chromium and 8 % nickel. The categories, martensitic and martensitic-austenitic SS alloys are hardenable, which means that it is possible to modify their properties via heat treatment in the same way as for hardenable carbon steels. The third category, the precipitation hardening steels, may also be hardened by heat treatment. The procedures used for these steels are special heat treatment or thermo-mechanical treatment sequences including a final precipitation hardening and ageing step. The steel categories, ferritic, ferritic-austenitic and austenitic are not

hardenable, but are basically used in the as received condition. The ferritic-austenitic SS alloys are often referred to as duplex SS alloys. It may be noted that there is only one category of SS that is non-magnetic: the austenitic steels. All the others are magnetic.

Austenitic SS in HNO₃ medium

It is mentioned in section 2.1 that PUREX is the main separation process in India for reprocessing of spent nuclear fuel. Reprocessing plants involve equipment/vessels such as fuel dissolvers, evaporators for various purposes and high active raffinate waste storage tanks. HNO₃ is the main process medium in the spent fuel reprocessing plants. The acid concentration may vary from dilute (1–4 N) to concentrated (10–14 N). The temperature of acid vary from room temperature (solvent extraction) to intermediate (warm, raffinate waste storage tanks) to boiling temperature (dissolver, evaporator). The presence of redox species (Pu⁶⁺ and Cr⁶⁺ in dissolvers, partitioners etc) can further aggravate environmental condition from corrosion point of view. Among austenitic Type 304L is extensively used for fabrication of vessels, tanks, piping and equipment in reprocessing plants wherein the concentration of the acid is below 8 N and temperature of operation is below 353 K [43]. The formation of a stable, adherent and self-healing passive chromium oxide (Cr₂O₃) film is responsible for good corrosion resistance of the material under the operating conditions employed in the reprocessing plants. Several incidences of failures of components made of Type 304L have been reported in spent nuclear fuel reprocessing plants when they were used in HNO₃ medium beyond 8 N concentration, and temperatures beyond 353 K [43]. Type 304L may contain significant quantities of other elements (Si-1%, Mn-2%, S-0.02%, P-0.04%, B-0.005, etc.) [43]. These elements segregate to the grain boundaries after solution annealing and heat treatment and this results in the formation of weak passive films at the grain boundaries. Weak passive films at the grain boundaries can cause IGC. When the concentration of the acid increases beyond 8N or the temperature of the acid increases beyond 353 K, the

normally protective Cr_2O_3 passive film gets oxidized to CrO_3 . Cr^{3+} ions start converting into soluble Cr^{6+} ions. This leads to excessive dissolution of the surface and higher corrosion rates of SS in boiling HNO_3 service. Type 304L is evaluated for the corrosion resistance as per practice C, A262, ASTM (HUEY test) in boiling concentrated HNO_3 for 240 h as recommended by United States Nuclear Regulatory Commission (USNRC) [43]. The alloy is permitted for application in HNO_3 service if it exhibits a corrosion rate of 0.45 mmy^{-1} (18 mil mpy) and below after sensitization at 948 K for 1 h. Even for nonactive and utility areas of reprocessing plants, an alloy with a maximum corrosion rate of 0.6 Mmy^{-1} (24 mpy) is acceptable. However, for any critical application in HNO_3 service the alloy must exhibit 0.45 mmy^{-1} (18 mpy) and below in the sensitized condition, which can occur during welding and heat treatment. Type 304L, and its improved varieties with extra low-carbon (Type 304ELC), with Nb (Type 347), with Ti (Type 321), or Type 310L and its equivalent with Nb stabilization and high Cr content, have been used in several reprocessing plants in the world for many critical applications. However, qualification of welding methods and carrying out the boiling HNO_3 (Huey test) on qualified specimens is essential to avoid failures. The challenge in materials development with respect to the manufacturing of austenitic SS lies in the elimination of the corrosion problems and finding improved varieties with controlled alloying elements and microstructure exhibiting higher corrosion resistance. The efforts are directed towards developing alloys which would show corrosion rates less than 18 mpy (0.45 mmy^{-1}).

Evolution of nitric acid grade austenitic SS

Nitric acid grade (NAG) austenitic SS alloys are the alloys inherently developed with (i) controlled chemical composition, (ii) modified microstructures leading to elimination of weaker sites for passive film break down and dissolution, and (iii) enhanced strength against transpassive dissolution. Several types of NAG alloys having compositions similar to Types

304L, 310L, and several new proprietary alloys have been developed worldwide [5]. NAG alloys show significant decrease in the corrosion rates compared to conventional Type 304L in boiling HNO_3 (Huey) test [43].

Increasing chromium content increases the stability and strength of passive film. However, in practice chromium levels below 30% are used. The reason for this is that increase in chromium contents beyond this level affects the stability of the austenite phase. Nickel is another element which improves the strength of passive films through stabilizing austenite. Nickel is kept within 15% as increases in nickel content increases the cost of the alloy. Molybdenum is completely removed from the alloy due to two important reasons namely, (i) increasing ferrite formation, and (ii) submicroscopic sigma precipitation during multipass welding of components thicker than 6 mm. Sigma phase can preferentially dissolve in hot oxidizing HNO_3 leading to excessive corrosion rates. Manganese, silicon, copper and aluminium are normally present as impurities in the steel making. Manganese content is controlled in order to reduce formation of MnS inclusions. These inclusions are harmful as they are preferentially attacked in HNO_3 service. In order to achieve lesser inclusions content, Mn content less than 1% is recommended. Copper and aluminium are also reduced to low levels as they enhance selective corrosion attack in HNO_3 service. Silicon has dual role with respect to corrosion of Type 304L in HNO_3 . It has been reported [5] that when Si content is less than 0.2%, an excellent corrosion resistance is achieved while enhanced performance is also achieved with silicon content beyond 1.6%. However, between 0.4 and 1% Si content, excessive IGC has been observed. Hence, two grades of NAG alloys have evolved, one with Si less than 0.2%, and the other with 4% Si. The impurity elements like S, P and B significantly affect the corrosion resistance of Type 304L in HNO_3 [43]. Sulphur forms MnS inclusions which degrade the alloy with selective dissolution.

One of the major problems in using bars and cut sections including tapered machined parts of Type 304L is “End Grain Corrosion” or tunnel corrosion [43]. The longitudinally aligned MnS inclusions are vertically cut and such cut faces expose MnS inclusions for selective attack leading to the formation of ‘corrosion tunnels’ or a puff candy appearance due to severe corrosion. The solubility of sulphur in the alloy is about 10 ppm. Decreasing the sulphur content below 50 ppm needs advanced steel making practices like electro slag remelting, electron beam melting, and combined double arc melting followed by vacuum induction melting (VIM), or argon oxygen decarburisation (AOD) or vacuum oxygen decarburisation (VOD) [5].

Another method to eliminate the problem of inclusion attack is ‘shape controlling’ of inclusions by either adding rare earth elements or Ca, or Ti or globularising the inclusions in order to have low surface to volume ratio through special fabrication processes [43]. In comparison to longitudinal stringers of MnS, the globular MnS inclusions pose less severe problems.

Phosphorus can segregate at the grain boundaries and interfaces to as high as 10^5 times of original concentration [5]. Passive films formed at such boundaries are weak. Phosphorous is controlled within 200 ppm in NAG grade alloys and both S and P together within 250 ppm to ensure good corrosion resistance. Boron is traditionally maintained in austenitic SS within 30 ppm to ensure adequate hot working and prevent cracking/fissuring during hot working [43]. However, it forms dichromium boride (Cr_2B) along grain boundaries even during water quenching after solution annealing. This results in significant deterioration in corrosion resistance of the conventional Type 304L and hence for NAG alloys, boron is kept within 10 ppm.

In HNO_3 environment, carbon content significantly affects the corrosion rate of SS depending on the heat treatment conditions. In a typical Type 304, the carbon content is kept

within a range of 0.06–0.08%. During welding or heat treatment whenever the alloy is slowly heated or cooled through the temperature regime 723–1073 K, carbon enhances the formation of chromium rich $M_{23}C_6$ carbide at grain boundaries. This leads to selective depletion of Cr in a narrow region adjacent to the grain boundary $M_{23}C_6$ carbides, thus promoting excessive corrosion along the grain boundaries due to the following reasons [43]: (i) galvanic cell formation between $Cr_{23}C_6$ and Cr-depleted zone, (ii) less Cr at depleted zone favouring more corrosion, and (iii) strain build up at carbide/matrix interface. Reduction of carbon below 0.03 wt% is an attractive proposal to overcome the selective IGC along the sensitized zones, and thus Type 304L alloys have been developed extensively for most of the components in reprocessing plants. As was described earlier, Type 304L has limitations when HNO_3 concentration is 8N and above, and the temperature is beyond 353 K. With the advancements taking place in steel making, ultra low-carbon alloys with carbon levels less than 0.015% are being developed for HNO_3 .

2.2.3.1 Passivity of Austenitic SS

The useful corrosion resistance of austenitic SS is due to the fact that it exhibits passivity in a wide range of environments. The passive film is thin, adherent, self-healing, and tenacious having thickness around 10-100 Å. The structure composition of this ultrathin passive film is a vast and complex subject, and depends upon the alloy composition, and also on the nature of the environment they are exposed to. The passivation of austenitic SS primarily dependent upon chromium content. In addition, the contribution of austenite stabilizers such as Ni, N and Mn also strengthen the passive film property. Apart from this, molybdenum also significantly contributes to the passivity in the corrosive environment containing aggressive ions. However, it is found that passive film formed on austenitic SS does not contain all the alloying elements that are added to stabilize the austenite phase [54]. The thickness, composition, and structure of passive film in austenitic SS are highly

dependent on the chromium content of the alloy as well as their formation potential. In austenitic SS passivation occurs by the rapid adsorption of hydrated complex largely associated with chromium in the form of bound water which deprotonates and changes to oxide layer with time and applied potential. Surface analysis of the passivated surface showed the existence of M-H₂O (aquo), M-OH (olation), and M-O (oxo) type of bonding between chromium and oxygen in the passive film [54-56]. All the above type of bonding between chromium and oxygen depends on the chromium content of the alloy and increases its bonding tendency with increase in chromium content [54-57]. However, with increase in passivation potential, the olation (MOH) type bonding decreases, and the oxo (M-O) type of bonding increases in proportion. The passivation potential, and the electrical field strength play an important role in deprotonation and influence the oxidation state of chromium which in turn governs the solubility of oxide layer. Iron, even though is the largest alloying element in austenitic SS, is found to present in less quantity in the passive film as the Cr/Fe ratio is always higher with increasing potential irrespective of specimen preparation conditions [54-57]. In general, iron is present in two oxidation states of Fe³⁺ and Fe²⁺, the higher proportion of the latter being observed on higher chromium alloys [54-57]. The beneficial effect of nitrogen on the passivity of austenitic SS is due to its segregation to the oxide-metal interface thereby forms the interstitial nitrides which largely hinder the anodic dissolution [50, 58]. Apart from this, in acidic solutions nitrogen forms ammonium ions which buffer the local pH, and increase the repassivation tendency by forming the nitrate compounds and providing local inhibition effects. Nevertheless, nitrogen is having solubility from 0.2 to 0.7 %, and higher content affects the hot ductility of austenitic SS. Molybdenum is one of the most effective elements added to austenitic SS to improve the pitting resistance. Extensive study was carried out to elucidate the role of molybdenum on the passivity of austenitic SS, and several mechanisms have been proposed. It is proposed that, molybdenum forms complex

with CrOOH, thereby inhibiting the transpassive dissolution [59] According to another mechanism, the active sites in the passive film are rapidly blocked by molybdenum oxyhydroxide or molybdate salts, thereby inhibiting the localized corrosion [60]. Many theories of metal passivity have been presented in the literature. The major theories which have been developed are the oxide film theory and the adsorption theory of passivity [61-66].

I. Oxide film theory

Oxide layer formation is one of the important hypotheses to account for the cause of passivity of metals, and alloys including different types of SS. The theory is usually ascribed to Micheal Farady on the study of passivation of iron in HNO₃ [56]. Later on, the protective oxide film theory gained support from the studies carried out by many researchers on different materials and in different environmental conditions. In the year 1934, Tronstad and Borgmann showed that some kind of film existed on 18-8 SS, and assumed that it must be an oxide layer [50]. They concluded from their study that the air formed film on 18-8 steels gets strengthened when passivated in HNO₃ media. According to this theory, the surface of the metal/alloy is oxidized or the atoms on the surface are in such a relation with the oxygen of the electrolyte, that it is equivalent to an oxidation process. The properties characterizing a typical oxide film are of low ionic conductivity, and low solubility. Moreover, it is assumed that such oxide layers are formed as a diffusion barrier separating metal/alloy from electrochemical environment and thereby decreasing the reaction rate. Due to these properties, the oxide layer prevents a large extent transport of metal ions from the sites in crystal lattice to the electrochemical environment thus preventing the anodic dissolution. Nevertheless, there is a slow dissolution corresponding to passive state of the materials since oxide layers directly formed in close connection with crystal structure often contain defects which allow electron conduction, and electrochemical reaction can occur at the top surface of the oxide layer.

II. Adsorption theory

The oxide film theory suffered a set back, from lack of coincidence of the potential marking the active to passive state transition with the potential for the reverse transition [50]. It was thought that the lack of coincidence in passivation potential could not be explained by oxide layer theory rather by a variable layer of adsorbed oxygen on the surface either by physical or chemical adsorption. Later on, Uhlig [56] proposed that adsorbed oxygen film is a common source of passivity, and such film forms on transition metals (Fe and Cr) as well as 18-8 SS in accordance with their uncoupled d-electrons interacting with oxygen atoms to form stable bond. The high sublimation energy of these metal-oxygen bond favors retention of the metal atoms in their lattice in preference to their removal to form the oxide lattice as per oxide layer theory. Even less than a monolayer of the adsorbed film has passivating effect, increases the anodic overvoltage and decreases the exchange current density. The characteristics of high energy of adsorption of oxygen on transition metals (Fe and Cr) mostly favour the formation chemisorbed films as compared to low-energy films formed on non-transition elements due to physical adsorption [56]. Thus, the chemisorbed film formed on the surface is thermodynamically more stable than the oxide layer formed on the surface due to oxidation according to oxide layer theory. However, the large recognition of adsorption theory does not preclude the existence of oxide layer theory. It is argued that both the theories are supplementary to each other because the adsorbed film in the process of nucleation and growth gradually changes into an oxide layer. The inclusion of adsorption is necessary to explain the observed property of passive film, and by and large is an overlap between the oxide layer and adsorption theory. The evidence for the change over from adsorbed layer to oxide layer was first pointed out by Flade on the observation that passive film on iron becomes more resistive to disruption when kept for longer duration in the passive state [50].

The observation was subsequently confirmed by others and can be explained on the basis of oxide film theory by formation of a thicker oxide film with time.

2.3 Corrosion Problems Associated With Reprocessing Plants

Situations prevailing in spent fuel reprocessing plants include, high concentration of HNO_3 in boiling condition ($\geq 8 \text{ M}$, $\geq 80 \text{ }^\circ\text{C}$), presence of long lived fission products, existence of various oxidizing agents having high oxidizing-reducing potentials (Cr^{6+} , Ce^{4+} , AmO^{2+}) and undissolved fuel elements. Owing to the existence of critical circumstances, the corrosion problems encountered in the fuel reprocessing plants are enumerated below [36, 43, 44, 68, 69]:

- Intergranular corrosion due to sensitization
- HNO_3 condensate corrosion problem even in non sensitized alloy
- Transpassive dissolution due to the presence of Cr^{6+} ions
- End-grain attack due to the presence of inclusions
- Crevice corrosion at joints
- Galvanic corrosion

2.3.1 Intergranular corrosion

If a metal corrodes, uniform attack results since grain boundaries are usually only slightly more reactive than the matrix. However, under certain conditions, grain interfaces are very reactive resulting in intergranular corrosion. “Localized attack at and adjacent to grain boundaries, with relatively little corrosion of the grains is intergranular corrosion” [1]. The alloy disintegrates (grain fallout) and/or loses its strength. Intergranular corrosion exhibited by an austenitic SS is shown in Fig 2.7 [70]. Fig. 2.7 (a) shows the surface of the specimen. The grain structure is visible due to the attack, and some grains have fallen out (grain dropping). The cross-sectional view (Fig 2.7 (b)) shows the depth of penetration of the attack

along the grain boundaries. In austenitic steels, intergranular failures occur in both sensitized and annealed conditions. Any physical or chemical heterogeneity is responsible for causing IGC in austenitic SS. The sensitization of austenitic SS, presence of secondary phases such as sigma, $M_{23}C_6$, TiC, NbC and delta ferrite, presence of inclusions, segregation of impurities as boron, sulphur, and phosphorus along the grain boundaries and aggressiveness of chemical environment are major contributors for failure of austenitic SS by severe IGC in HNO_3 service [1].

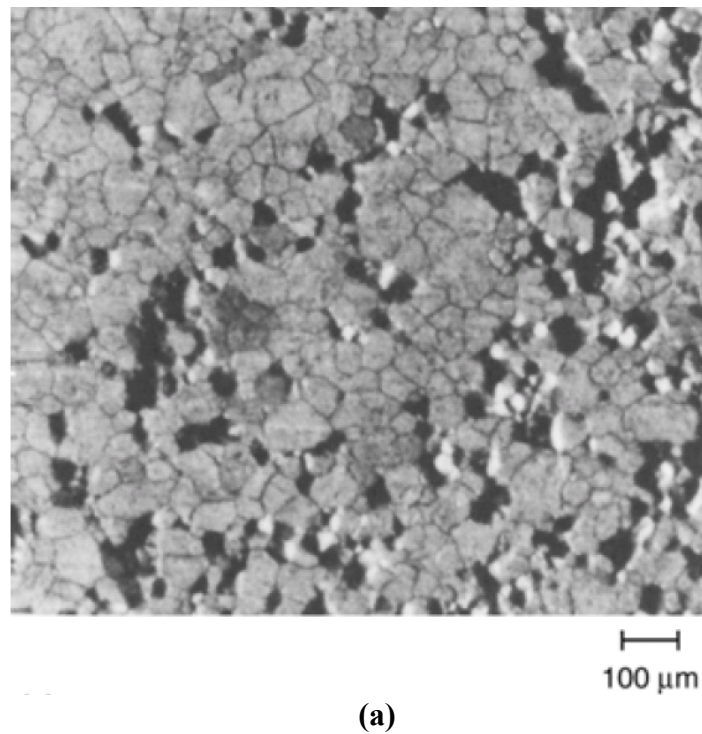
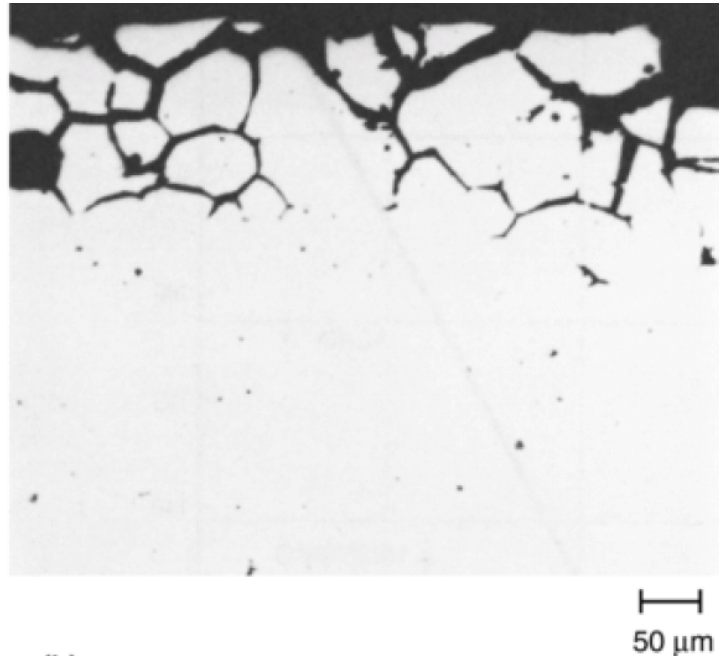


Fig. 2.7 Intergranular corrosion exhibited by an austenitic steels: (a) surface of the specimen and (b) cross-sectional view shows the depth of penetration of the attack along the grain boundaries [70].



(b)

Fig. 2.7 Continued

Sensitization and intergranular corrosion

When austenitic SS alloys are subjected to a temperature range of 450 - 850 °C they become sensitized or susceptible to intergranular corrosion. In this temperature range Cr_{23}C_6 and carbon are insoluble and precipitate out of solid solution if carbon content is 0.02 % or higher. Chromium is thereby removed from solid solution. This results in depletion of chromium content adjacent to the grain boundary areas. These chromium depleted areas do not possess sufficient corrosion resistance to resist attack in many corrosive environments. At sensitizing temperature carbon diffuses towards the grain boundary at a faster rate while diffusion of chromium is slower due to its larger size. The surface available at the grain boundary facilitates formation of a new surface. Therefore Cr_{23}C_6 precipitates at the grain boundary at sensitizing temperature. The chromium content at the grain boundary can be reduced to a very low level or zero. The chromium content within the grain is 18%. Thus two dissimilar metal compositions are in contact and a large unfavorable area ratio is present. The depleted area protects the grain. This results in rapid attack in chromium depleted areas while

little or no attack on the grain. In practice, susceptibility to intergranular attack will result usually from one of three situations:

1. Slow cooling from an annealing treatment. This factor is very important in large product sizes where the rate of cooling through the sensitization range is slower.
2. Stress relieving for several hours in the sensitization range, for example at 593 °C.
3. During welding.

Welding is probably the most common cause of intergranular corrosion. Parent metal on both sides of a weld is heated in the sensitization range for several seconds or minutes during welding, and this can result in susceptibility as shown in Fig. 2.8 [71]. This type of attack is sometimes called "weld decay" or "low-temperature heat affected zone corrosion" [71].

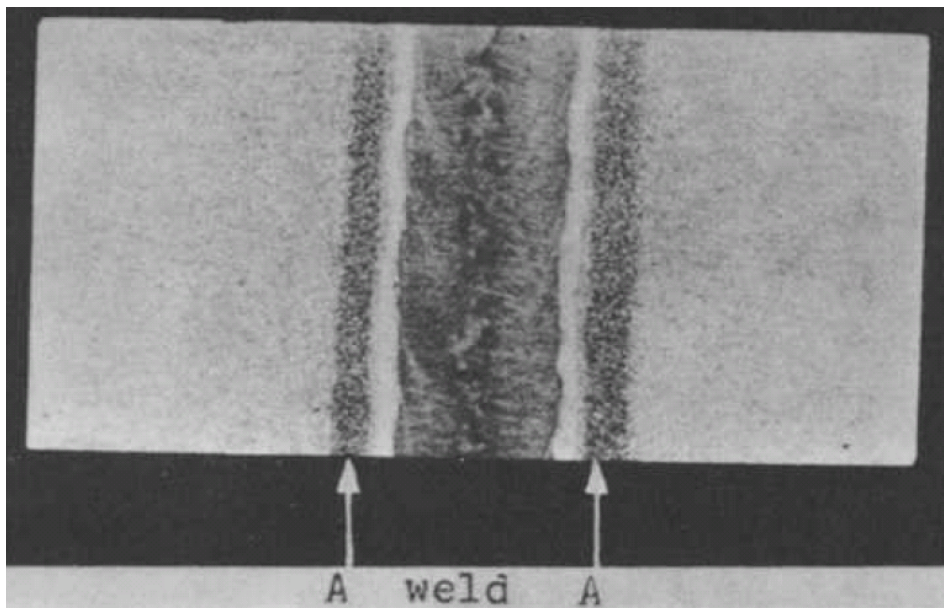


Fig.2.8 Preferential attack in low-temperature heat affected zones (A) of Type 302 steels welded strip [71]

Three methods are used to avoid IGC by using:

1. Annealed material.
2. Stabilized grades such as Type 321 (titanium added) or Type 347 (columbium added)
3. Low-carbon grades such as Type 304L (< 0.03 %)

Commercial solution – quenching treatments consist of heating to 1000 to 1050°C followed by water quenching. Chromium carbide is dissolved at these temperatures, and a more homogeneous alloy is obtained. Most of the austenitic SS alloys are supplied in this condition. If welding is used during fabrication, the equipment must be solution annealed/quench annealed to eliminate susceptibility to weld decay. This poses an expensive problem for a large equipment as furnaces are not available for heat treating large components. In case welding is carried out at plant location for repairs etc. in such situations heat treatment post welding is impossible. The stabilized grades take a different approach of putting in a strong carbide former to tie up carbon before chromium gets a chance to do so. Lowering the carbon content below 0.03% (Type 304L) does not permit sufficient carbide to form to cause intergranular corrosion.

In welding applications, the stabilized grade can be at a disadvantage (compared to the low-carbon alloys), because the titanium or columbium carbide goes into solid solution at the high temperatures associated with welding and they remain in the solution when cooled rapidly from this temperature. The stabilizing elements remain in the solution when the temperature reaches the chromium carbide precipitation range and thus the area adjacent to the weld which is now rich in carbon content forms chromium carbide precipitates. This area becomes depleted in chromium and IGC occurs in corrosive environments. Knife-line attack (KLA) is similar to weld decay in that they both result from IGC and both are associated with welding. The two major differences are:

1. KLA occurs in a narrow band in the parent metal immediately adjacent to the weld, whereas weld decay develops at an appreciable distance from the weld, and
2. KLA occurs in the stabilized steels.

2.3.1.1 Theories of Intergranular Corrosion

There were four major theories, which explain the carbide and nitride precipitation mechanism and its role in IGC [6].

I. Chromium depletion theory

According to this theory, the carbon and nitrogen diffuse to grain boundary much faster than chromium and combines with chromium to form carbides/nitrides of chromium. For the formation of chromium carbide, initially chromium is used from grain boundary but later chromium is supplied from grain periphery. This results in depletion of chromium concentration below 12% in the vicinity of grain boundary (Fig. 2.9), which is minimum chromium concentration required for the formation of strong, protective oxide film (*Passivation*) on the surface of SS [6]. The reduction in chromium in the vicinity of grain boundary makes it prone to IGC [1-3, 5, 6]. Recent analytical and quantitative refinement to this theory for IGC in sensitized SS has demonstrated the widespread applicability and validity of this model.

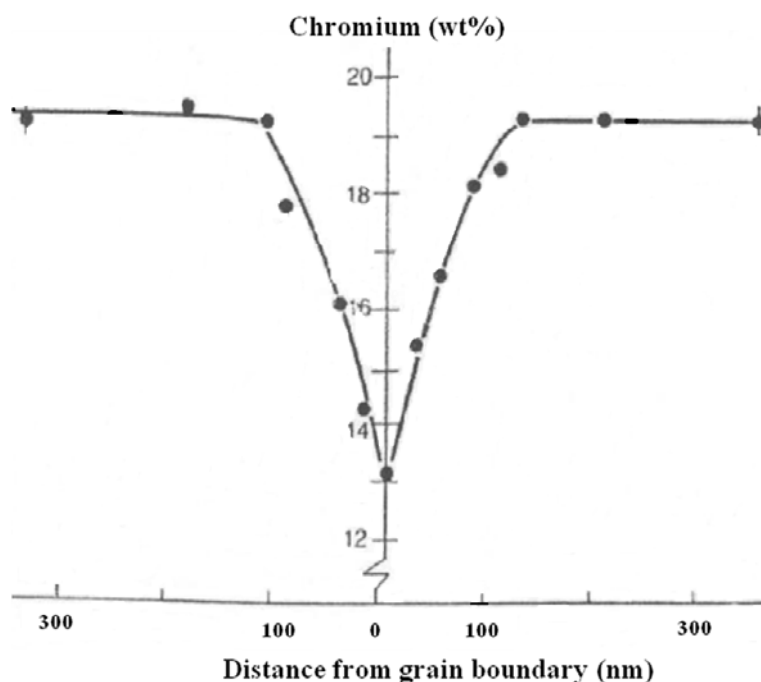


Fig.2.9 Chromium distribution profile at grain [5]

II. Stress Theory

According to this theory, local stresses arise in those areas where secondary phase begin to precipitate and grows [52]. Due to this considerable energy differentials are produced in these zones. This leads to imperfect passivation which results in poor corrosion resistance.

III. Microcell Theory

This theory is based on the dissolution of grain boundary due the formation of local cells, the precipitate acting either as anode or cathode as proposed by Stickler and Vinckier [72]. They proposed that IGC is an electrochemical reaction between the noble carbide particle acting as a cathode and matrix acting as an anode and proceeds rapidly along the grain boundary where there is a continuous path provided by carbide particles. This theory could not explain desensitization as well as resistance to IGC during the onset of precipitation.

IV. Segregation Theory

According to this theory, IGC takes place due to the presence of continuous grain boundary path of either second phase or soluble segregate resulting from solute-vacancy interaction. This model can explain the IGC arising due to the segregation of impurity elements. The observation that IGC takes place even in annealed steel in highly oxidizing solution can be explained by this model. Although this model holds good for IGC in non sensitized austenitic SS, attempts to extend the model to carbide-sensitized SS have been inconclusive.

It can be concluded that chromium depletion theory is able to explain most of the cases of IGC resulting from chromium carbide precipitation. Various theories do not contradict each other substantially but rather supplement each other in explaining IGC problems.

2.3.1.2 Factors Affecting Intergranular Corrosion

I. Compositional Factors

All three major constituents of SS namely iron, chromium and nickel have highly cathodic potential [6] but exhibit very good corrosion resistance due to passive film formation on them. Both iron and nickel owe passivity in their alloys to chromium. Addition of chromium to iron shift the polarization curve towards pure chromium, and with 20 % chromium stable passivity is achieved. The passivity is due to thin metal oxide films of thickness 30-50 Å. Drastic increase in chromium content in the films was reported when chromium content in the base alloy exceeds 13% [73]. Fig 2.10 shows corrosion behavior of austenitic SS with respect to Cr content in 65 wt % boiling HNO₃ [36]. It can be seen that high chromium content makes austenitic SS more corrosion resistant.

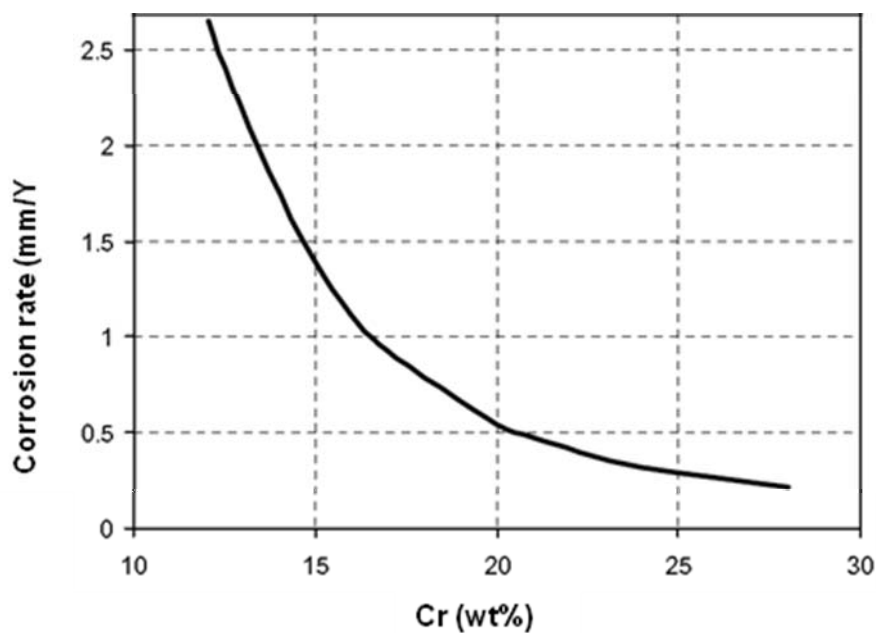


Fig. 2.10 Effect of the chromium content on the corrosion behavior of austenitic SS in HNO₃ (65 wt%, boiling temperature) [36].

Nickel is required in austenitic SS to stabilize the austenitic phase and must be increased with increasing Cr concentration. Increasing the bulk nickel content decreases the

solubility and increases the diffusivity of carbon. This effect is much more pronounced when nickel content is above 20%. It is generally recommended that in 25/20 Cr-Ni steel, carbon content should be less than 0.02% to guarantee resistance to IGC.

Molybdenum reduces the solubility of carbon in austenite. Carbide precipitation is accelerated at higher temperatures whereas at lower temperatures it is slowed down [52]. When molybdenum is present, it is also incorporated in $M_{23}C_6$. Therefore in addition to chromium depletion molybdenum depletion is also observed. With increasing molybdenum content, $M_{23}C_6$ precipitation and IGC are increasingly influenced by the precipitation of intermetallic phases [52].

Carbon is a more powerful austenitic phase stabilizer than nickel. But it promotes sensitization of material, when austenitic SS alloys are heat treated in the temperature range of 450-850 °C. Among the chromium carbides $Cr_{23}C_6$, Cr_7C_3 , Cr_6C and Cr_3C_2 that are formed during the process of sensitization, $Cr_{23}C_6$ is the most stable. A carbon content below 0.03% or preferably below 0.02%, and optimized quench annealing temperatures and heating time prevent from IGC resulting from the chromium depleted zones due to sensitization after a thermal treatment or by welding [36]. The effect of carbon content on the behavior of AISI 304L steel is illustrated by using the double loop EPR test in Fig. 2.11 [36].

The effect of Si content on IGC is more complex. Whereas a maximum IGC is observed for about 1 % Si content, the absence of IGC is observed for Si values higher than 3 % in boiling HNO_3 containing oxidizing species (Fig. 2.12) [36]. The dual effect of Si on IGC of austenitic SS in boiling HNO_3 containing Cr^{6+} ion can be explained as follows [26]: Si accelerates anodic dissolution of grain boundaries but simultaneously it forms a passivating film. This film retards the cathodic process which in turn reduces the anodic process. The maxima in corrosion data (shown in fig 2.12) is due to competition between these two processes.

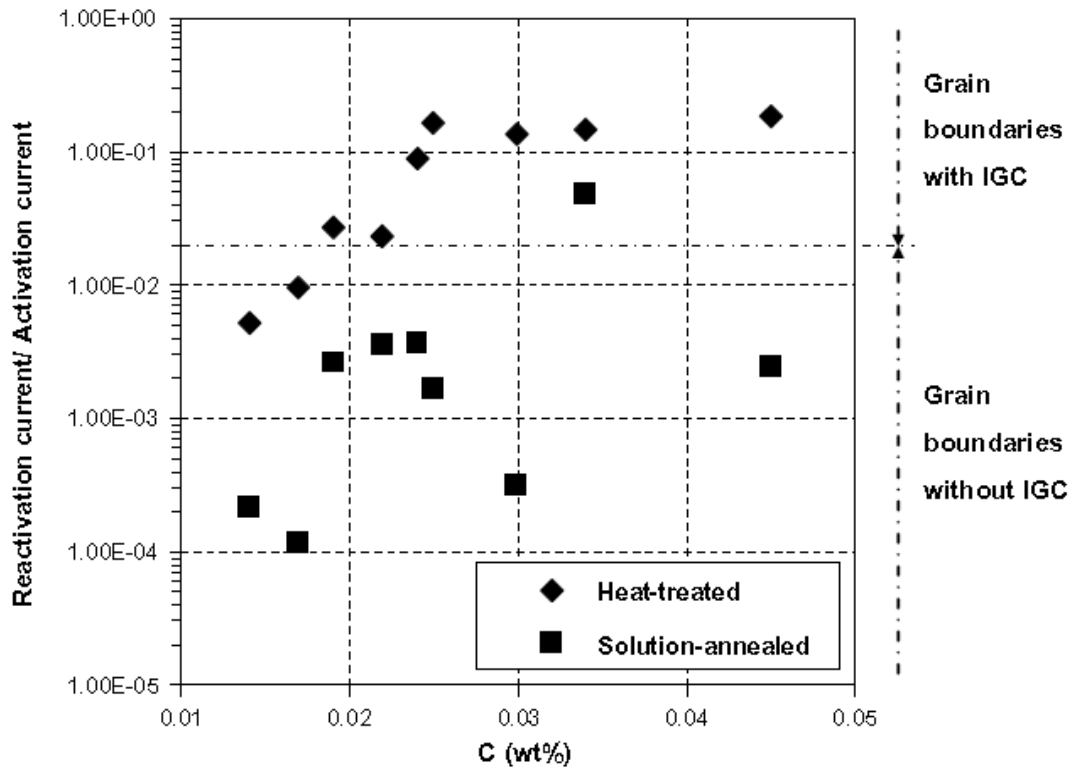


Fig. 2.11 Effect of the carbon content on the behavior of 304 SS in HNO₃, as revealed by the double loop EPR technique [36].

In pure boiling HNO₃, the uniform corrosion rate increases continuously as the Si-content of steel increases [36]. Therefore, when immunity to IGC is required and a relatively high general corrosion rate can be tolerated, the use of high purity grades containing at least 4% silicon such as Uranus S1N steel (AFNOR Z1 CNS 17.15) offers a safe choice.

Fig. 2.13 shows that phosphorous when its concentration is above 100 ppm is deleterious from IGC point of view [5].

The effect of nitrogen is quite complex and is dependent on the presence of other alloying elements. Nitrogen content up to 0.16 wt% is reported to improve sensitization resistance by retarding the precipitation and growth of Cr₂₃C₆. In essence, nitrogen retards Cr₂₃C₆ precipitation by decreasing the diffusivity of chromium [52].

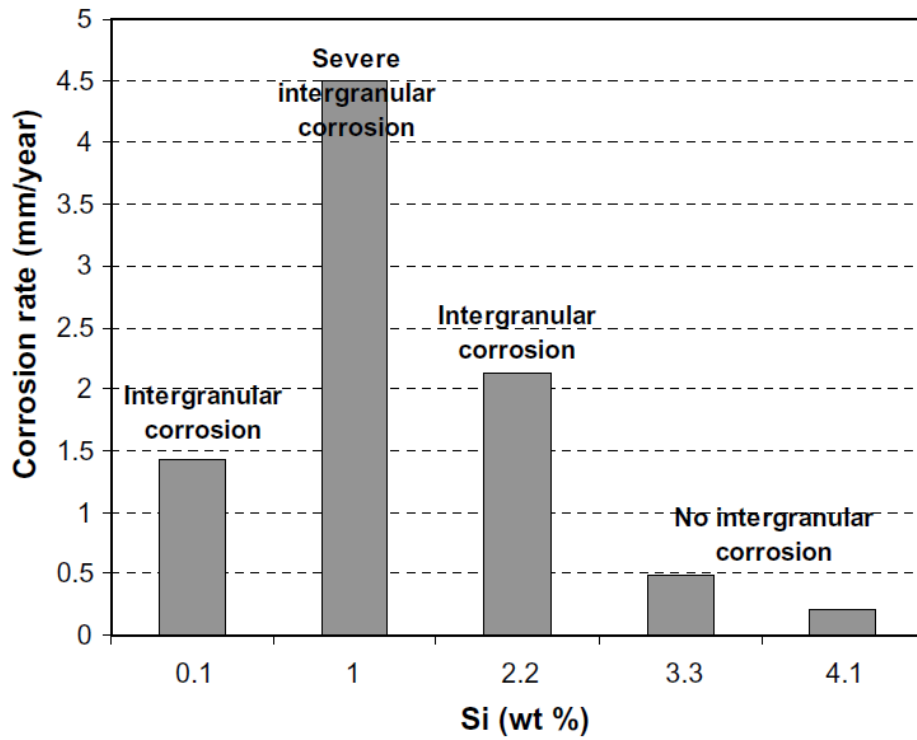


Fig. 2.12 Effect of the silicon content on the behavior of austenitic SS in boiling 5M L⁻¹ HNO₃ + 1 g L⁻¹ Cr⁶⁺ [36].

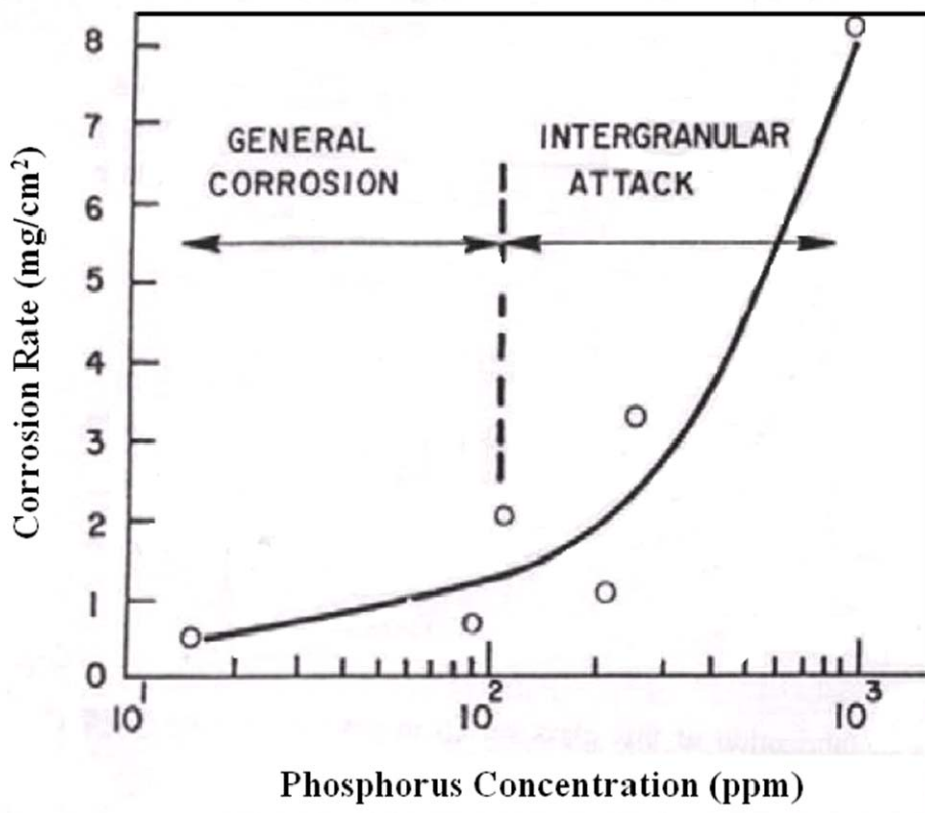


Fig. 2.13 Effect of phosphorus concentration on corrosion rate [5].

II. Grain Size

Sufficient data are available to state that IGC in SS reduces with smaller grain size. Greater grain boundary area present may retard continuous formation of carbide at grain boundaries [6]. The grain size effect on IGC also depends upon the type of material (forged, wrought) and testing methods. In HNO₃ corrosion, however there is rapid opening of small grains in the structure, so that fine grain steels are often corroded in shorter span of time than coarse grained steels which confirms the difference in characteristic in IGC in HNO₃. But as whole grain size seems not to affect significantly to the IGC behavior of SS in boiling HNO₃ as the influence of grain size is overshadowed by the influence of accumulated corrosion products, which speed up the attack.

III. Cold Work and Annealing parameters

Several Studies have shown that kinetics of sensitization can be influenced by prior deformation [74-78]. Experimental study by Parvathavarthini shows that cold work accelerates the sensitization up to 15% but after this limit, time required for sensitization increases IGC at low deformation level [79]. Annealing parameters like time, temperature and method of cooling also affect IGC. Furnace cooled austenitic SS sensitize at lower rate as compared to water quenched steels after solution annealing at 1083 °C [80].

IV. β , γ -Radiation

The γ radiation affects process fluid as well as material. It may cause defects in the material. The radiolysis of boiling HNO₃ occurs to generate nitrous acid and NO_x [81, 82]. Nitrous acid affects the autocatalytic reduction of HNO₃ and causes reduction in the potential in solution as shown in Fig. 2.14. But immersion test shows contradictory results with regard to potential. The corrosion rates in immersion tests are slightly enhanced due to irradiation as shown in Fig. 2.15 [82]. Metallic oxidizing species like Cr⁶⁺, Ru⁴⁺, V⁵⁺ and Ce⁴⁺ are converted to their respective reduced forms viz. Cr³⁺, Ru³⁺, V⁴⁺ and Ce³⁺ in the

presence of radiation activity ($1300 \text{ CuriesL}^{-1}$) [83]. This leads to reduction of oxidation potential of solution.

Reduction of redox potential on one hand and increase of corrosion rate on the other hand as a consequence of radiolysis can be explained by considering the role of HNO_2 . Redox potential of HNO_3 solution increases with concentrations of NO_3^- and H^+ . It decreases when HNO_2 concentration increases. HNO_2 increases the reduction rate of HNO_3 by autocatalytic mechanism (Electrochemical reactions in HNO_3 will be discussed in detail in section 2.4). As a consequence of this corrosion potential and the corrosion rate of the steel increases.

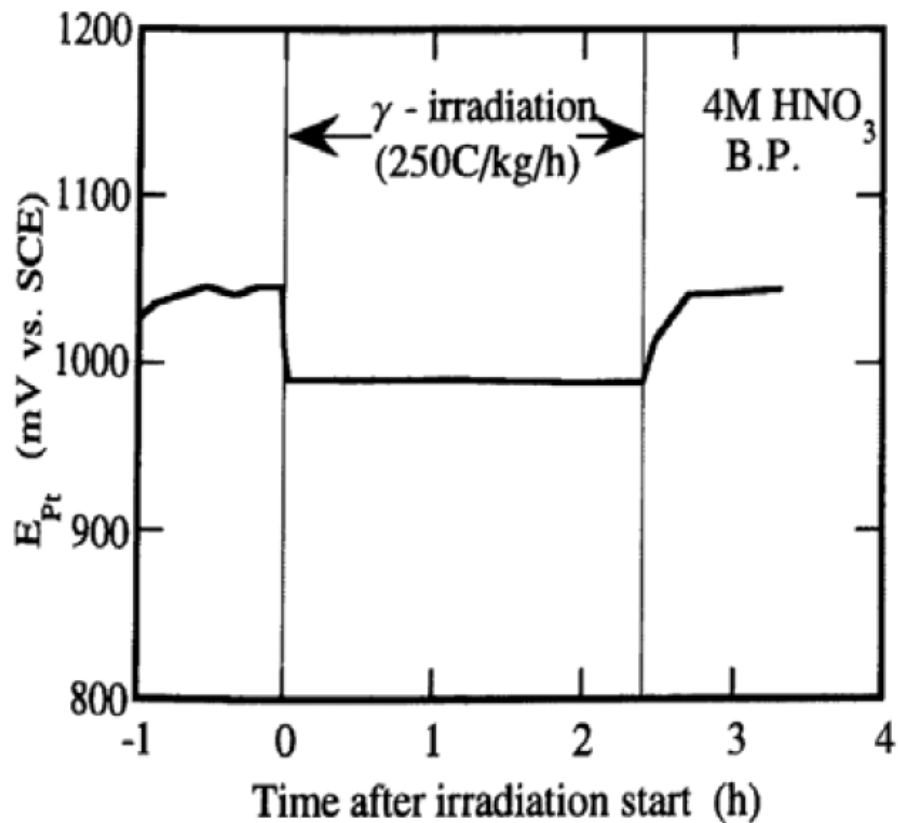


Fig. 2.14 Reduction in solution potential [82]

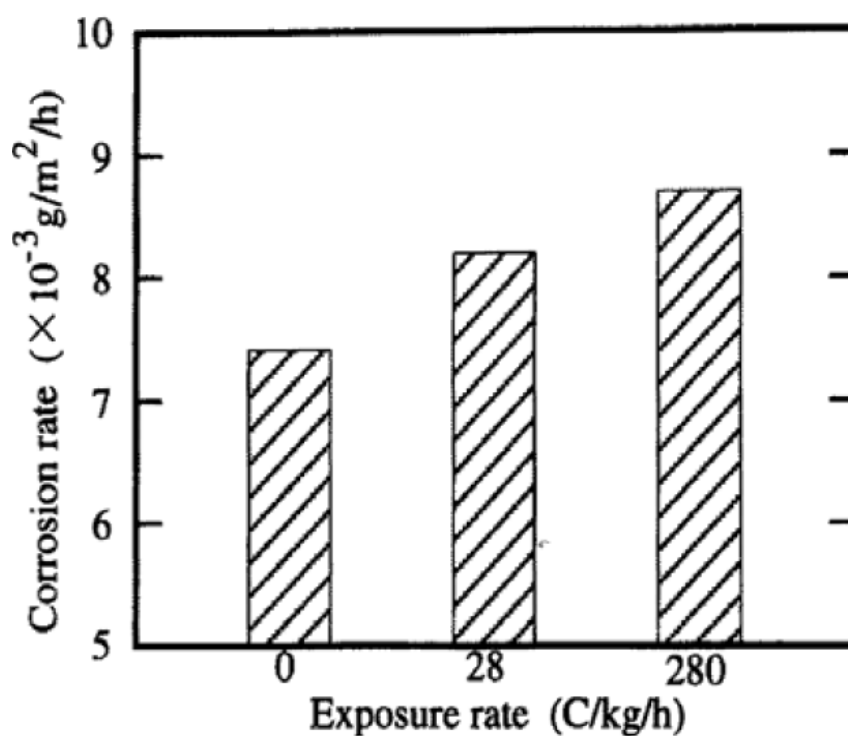


Fig. 2.15 Corrosion rate variation with exposure for 4 M HNO₃ [83].

2.3.2 End Grain Corrosion

This is an unusual form of localized corrosion in austenitic SS that occurs in the nuclear fuel reprocessing plants as well as other chemical processing plants that are using concentrated HNO₃. “End Grain Corrosion” also known as tunnel corrosion. It takes place on tubular and forged surfaces that are perpendicular to hot working direction. It appears as localized “pitting” type attack and penetrates along the hot working direction and finally the corrosion occurs as intergranular attack. The SS, especially tubular products like bars, pipes and tubes, are prone to “End Grain Corrosion”. End Grain Corrosion” is specifically related to highly oxidizing HNO₃ environment. The schematic of “End Grain Corrosion” is shown in Fig. 2.16a. A typical example of “End Grain Corrosion” in 18 Cr-10 Ni austenitic SS, caused due to exposure to simulated dissolver solution containing highly oxidizing HNO₃ is shown in Fig. 2.16b [84].

In the reprocessing plants that use sensitization resistant SS alloys (L grade or NAG grade), “End Grain Corrosion” is shown to be a major degradation mode in the components such as instrument tubing and tube to tube sheet welds. Forgings and set in pipe branches are reported /to be most affected by End Grain Corrosion [23]. Exposure studies done in a dissolver in a reprocessing plant (in vapor phase) showed very heavy corrosion rates of 0.6 – 2 mm^y⁻¹ even for NAG grade of SS and was attributed mainly to “End Grain Corrosion” [23]. It has been shown by earlier studies that inclusions in the form of stringers (sulfides or oxysulfides of manganese and iron) cause IGC in austenitic SS [11, 24, 25, 29, 31]. The corrosion rates of sensitized SS increase manifold due to presence of these inclusions. Annealed (non sensitized) SS containing these types of inclusions also undergo IGC. This is due to dissolution of stringer types of sulfide inclusions from the exposed end (cross sectional) faces. This causes accumulation of Cr⁶⁺ ions in the cavities that form due to dissolution of inclusions. It makes the environment within the dissolved inclusions even more aggressive and the high energy grain boundaries start corroding leading to IGC. This is minimized by specifying total inclusion rating of less than 4.5 as per ASTM for the NAG grade. Specifically the sulfide type of inclusions, termed as “active inclusions” have to be avoided. The control of inclusions in NAG grade SS is done by controlling the levels of sulfur and oxygen. Low levels of sulfur and manganese ensure that manganese sulfide type of inclusions do not form. Other types of inclusions are controlled by limiting the dissolved oxygen content in the SS to less than 0.01% but preferentially below 50 ppm. Another method by which End Grain Corrosion takes place in austenitic SS is by preferential attack on the segregated elements along accumulated dislocations [11, 23, 25, 24, 30] due to cold working and insufficient solution annealing. The dislocation banding taking place along the direction of working as a result of cold working leads to segregation of elements. Niobium in stabilized SS and silicon and phosphorus in non stabilized grades can be segregated along

dislocation banding. This makes such regions more prone to corrosion in strong oxidizing environments and the exposed end faces of tubular products get corroded. A recent study [30] has shown that the “End Grain Corrosion” in HNO_3 environments can be controlled by any of the following methods:

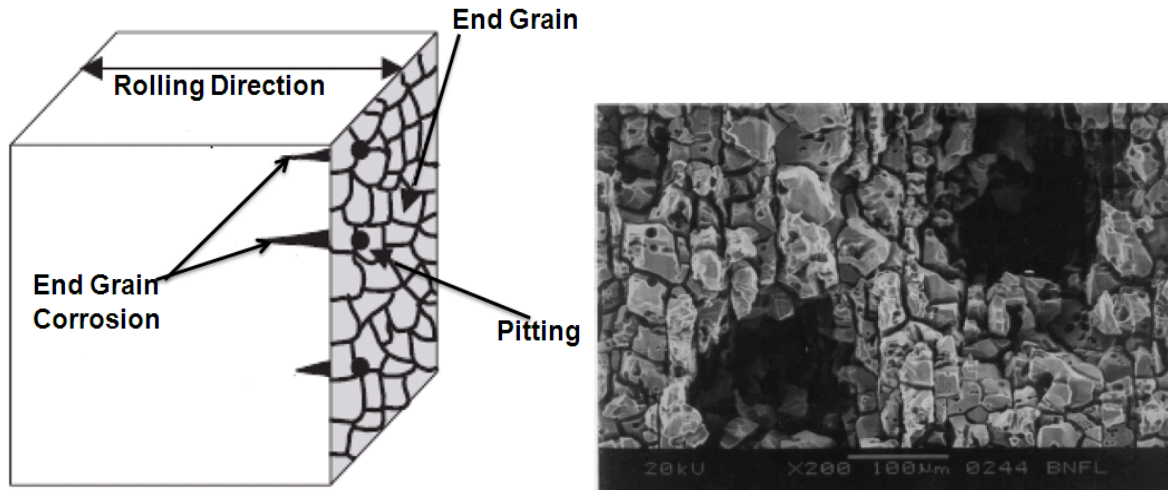


Fig. 2.16 (a) Schematic of “End Grain Corrosion” and **(b)** a typical “End Grain Attack” in austenitic SS [84].

(a) A controlled solution annealing heat treatment on the as received SS which is otherwise prone to “End Grain Corrosion”. A re-solution annealing at $950\text{ }^\circ\text{C}$ for 90 minutes has been shown to be effective in achieving this. This heat treatment does not result in grain coarsening. It was shown that this heat treatment results in proper homogenization of alloying elements thereby erasing segregation in the material.

(b) Laser surface remelting of the exposed end faces (cross-sectional surfaces) was shown to result in immunity from End Grain Corrosion. A modified cast microstructure and presence of ferrite was shown to be the main features of the laser remelted surface.

(c) Weld overlay on the exposed end faces (e.g. cross-sectional areas of a tubular product) with a weld filler material e.g. Type 308L avoids End Grain Corrosion. This method, or welding a ring of a SS material (that is not prone to End Grain Corrosion) over the susceptible end face are the best practical methods to avoid End Grain Corrosion during fabrication of component. This brought down the End Grain Corrosion rate from 4.57 mmy^{-1}

to 0.24 mmy^{-1} in practice C, A262, ASTM [30]. The main advantage of using either weld overlay or the laser surface remelting is masking (breakdown) of the stringer shape of the inclusions/flow lines along which segregation of elements usually takes place. Weld overlay is certainly a more practical approach that can be easily adopted during fabrication of components.

2.3.3 Transpassive Corrosion

All the austenitic SS alloys in HNO_3 medium exhibit passive to transpassive transition behavior. The SS alloys develop a passive film (chromium rich oxide) and current densities in the domain of passive potentials are very low ($\mu\text{A cm}^{-2}$). At sufficiently high potentials, many passive metals and alloys, including SS alloys, enter the transpassive state in which the current density begins to increase exponentially with the applied voltage. This behavior in the transpassive potential regime is similar to that exhibited during active dissolution. At still higher potentials, oxygen evolution occurs and may mask the transpassive behavior. The main reason for increased current density at the onset of transpassivity for SS is conversion of Cr^{3+} to Cr^{6+} in the passive film itself. As potentials increase further in the transpassive potential regime, faster dissolution of chromium occurs through the oxide film. It has been shown clearly that thickness of the oxide film increases over SS in the transpassive regime of potentials [32-34]. The characteristic feature of transpassive dissolution is mainly intergranular corrosion with opening up of grain boundaries and observed intergranular ditches [39, 43-45, 85-87].

2.3.4 Pitting Corrosion

Pitting is a form of extremely localized corrosion that results in holes in the metal as shown in Fig. 2.17. Generally a pit may be described as a cavity with the surface diameter about the same as or less than the depth. In general austenitic SS undergoes pitting corrosion, and passivation property decreases when HNO_3 is contaminated with halide ions [88, 89].

Pitting corrosion is one of the major concerns for austenitic grade SS alloys used in the spent nuclear fuel reprocessing plant as all Indian plants are located in the saline atmosphere of coastal region. The combined action of both powerful oxidizing (HNO_3) and de passivating (Cl^-) agents on the corrosion properties of austenitic SS depends upon the alloy composition, solution composition and pH of the solution. Alloying elements such as Cr, Mo and N increase the passive film breakdown potential, and C, S and P reduce the breakdown potential [5].

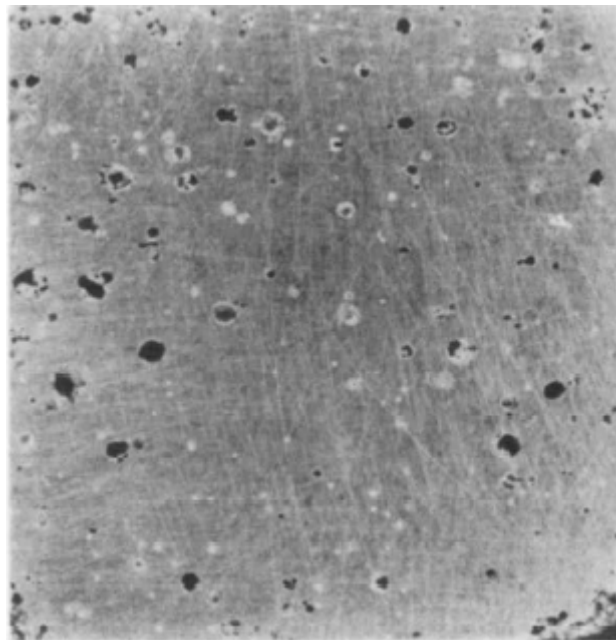


Fig. 2.17 Pitting corrosion of austenitic SS in HNO_3 medium containing chloride ions [89].

Studies reported showed that for HNO_3 concentrations from 0.1 to 4 M at room temperature, the chloride contamination (even up to 3M NaCl) did not cause pitting during anodic polarization tests done in open to air solutions [90]. It was suggested that certain combinations of HNO_3 concentration and chloride ion concentration may lead to pitting. Another study reported that no corrosion occurred when HNO_3 is between concentrations of 0.1 and 1 N and chloride ion concentration was below 0.2%. The chloride influence was reported to decrease when the nitric concentration was increased [90]. When the nitric solution became less oxidizing, the chloride ions gave rise to pitting, but independent of the

chloride concentration. However oxidizing solutions ($> 1.5 \text{ N HNO}_3$) gave rise to intergranular corrosion.

2.3.5 Crevice corrosion

Intensive localized corrosion frequently occurs within crevices and other shielded areas on the metal surfaces exposed to corrosives. This type of attack is usually associated with small volume of stagnant solution caused by holes, gasket, lap joints surface deposits and crevices under bolt and rivet head. Austenitic SS does suffer from crevice corrosion in HNO_3 medium containing aggressive ions. Crevice corrosion indeed has been observed in nuclear fuel reprocessing plant behind weld backing strip at the closing seam of Type 304L vessels handling hot concentrated HNO_3 [5]. Corrosion by stagnant acid in the crevices creates hexavalent chromium ions (Cr^{6+}) which causes accelerated attack while other exposed surfaces remains unaffected.

2.4 General Electrochemical Behavior of Austenitic SS in Nitric Acid Media

Fig. 2.18 shows a diagram which illustrates the behavior of an austenitic SS in acidic media as a function of its potential [36]. The partial anodic process, which relates to the oxidation of the elements (mainly Fe, Cr and Ni) of the steel, includes following domains:

- I.** An active domain where the uniform dissolution rate of the SS is high, if the medium conditions are sufficiently reducing.
- II.** For moderately oxidizing medium conditions, austenitic SS alloys are in their passive state characterized by uniform and low rate of dissolution [91]. Steels treated with HNO_3 are then protected by a passive layer as revealed by XPS analysis of the specimen. For AISI 304L type steel, this passive layer, a few nm thick, is mainly composed of Cr_2O_3 [36].
- III.** If the medium becomes excessively oxidizing, passive film dissolution occurs,

specially by oxidation of Cr^{3+} (as insoluble Cr_2O_3) to Cr^{6+} (as soluble $Cr_2O_7^{2-}$) [36]. This results in fast and accelerating transpassive corrosion.

2.4.1 Pure HNO_3 Solutions

In most of the HNO_3 medium, the electrochemical reaction which imposes the redox potential of the solutions is the global reduction reaction of HNO_3 to nitrous acid



$$E_{25^\circ C}^\circ = 934mV / SHE$$

From this reaction, the redox potential increases with concentrations in NO_3^- and H^+ and with temperature. It decreases when HNO_2 concentration increases [92]. However, in order to conclude on the modifications in the corrosion potential induced by these different species, it is necessary to detail the specific reduction mechanism of HNO_3 , which has been explained in many studies [93, 94].

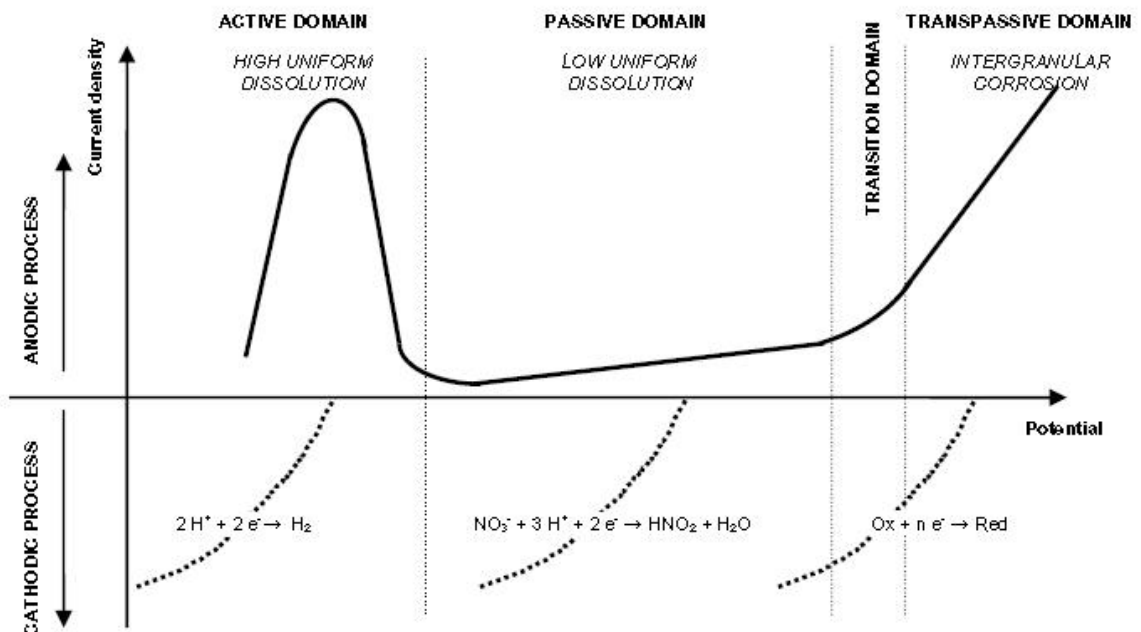


Fig. 2.18 General electrochemical behavior of austenitic SS in acidic media as a function of the potential [36].

A thermodynamic study of the equilibrium between gas and liquid phases for concentrated aqueous solutions of HNO₃ allowed identifying the predominant species involved in the process of reduction of HNO₃. These are two gaseous species (NO and NO₂) and an aqueous specie (HNO₂) [93]. The study of the influence of the HNO₃ concentration on the nature of the species limiting the stability of HNO₃ in reduction shows: (a) the final reduction product is nitrogen monoxide (NO) for concentrations lower than 8 ML⁻¹ and (b) nitrogen dioxide (NO₂) for concentrations higher than 8 ML⁻¹. The electrochemical study of the reduction process of HNO₃ was carried out first on a platinum electrode and then on a SS electrode. Similar results were obtained in both the cases. It allowed to confirm the predictions of thermodynamics and led to a better understanding of the mechanism [94]. HNO₃ is indirectly reduced by an autocatalytic mechanism including a charge transfer step and a chemical reaction which regenerates the electro-active species.

The electro-active species is nitrous acid which is reduced into nitrogen monoxide



Nitrous acid is then regenerated by a heterogeneous chemical reaction between HNO₃ and nitrogen monoxide



A third reaction occurs between HNO₃ and nitrous acid:



Reactions (2.2)–(2.4) are the elementary reactions of the reduction mechanism of HNO₃. They are valid on the whole concentration range. For low to moderate (<6 ML⁻¹) HNO₃ concentrations, the reaction of regeneration of nitrous acid (2.3) is slow. The nitrogen monoxide formed during the charge transfer step (2.2) may accumulate. Reaction (2.4) is also drawn back towards HNO₂ formation, because NO₂ is not thermodynamically stable for

concentrations lower than 8 ML^{-1} . Thus, for low to moderate HNO_3 concentrations, the mechanism of reduction of HNO_3 is as shown in Fig. 2.19a.



For more concentrated media ($>8 \text{ ML}^{-1}$), the reaction of regeneration of nitrous acid (2.3) is fast, because it is enhanced by the high HNO_3 concentration. This reaction leads to a gaseous evolution of NO_2 which is stable at these HNO_3 concentrations. The mechanism of HNO_3 reduction is then as shown in Fig. 2.19b. The kinetics of HNO_3 reduction can be modified by:

- Products resulting from the corrosion of the steels themselves namely Fe^{3+} ions and to a lesser extent Cr^{3+} ions which catalyze this reduction reaction.
- Dissolved oxygen, which slows it down.

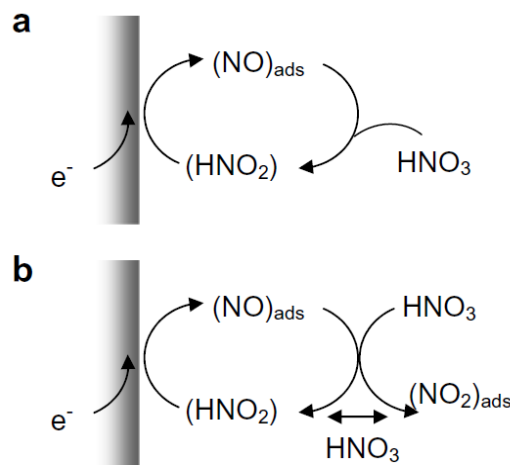


Fig.2.19 Pictorial representation of the mechanism of reduction of HNO_3 [36]. (a) Low to moderate concentrations ($<6 \text{ ML}^{-1}$) and (b) high concentrations ($>8 \text{ ML}^{-1}$).

It can be concluded that nitrous acid and nitrogen monooxide and dioxide play an ambivalent role in nitric acid medium:

- From a thermodynamic point of view, HNO_2 is the reduced species of HNO_3 (Reaction 2.1). Therefore the higher the HNO_2 concentration, the more reducing the

medium is. The redox potential of the medium is imposed by the $[HNO_2]/[HNO_3]$ ratio.

- From a kinetic point of view, it increases the reduction rate of HNO_3 by the autocatalytic mechanism described above. Consequently, the corrosion potential and the corrosion rate of the steel increase, although the medium is more reducing. In extreme cases, the corrosion potential may be shifted in the transpassive domain, and IGC may occur.

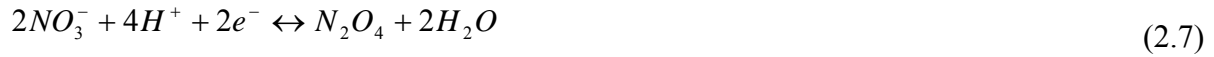
2.4.2 HNO_3 media Containing Oxidizing Species

Reprocessing media can contain metallic ions coming from oxido-reduction couples the standard potential of which is higher than the value of the NO_3^- / HNO_2 couple. Data concerning these so-called ‘oxidizing’ ions susceptible to be present in spent fuel treatment medium are summarized in Table 2.1, together with relevant data. In HNO_3 medium containing oxidizing ions [for example Cr^{6+} , Ce^{4+} and Mn^{6+}] the reaction of reduction of the medium is not any more reaction (2.1), but the reduction reaction of the oxidizing ion by the metallic elements of the steel is:



From a thermodynamic point of view, the standard potentials shown in Table 2.1 allow to classify the relative aggressiveness of the different oxidizing ions. However, the corrosion potential taken by the SS, and thus the dissolution rate of the material, depends on the kinetics of Reaction 2.6. In a closed medium without any external addition of oxidizing ion, the stationary concentration of the oxidizing ion results from the difference between its rate of formation by re-oxidation of the reduced species by the HNO_3 medium and its rate of consumption by oxidizing the elements of the steel. The ability of the HNO_3 medium to re-oxidize the reduced species depends on the real potential achieved by reaction (2.1). So, it is enhanced by high HNO_3 concentration and temperature and by low nitrous acid

concentration. For instance, boiling high concentrated HNO₃ solutions from which nitrous acid escapes by evaporation favors re-oxidation of the reduced species. On the contrary, NO₂ (or N₂O₄) generated or introduced in the medium acts as a reducing species according to the reaction.



Thus, many oxidizing species can be reduced and the corrosion of SS be lowered in their presence [95]. Studies carried out with a variety of oxidizing ions showed that, either for 310Nb SS or for 304L SS, the corrosion rate of the steel depends mainly on the corrosion potential it takes in the solution, whatever the nature or the concentration of the oxidizing ion are [36, 95].

Table 2.1 Data on the ‘oxidizing’ ions susceptible to be present in spent fuel treatment media [36]

Oxido reduction couple	Oxido reduction reaction	Standard potential $E_{25^0C}^0$ mV/SHE
<i>N(V)/N(III)</i>	$NO_3^- + 3H^+ + 2e^- \leftrightarrow HNO_2 + H_2O$	934
<i>Pu(IV)/Pu(III)</i>	$Pu^{4+} + e^- \leftrightarrow Pu^{3+}$	970
<i>Pu(VI)/Pu(IV)</i>	$PuO_2^{2+} + 4H^+ + 2e^- \leftrightarrow Pu^{4+} + 2H_2O$	1040
<i>Np(VI)/Np(V)</i>	$NpO_2^{2+} + e^- \leftrightarrow NpO_2^+$	1150
<i>V(V)/V(IV)</i>	$V(OH)_4^+ + 2H^+ + e^- \leftrightarrow VO^{2+} + 3H_2O$	1000
<i>Cr(VI)/Cr(III)</i>	$Cr_2O_7^{2-} + 14H^+ + 6e^- \leftrightarrow 2Cr^{3+} + 7H_2O$	1232
<i>Ce(IV)/Ce(III)</i>	$Ce^{4+} + e^- \leftrightarrow Ce^{3+}$	1610
<i>Mn(VI)/Mn(IV)</i>	$MnO_4^- + 4H^+ + 3e^- \leftrightarrow MnO_2 + 2H_2O$	1679
<i>Ag(II)/Ag(I)</i>	$Ag^{2+} + e^- \leftrightarrow Ag^+$	1980

2.4.3 HNO₃ medium with Metallic Elements

In the framework of the spent fuel treatment process, metallic elements can be in contact either with SS and HNO₃ medium acting as an electrolyte. If the corrosion potentials of the steel and of the metallic elements are different in the HNO₃ medium, a corrosion cell forms and galvanic corrosion occurs. The metallic elements which can be in contact with SS and might be responsible for galvanic corrosion can have several origins:

- Structural materials of some specific nuclear fuels (Al, graphite).
- Fission products from irradiated fuels, and especially platinoids (Pd, Rh, Ru and Tc);
- Other structural materials of equipments in the plants (Zr and Ti) these equipments are connected to SS equipments by explosion-bonded junctions which are composed of Zr (or Ti) /Ta sheet/ SS [36].

Experience in HNO₃ allows at least, if not to establish a galvanic series, to classify the metallic elements in comparison with the corrosion potentials of Type 304L and Type 316L steels in their passive state. Table 2.2 summarizes this classification in hot and concentrated HNO₃: qualitatively and the trends are the same as the galvanic series in flowing seawater [36]. The corrosion mechanism of galvanic corrosion in HNO₃ is the same as in other aqueous electrolytes. It is explained by a classical Evans diagram. However, the cathodic reaction occurring on the more noble material is the reduction reaction of HNO₃ (2.1).

Table 2.2 Metallic elements susceptible to induce a galvanic corrosion of SS in hot and concentrated HNO₃ medium

Metallic elements less noble than 304L and 316L SS (passive state) (acting as anode in the galvanic coupling with steel)	Metallic elements more noble than 304L and 316L SS (passive state) (acting as cathode in the galvanic coupling with steel)
Al	Platinoids
Ti	Pt
Zr	graphite
Ta	Au
	Zircaloy

2.5 Techniques for Measuring the Tendency to IGC in Austenitic SS

2.5.1 Acid Tests

The ASTM standard test developed to detect IGC in austenitic SS are listed in Table 2.3.

ASTM A393 [5]

The ASTM A393 is commonly known as the “Strauss test”. Earlier it was used to test IGC of sensitized SS. The test specimen was exposed to boiling 15.7% H₂SO₄ + 5.7% CuSO₄ for 72 h and damage was measured by bending through 180° and examining the outside surface for accentuated IGC. This test was adequate for the high carbon austenitic SS alloys but its severity is not sufficient for low carbon austenitic SS alloys. This practice was discontinued in 1972. It was reintroduced as ASTM A708 in 1974 as a test that detect only severe sensitization, and discontinued again in 1993.

Practice E, A262, ASTM [22]

Strauss test was modified to incorporate contact with metallic copper during exposure. This accelerates the attack. Coupling of SS specimen with metallic copper move the corrosion potential in active direction. The testing time is reduced to 24 h. Specimen are classified as acceptable or unacceptable, depending on whether cracks that are seen in bent specimens.

Practice A, A262, ASTM [22]

The oxalic acid etch test is used to identify specimens of certain SS grades that are essentially free of susceptibility to intergranular attack associated with chromium carbide precipitates. It is a rapid test involving simple etching of the specimen. This test is used for acceptance of material but not for rejection of material. This may be used in connection with

the other evaluation tests to provide a rapid method for identifying those specimens that are certain to be free of susceptibility to rapid intergranular attack in these other tests.

Apparatus

Source of Direct Current: Battery, generator, or rectifier capable of supplying about 15 V and 20 A.

Table 2.3 Standard IGC tests for austenitic SS

ASTM Standard (Common Name)	Environment	Exposure	Evaluation	Species Attacked
A393 (Strauss)	15.7 % H ₂ SO ₄ + 5.7 % CuSO ₄ boiling	Several 72 h periods, Fresh solution in each period	Appearance after bending	Chromium-depleted area at carbides
A262, Practice A (Oxalic acid etch)	10 % H ₂ C ₂ O ₄ , anodic at 1 A cm ⁻² , ambient temperature	1.5 min	Type of attack	Chromium – depleted area at carbide
A262, Practice B	50 % H ₂ SO ₄ + 2.5 % Fe ₂ (SO ₄) ₃ , boiling	One 120 h period	Weight loss per unit area	Chromium – depleted area at carbides and at sigma phase
A262, Practice C (Huey)	65 % HNO ₃ , boiling	Five 48 h periods, fresh solution in each period	Average weight loss per unit area	Chromium – depleted area at sigma and carbide and other phases
A262, Practice E (Copper Accelerated Strauss)	15.7 % H ₂ SO ₄ + 5.7 % CuSO ₄ , specimen in contact with copper boiling	One 24 h period	Appearance after bending	Chromium-depleted area at carbides
A262, Practice F	50 % H ₂ SO ₄ + CuSO ₄ , solid copper in solution, not in contact with specimen, boiling	One 120 h period	Weight loss per unit area	Chromium-depleted area at carbides

Ammeter: Range 0 to 30 A

Variable Resistance

Large Electric Clamp: To hold specimen to be etched.

Electrodes of the Etching Cell: The specimen to be etched is made as anode, and a SS beaker or a piece of SS as large as the specimen to be etched is made as cathode.

Metallurgical Microscope: For examination of etched microstructures at 250 X to 500 X diameters.

Procedure

The specimen is polished to achieve mirror finish. The polished specimen is etched in oxalic acid, ($\text{H}_2\text{C}_2\text{O}_4 \cdot 2\text{H}_2\text{O}$), reagent grade, 10 weight% solution at 1 Acm^{-2} for 90 S. Following etching, the specimen is rinsed in hot water and in acetone or alcohol. Rinsing avoids crystallization of oxalic acid on the etched surface during drying. The etched surface is examined on a metallurgical microscope at 250X to 500X for wrought steels and at about 250X for cast steels. The microstructure of specimen can be classified as follows.

Step Structure: Steps only between grains, no ditches at grain boundaries as shown in Fig.2.20 [22].

Dual Structure: Some ditches at grain boundaries in addition to steps, but no single grain completely surrounded by ditches as shown in Fig.2.20 [22].

Ditch Structure: One or more grains completely surrounded by ditches as shown in Fig.2.20 [22].

Materials showing “step” microstructure (no precipitation of chromium carbides at grain boundaries) or “dual” microstructure (discontinuous chromium-depleted regions at the grain boundaries but no single grain completely encircled) are considered resistant to IGC. However materials showing “ditch” microstructure (continuous chromium-depleted regions at the grain boundaries for at least one grain) may be susceptible to IGC in HNO_3 medium.

As practice A is not a rejection test, such materials have to be tested as per practice C, A262, ASTM [22].

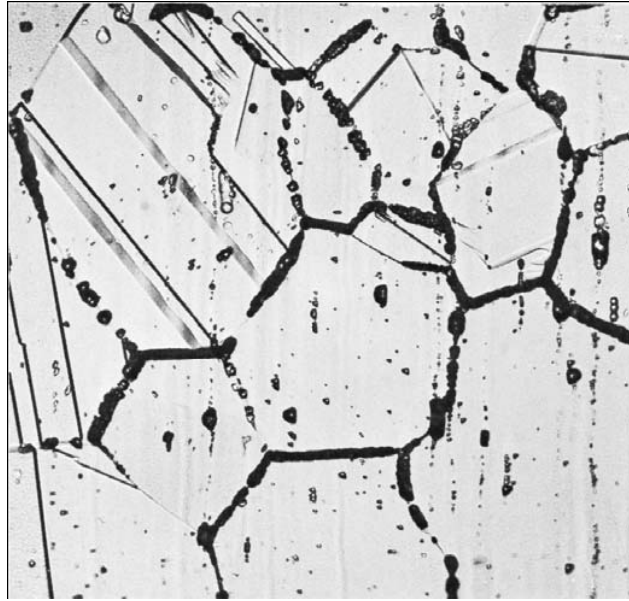
Practice B, A262, ASTM [22]

Practice B A262 ASTM (ferric sulfate–sulfuric acid test) detects susceptibility to IGC associated with the precipitation of chromium carbides in unstabilized austenitic SS. It does not detect susceptibility to IGC associated with sigma phase in wrought austenitic SS containing molybdenum, such as Types 316, 316L, 317, and 317L. The ferric sulfate–sulfuric acid test will detect IGC associated with sigma phase in the cast SS CF-3M and CF-8M.

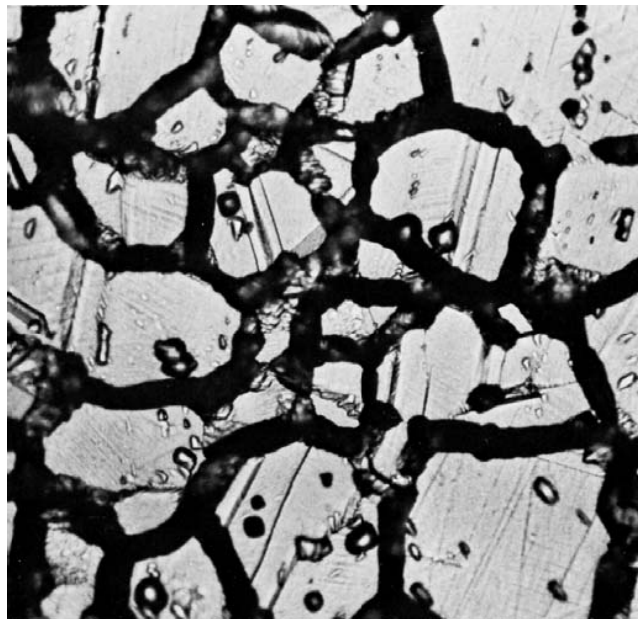


(a)

Fig. 2.20 (a) “step” microstructure (500X). (b) “dual” microstructure (250X) and (c) “ditch” microstructure (500 X) [22].



(b)



(c)

Fig. 2.20 continued

Practice C, A262, ASTM [22]

This test is used to measure the relative susceptibility of austenitic SS to IGC in boiling HNO_3 . The presence or absence of IGC in this test is not necessarily a measure of the performance of the material in other corrosive environments. This test does not provide a basis for predicting resistance to forms of corrosion other than IGC. Specimens of extra-low-

carbon and stabilized grades are tested after sensitizing heat treatments. Sensitizing heat treatment is conducted at 650 to 675 °C, which is the range of maximum carbide precipitation. The maximum permissible corrosion rate in this test is determined by duration of this sensitizing heat treatment. Commonly heat treatment at 675 °C for 1 h is used for sensitization [22].

This test is conducted in Erlenmeyer flask equipped with a cold finger-type condenser. A sufficient quantity of HNO₃ test solution is used to cover the specimens and to provide a volume of at least 20 mL cm⁻² of specimen surface. Normally, a volume of about 600 cm³ is used. The specimens are placed in the acid in the container and then cooling water is passed through the condenser. Acid solution is boiled on the hot plate and then kept boiling throughout the test period (48 h). After each test period, specimens were rinsed with water and scrubbed with rubber or a nylon brush under running water to remove any adhering corrosion products. After which they are dried and weighed. The procedure is repeated for five test periods of 48 h each. The effect of the acid on the material is measured by determining the loss of weight of the specimen after each test period and for the total of the test periods. The corrosion rates are usually reported as mils per year, calculated using following rate of corrosion equation:

$$r = \frac{472 \times 7290 \times W}{A \times d \times t} \quad (2.8)$$

where:

r = corrosion rate, mils per year

t = time of exposure, h,

A = total surface area, cm²,

W = weight loss, g, and

d = density of the sample, g cm⁻³

for chromium-nickel steels, $d = 7.9 \text{ g cm}^{-3}$

for chromium-nickel-molybdenum steels, $d = 8.0 \text{ g cm}^{-3}$

2.6 Grain Boundary Engineering

The concept of grain boundary design and control was introduced by Watanbe [96] and since then it is called Grain Boundary Engineering. Besides grain size, bulk properties of polycrystalline materials are affected by the grain boundary character distribution (GBCD) and connectivity of grain boundaries. Grain boundary engineering emphasizes on this fact and it involves tailoring of properties of polycrystalline materials through optimum thermomechanical process (optimum combination of amount of deformation, annealing temperature and annealing time). The favourable GBCD is achieved by optimum combination of these three parameters namely amount of deformation, annealing temperature and annealing time.

2.6.1 Grain Boundaries and its Classification

Grain boundaries are boundaries that separate adjacent crystals (grains) with identical chemical composition and crystallography, that differ only by mutual misorientation of their crystal lattices [97]. Regular atomic packing is disrupted at the grain boundary. In most crystalline solids, a grain boundary is very thin (one/two atoms). Disorder is unavoidable for geometrical reasons at the grain boundaries. Therefore grain boundaries have large excess free energy. Grain boundaries vary a great deal in their characteristics (energy, mobility and chemistry). Many properties of a material - and also processes of microstructural evolution depend on the nature of the grain boundaries. Materials can be made to have good or bad corrosion properties, mechanical properties depending on the type of grain boundaries present. Some grain boundaries exhibit good atomic fit and are therefore resistant to sliding, show low diffusion rates, low energy, etc.

Grain boundaries can broadly be classified in two categories: low-angle grain boundaries and high-angle grain boundaries. Low-angle grain boundaries are boundaries in which the difference in the orientation across the boundary may be only at most a few

degrees. A low-angle grain boundary contains a relatively simple arrangement of dislocations. High angle grain boundaries are boundaries of rather high surface energy and the difference in the orientation across the boundary is high. A system tends to reduce its total energy by interaction of grain boundaries with other lattice defects, such as solute or impurity atoms. Consequently these atoms accumulate at the grain boundaries. In this way grain boundary may become qualitatively different in chemical nature as compared to the bulk. As a result, further changes of grain boundary properties such as plasticity (temper embrittlement) or chemical resistance (corrosion cracking) occur.

The atomic arrangement in a perfect crystal is determined by the minimum of free energy. Any deviation of the atomic arrangement from ideal positions causes an increase of the free energy. Therefore atoms will remain close to their ideal position. At certain misorientations between two grains, crystallographic planes exist that transcend the grain boundary from one grain to the other, i. e. certain atomic positions in the grain boundary coincide with ideal positions in both neighboring grains. These atomic positions are termed coincidence sites and the super lattice containing these sites on the other hand is called coincidence site lattice (CSL). The elementary cell of the CSL is self-evidently larger than the elementary cell of the crystal lattice and its volume may be calculated in terms of the lattice parameters of the crystal lattice. The CSL is characterized by the density of its coincidence sites, which in turn are defined by the quantity Σ . Quantity Σ is the reciprocal density of coinciding atomic lattice sites [98] Since coincidence sites are representations of atoms located at ideal fit positions, it is safe to assume that grain boundaries preferably stretch along coincidence sites. Grain boundaries containing a high density of coincidence sites are called CSL boundaries or special boundaries. Grain misorientations are determined using Electron Backscattered Diffraction (EBSD) technique [98].

EBSD is a scanning electron microscope (SEM) based technique that involves positions of an electron beam on a specimen surface and relating the resulting diffraction pattern (Kikuchi lines) to its original position on the specimen to obtain crystallographic information. In this way, grain misorientations can be easily evaluated and the nature of a grain boundary is determined by extrapolating the orientation of the two grains and calculating the nature (Σ) of the grain boundary. On the basis of that, any grain boundary can be classified as either special or random. A classification of special boundaries require a coincidence site lattice (CSL) value, Σ , of less than or equal to 29 [99]. This Σ -value is based upon the reciprocal density of coincident atomic lattice sites between two grains assuming interpenetration between one and another. Low value indicates better fit between two grains and lower interfacial energy. Since exact CSL misorientations are unusual, a grain boundary's measure value is allowed to deviate to a maximum angle, which is calculated by Brandon's criterion [100] or more restrictive Palumbo-Aust criterion [101].

2.6.2 Methods of Grain Boundary Engineering

Grain boundary engineering (GBE) is a group of thermo-mechanical process to tailor GBCD to improve various material properties. GBE is an iterative process and most of the time it involves more than one cycle of cold-working and subsequent annealing [98]. Usually GBE is applied to fcc materials with low stacking fault energy (SFE). Common example of these materials include austenitic SS, nickel-base alloys, copper alloys and lead alloys [98]. Low SFE materials allow $\Sigma 3$ twins to proliferate easily during annealing process (after cold-working) and therefore, twins account for the larger part of the special boundary fraction increase in nearly every case, leading to more accurate level of twin-related grain boundary engineering [98]. Twin boundaries are low energy segments and are more resistant to segregation, corrosion and cracking. Two types of GBE processes viz. strain annealing and

strain recrystallization use distinctly different routes. GBE can be accomplished through either process as long as twin generation can take place.

2.7 Scope of the Present Study

Based upon the literature survey it was found that even though the mechanism of different forms of corrosion of austenitic SS in HNO₃ medium has been investigated, the correlation between potential developed on SS and corrosion rate, for different metallurgical conditions such as (chemical composition, and microstructure, grain size and grain boundary character) of SS and environmental conditions (.acid concentration and temperature) have not been addressed to date. The potential developed in HNO₃ is a function of concentration of acid, temperature and the concentration of specific oxidizing ions. In this work potential has been applied to SS in near boiling HNO₃ for 48 hours and the resultant corrosion rate is measured. Attempts were made to explore possible relation between the applied potential (in passive to transpassive potential range) and the corrosion rate. Effect of various material parameters such as microstructure, chemical composition, grain size, and grain boundary character on corrosion of SS at transpassive potential regimes have been studied. The effect of acid concentration and temperature on corrosion behavior of SS at transpassive potential were investigated. The causes and mechanism of “End Grain Corrosion” is not significantly investigated. An attempt has been made to investigate the causes of End Grain Corrosion. This work includes corrosion experiments in near boiling HNO₃, corrosion experiments in boiling HNO₃ containing hexavalent Cr⁶⁺ ions, measurement of open circuit potential (OCP) and polarization in HNO₃ at near boiling temperature, morphological study of corrosion attack by optical microscopy and SEM, grain boundary character study by EBSD. The results can be used as on-line technique for predicting corrosion rate based on potential measurement. A “safe/limiting” OCP has been established that would keep the structural material safe from corrosion attack in the plants and can be used as a “control parameter”

during plant operation. Attempts were also made to understand the mechanism of “End Grain Corrosion”.

CHAPTER 3

MATERIALS AND EXPERIMENTAL METHODOLOGY

This chapter includes experimental methodologies used in the present investigation. This comprises of materials of investigation and experimental techniques such as microstructure characterization techniques, electrochemical techniques, weight loss techniques and surface morphological techniques that have been used in the present study.

3.1 Materials and Processing

The materials used for this study were AISI (american iron and steel institute) (Type 304L CP (commercial purity), Type 304L NAG and Type 310L austenitic SS alloys. The chemical composition of the materials is reported in Table 3.1. It should be noted that the Ni content in Type 304L1 used in this study is 7.95 wt % against the specified limits of 8 wt % to 12 wt %.[102]. Type 304L1 was cold-rolled by unidirectional rolling in a laboratory rolling mill to obtain a thickness reduction by 5 %. These alloys were subjected to heat treatment as per requirement of various investigations. The heat treatments given to various materials are mentioned in Table 3.2. The size of the specimen prepared for the investigation varies depending upon the suitability and requirement of the particular experimental technique.

Table 3.1 Chemical composition of austenitic SS alloys used in the present study (wt %)

Elements	Composition (wt %)				
	Type 304L1	Type 310L	Type 304L NAG 1	Type 304L NAG2	Type 304L2
Fe	balance	balance	balance	balance	balance
Cr	18.0	24.3	18.7	18.0	18.1
Mn	1.47	1.63	1.58	1.17	1.54
Ni	7.95	20.17	10.19	10.87	8.00
C	0.024	0.011	0.014	0.012	0.023
S	0.003	0.0005	0.004	0.003	0.007
P	0.034	0.019	0.024	0.018	0.04
Si	0.49	0.09	0.31	0.25	0.04

3.2 Microstructural Characterization

The specimens of appropriate dimensions were cut from the Type 304L1, Type 310L Type 304L NAG1, Type 304L NAG2 and Type 304L2. The microstructure was evolved using practice A, A 262, ASTM in as-received condition and after heat treatment of these specimens. Cross sectional and longitudinal sections of as- received and heat treated specimens were mounted in cold setting resin. Such sections were ground with silicon carbide papers and final polishing was done with a diamond paste to obtain 1 μm finish. The specimens were degreased in soap solution, rinsed in water and then dried with acetone. Electrolytic etching of the specimens was carried out in 10 % oxalic acid solution at a current density of 1 A cm^{-2} for 90 s as per practice A, A 262, ASTM [22]. Fig. 3.1 shows the test specimen used for the microstructural study. Practice A, A 262, ASTM was carried out to evaluate the presence of chromium depletion and/or chromium rich carbide (M_{23}C_6) at the

grain boundaries. The microstructures revealed after practice A, A 262, ASTM were classified as: (I) “step” (i.e. no chromium carbide/chromium depletion regions at the grain boundaries), (II) “dual” (i.e. discontinuous chromium carbide/chromium depletion regions at the grain boundaries) and (III) “ditch” (i.e. at least one grain having complete encirclement with chromium carbide/chromium depletion regions) as shown in Fig. 2.20 in chapter 2 [22].

Table 3.2 Heat treatments used in the present study

Materials	Heat Treatment
Type 304 L1	675 °C for 1h
Type 304 L1	675 °C for 142 h
5 % cold-rolled Type 304L 1	927 °C for 72 h
Type 304L 2	675 °C for 1 h
Type 304L 2	1050 °C for 45 min then 675 °C for 1 h
Type 304L 2	1050 °C for 2 h then 675 °C for 1 h
Type 310L	675 °C for 1 h
Type 304L NAG 1	675 °C for 1 h
Type 304L NAG 1	675 °C for 171 h
Type 304L NAG 2	650 °C for 3 h
Type 304L NAG 2	650 °C for 100 h
Type 304L NAG 2	650 °C for 100 h and then 950 °C for 90 min
Type 304L NAG 2	990 °C for 5 min



Fig. 3.1 Photograph of Type 304L NAG 1 specimen mounted in cold setting resin for microstructure evolution.

3.3 Electrochemical Techniques

3.3.1 Double Loop Electrochemical Potentiokinetic Reactivation

Test

Double loop electrochemical potentiokinetic reactivation (DL-EPR) test was carried out on the austenitic SS specimens in as-received condition as well as after the heat treatment to establish its degree of sensitisation [103-109]. DL-EPR tests for austenitic SS specimens were conducted in a solution of 0.5 M H_2SO_4 + 0.01 M KSCN at room temperature. In this test solution potassium thiocyanate acts as a catalyst. The tests were carried out in a conventional three-electrode cell (Fig.3.2) using a platinum foil as the auxiliary electrode and a saturated calomel electrode (SCE) as reference electrode. The working electrode was the austenitic SS specimen embedded in the epoxy resin (Fig. 3.3). Specimen was polished with a diamond paste to a finish of $1\mu m$, degreased with soap solution, rinsed with water and allowed to dry after rinsing with acetone before each experiment. Prior to each experiment, deaeration of the test solution was done by bubbling purified argon gas for about 1 h and deaeration was continued during the experiment. Before each measurement, the specimen was cathodically polarised at -1 V (vs. SCE) for 60 s to remove the air-formed oxide film.

After steady-state open circuit potential (OCP) had developed, the DL- EPR test was initiated by scanning the potential in the anodic direction at 100 mV min^{-1} until the potential of 0.3 V (vs. SCE) was reached (forward scan), and then the scan was reversed in the cathodic direction until the OCP was reached (reverse scan) at the same scan rate [Fig 3.4]. The highest current density shown by the anodic curves during the forward scan and the reverse scan are referred to as the activation peak current density (i_a) and reactivation peak current density (i_r) respectively [Fig 3.4]. The DL-EPR value which is the ratio of i_r to i_a multiplied by 100 (equation 3.1) was calculated from the tests and is taken as an indication of Cr-depletion in the sample.

$$\text{Degree of sensitization (\%)} = \frac{i_r \times 100}{i_a} \quad (3.1)$$

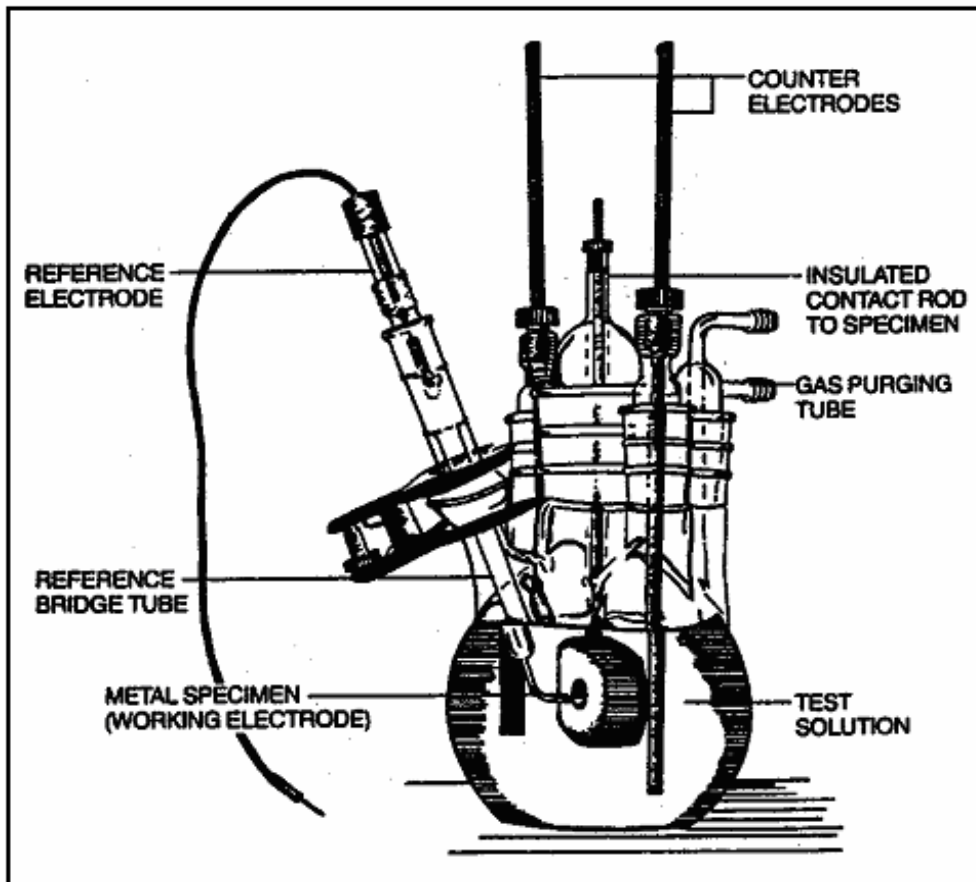


Fig. 3.2 Cross sectional view of an electrochemical cell for corrosion study [110].

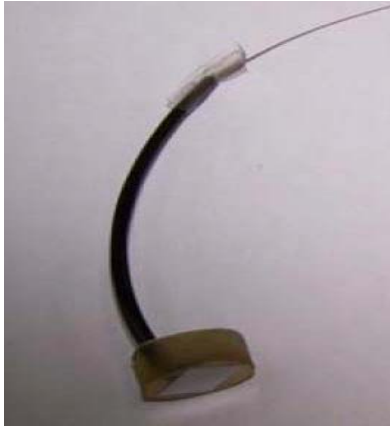


Fig.3.3 Photograph of specimen for DL-EPR test.

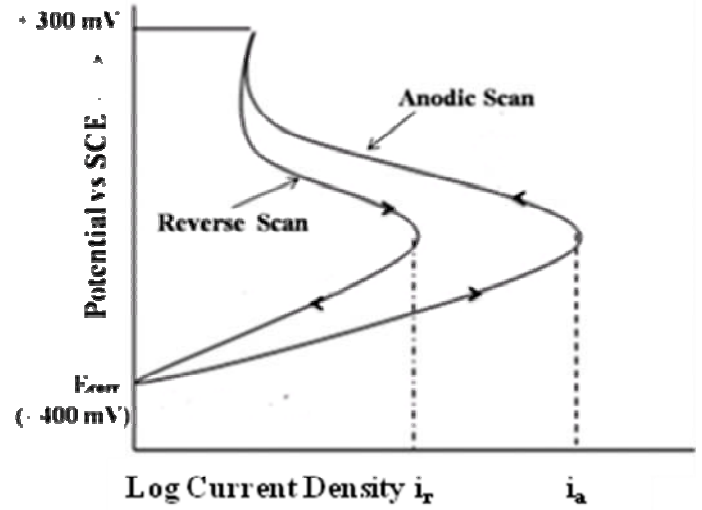


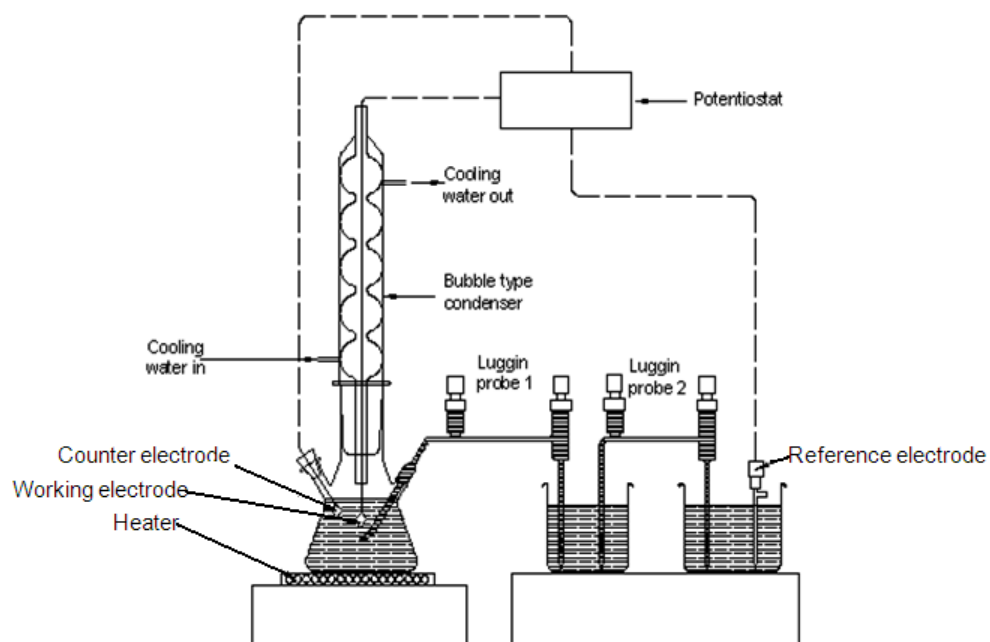
Fig.3.4 Schematic diagram of the DL-EPR test.

3.3.2 Potentiodynamic Polarization

The instrumentation for carrying out the polarization study consists of a potentiostat which maintains the potential of the working electrode according to the preset value. An electrometer was used for measuring the current produced due to the applied potential. Three electrodes system consist of (a) a working electrode (specimen to be tested), (b) a non-polarizable counter electrode for completing the circuit, (platinum foil was used for this purpose) and (c) a reference electrode (saturated calomel electrode) with respect to which potential has to be applied The experimental set up used in this study was the same as was used in a study carried out in our lab earlier and reported elsewhere [35] and is shown in Fig.3.5 [35]. Streicher used a similar set up for electrode potential measurements in boiling acid [37]. Temp and junction potential corrections were not applied as the solution used was highly conductive [37]. In this set-up calomel electrode was kept in a beaker filled with saturated potassium chloride solution. An acid bridge provided electrical connectivity while avoiding direct immersion of calomel electrode in near boiling HNO_3 . A second beaker was filled with test solution at room temperature. Temperature of test solution in a conical flask

was maintained at near boiling point by controlling voltage supply to heating mantle. Test specimens having a ratio of total cross-sectional area to the total surface area of 14 % were cut from the as-received materials. A 2 mm diameter hole was drilled on one side of the specimen. The specimens were ground on successively finer grits of emery papers till 600 grit was reached. The edges and corners were smoothed. Polished specimens were washed in soap solution, rinsed with water and dried with acetone. A SS wire was fastened through the hole on specimens to provide electrical contact. The connecting wire was covered by an insulative sheathing and the contact surfaces between the specimen and the wire were covered using a polytetrafluoroethylene (PTFE) tape. The test solution was 6M HNO₃ at a temperature close to boiling point (95± 2°C). The polarization curves were measured using a portable field potentiostat. The scan rate was maintained at 0.1 mVs⁻¹.

Polarization tests were performed on Type 304L1 in the as-received condition and after heat-treatment at 675 °C for 1 h and at 675 °C for 142 h. Type 304L NAG1 specimens in as-received condition and after heat-treatment at 675 °C for 1 h and at 675 °C for 171 h were subjected to polarization test. Polarization behavior of Type 310L (heat-treated at 675 °C for 1 h) was also studied.



(a)



(b)

Fig.3.5 Experimental set-up used for measurement or application of potential at 95 °C (a) schematic of set-up and (b) photograph of the actual set-up [35].

3.3.3 Potentiostatic Tests

In these experiments potentials were applied with the help of a potentiostat to an austenitic SS specimen immersed in the test solution for the whole duration of exposure (48 h). The values of the potential to be applied were determined based on the result obtained from polarization experiments and ranged from passive to transpassive potentials. The weight loss measured after the test shows effect of acid on the material. Weighing was done using an analytical balance of accuracy 0.0001 g. The corrosion rates were calculated in millimeter per year as per equation 3.2 [22]:

$$r = \frac{87480 \times W}{A \times d \times t} \quad (3.2)$$

where r is corrosion rate in millimeters per year, W is weight loss in grams, A is total exposed surface area (cm^2), d is density of sample (gcm^{-3}) and t is time of exposure (h).

The setup used for the application of potential to the test specimens was the same as described for ‘potentiodynamic polarisation experiments’ in section 3.3.2 (Fig 3.5). Specimens for these studies were prepared by the method described in section 3.3.2. The test solution was 6M HNO_3 at near boiling point for majority of these tests. It may be noted that to study the effect of HNO_3 concentration on corrosion behavior of austenitic SS test solutions used were 3M, 6M and 9M near boiling HNO_3 . Similarly to study the effect of solution temperature on corrosion behavior, solution temperature was varied in different tests.

3.3.3.1 Effect of alloy composition

To study effect of alloy composition on corrosion, three austenitic SS alloys namely Type 304L1, Type 304L NAG1 and Type310L were used. Specimens of all the three austenitic SS were heat treated at 675 °C for 1h followed by water quenching to simulate the worst microstructure in the HAZ of the weldment [4, 20, 22]. Potentiostatic tests were

conducted on these sensitized specimens in 6M near boiling HNO₃ as described in section 3.3.3.

3.3.3.2 Effect of microstructure

Type 304L1 and Type 304L NAG1 were used to study effect of microstructure on corrosion behavior. Specimens of these alloys were subjected to different heat treatment to produce “dual” and “ditch” microstructures. Heat treatment conditions to produce “ditch” microstructure was arrived at by subjecting several specimens to heat treatment of 675 °C for different periods followed by water quenching. A set of specimens of both the alloys were heat treated at 675 °C for 1 h and another set of specimens at 675 °C for 142 h. A set of specimens of Type 304L NAG1 were heat treated at 675 °C for 171 h. Potentiostatic tests on as-received as well as heat treated specimens were conducted in 6M HNO₃ as described in section 3.3.3 to establish a correlation between corrosion rate and applied potential.

3.3.3.3 Effect of grain size

Type 304L2 was used to study the effect of grain size on corrosion behavior at different applied potentials in 6M HNO₃ for a period of 48 h. A few specimens of as-received material were subjected to annealing heat treatment at 1050 °C for 45 min, and another set of specimens were annealed at 1050 °C for 2 h. Solution annealing heat treatment was done in Argon atmosphere followed by water quenching. As-received specimens and solution - annealed specimens were subjected to a sensitization heat treatment at 675 °C for 1 h followed by water quenching and exposed to potentiostatic test in near boiling 6M HNO₃ as described in section 3.3.3.

3.3.3.4 Effect of grain boundary engineering

To study the effect of grain boundary character distribution on corrosion behavior, Type 304 L1 was 5 % cold-rolled and then heat-treated at 927 °C for 72 h and designated as strain-annealed Type 304L1. EBSD (Electron backscattered diffraction) examination of as-

received Type 304L1 specimens and strain-annealed Type 304L1 specimens were carried out to establish GBCD (grain boundary character distribution). The procedure for EBSD examination will be given in section 3.6. As-received Type 304L1 specimens and strain-annealed Type 304L1 were subjected to potentiostatic tests in 6M near boiling HNO₃ (section 3.3.3). The potential was maintained at 0.99 V_{SCE} in these tests.

3.3.3.5 Effect of solution temperature

Type 304L NAG1 specimens heat treated at 675 °C for 1 h were used to study the effect of solution temperature on corrosion behavior. Specimens were exposed to 6M HNO₃ and temperature of solution was maintained at 55 °C, 75 °C, 85 °C and 95°C by controlling voltage supply to heating mantle in separate tests. Solution temperature was measured with the help of mercury thermometer before the test was started and also in between the test to check if there was any temperature fluctuation. A temperature fluctuation of ± 2.5 °C from the set temperature was observed in these tests. A potential of 0.99 V_{SCE} for 48 h was applied to the specimen in each test.

3.3.3.6 Effect of solution concentration

Type 304L1 specimens heat treated at 675 °C for 1 h were used to study the effect of solution concentration on corrosion behavior. HNO₃ solution of concentration 3M, 6M and 9M were used in three sets of potentiostatic tests (section 3.3.3) to establish effect of solution temperature on corrosion behavior. The test temperature was maintained at near boiling point.

3.4 Study of End Grain Corrosion by Weight Loss Techniques

Type 304 LNAG2 was used to study “End Grain Corrosion”. The specimen geometry and size were chosen such that the cross sectional area was 32 % of total surface area of the specimen. Specimens were subjected to heat treatments (listed in Table 3.2). The influence of these heat treatment on microstructural feature is given in Table 3.3. Specimens were polished on successively finer grits of silicon carbide papers to a finish with 600 grit, cleaned

with soap solution and dried with acetone. These specimens were used for practice C, A262, ASTM , “End Grain Corrosion” test, and OCP (open circuit potential) measurement.

Table 3.3 Heat treatment and its influence on the microstructure

Heat treatment	Influence on microstructural feature
650 °C for 3 h	Cr and P segregation [111]
650 °C for 100 h	P segregation [111]
650 °C for 100 h and then 950 °C for 90 min	Equilibrate segregations without altering grain size [30]
990 °C for 5 min	S segregation [112]

3.4.1 Practice C, A262, ASTM

This test was conducted on Type 304L NAG2 specimens in as-received condition and after heat treatment at 650 °C for 100 h and at 990 °C for 5 min. The objective of this test was to investigate whether these specimens are susceptible to IGC in HNO₃. Erlenmeyer flask equipped with cold finger type condenser was used for this test (Fig. 3.6). Specimens were exposed to 65 % boiling HNO₃ for 240 h (48 h x 5 periods). In each period fresh HNO₃ was used. It dissolves chromium carbide, chromium depleted zones and sigma phase [74]. Surface to volume ratio of specimen and solution is important from corrosion rate point of view, with increase in surface to volume ratio, corrosion rates are increased, and hence it is recommended that this ratio can be maintained at 20 mL cm⁻² [22]. The weight loss measured after each period was used to calculate corrosion rates by using equation 3.2 described in section 3.3 3. Test results can be reported as corrosion rate of individual period as well as average of five or three periods. In the reprocessing plants, the acceptable corrosion rates for material of construction depend on the position of the equipment (in cell or out of cell) and service fluid. However the corrosion rates for fabrication of critical equipments like dissolver are limited to 10 mpy.



Fig.3.6 Photograph of the set up used for Practice C, A262, ASTM.

3.4.2 End Grain Corrosion Test

This test was conducted to investigate Type 304LNAG2 susceptibility to “End Grain Corrosion”, in as-received condition and after selective heat treatment (Table 3.2). The test set-up and specimen preparation were similar as it is for Practice C, A262, ASTM (section 3.4.1). Modification was done in test solution and test periods. Following test solution and test periods were used.

9M HNO₃ + 1 g L⁻¹ Cr⁶⁺, four periods each of 24 h duration.

9M HNO₃ + 1.25 g L⁻¹ Cr⁶⁺, twenty periods each of 3 h duration.

9M HNO₃ + 1.5 g L⁻¹ Cr⁶⁺, twenty periods each of 3 h duration.

As-received as well as heat treated specimens were exposed to boiling 9M HNO₃ + 1 g L⁻¹ Cr⁶⁺ solutions for four periods each of 24 h duration in separate tests. Corrosion rate was calculated by weight loss measurement after each period. Specimens were washed in tap water and dried with acetone after the completion of fourth period. To study the morphology of pitting like attack longitudinal section of specimens were then mounted in cold setting resin and then ground with emery paper and final polishing was done with diamond paste to 1 μm finish. Polished specimens were then degreased with soap solution, cleaned with water

and dried with acetone. These specimens were then etched in 10 % oxalic acid solution for 20 s. The morphology of corrosion attack was then studied under optical and scanning electron microscope. The depth of “End Grain Corrosion” was measured with the help of inbuilt scale present in optical microscope. In order to study the effect of Cr^{6+} concentration on 304L NAG2 susceptibility to “End Grain Corrosion”, as-received specimens were exposed to boiling $9\text{M HNO}_3 + 1 \text{ g L}^{-1} \text{ Cr}^{6+}$, $9\text{M HNO}_3 + 1.25 \text{ g L}^{-1} \text{ Cr}^{6+}$ and boiling $9\text{M HNO}_3 + 1.5 \text{ g L}^{-1} \text{ Cr}^{6+}$ in two separate tests. Each exposure period was for 3 hours duration and the solution was refreshed after each period. The test was carried out for twenty periods in both the test solutions. The OCP of $9\text{M HNO}_3 + 1.25 \text{ g L}^{-1} \text{ Cr}^{6+}$ and $9\text{M HNO}_3 + 1.5 \text{ g L}^{-1} \text{ Cr}^{6+}$ solutions at near boiling temperature were recorded by using experimental setup shown in Fig. 3.5. (section 3.3.2).

3.5 Surface Morphological Characterization Techniques

3.5.1 Optical Microscopy

In the present work an optical microscope was used to study microstructures of as received as well as heat treated specimens after they were subjected to practice A, A262, ASTM. The morphology of corrosion attack on specimens after they were subjected to potentiostatic tests (section 3.3.3) and “End Grain Corrosion” test (section 3.4.2) were also studied with the help of optical microscope.

3.5.2 Scanning Electron Microscopy

In present investigation the corrosion attack on specimens exposed to “End Grain Corrosion” test (section 3.4.2) and specimens exposed to potentiostatic tests (section 3.3.3) were observed under SEM (scanning electron microscopy). SEM analysis was done in secondary electron imaging (SEI) and backscattered electron imaging (BEI) modes. In SEM analysis electron beam energy was kept 20 kV.

3.6 Electron backscattered diffraction examination

Type 304L1 and strain-annealed Type 304L1 specimens were analyzed using EBSD. The EBSD measurements were carried out after electropolishing the specimens in the solutions of methanol and perchloric acid (80:20 ratio) for 30 s at 15 V. The temperature of the solution was maintained at -35 °C by using dry ice. Type 304L1 specimen was used as anode and another piece of SS was used as cathode. The EBSD operating parameters such as an accelerating voltage of 20 kV, a beam current 16 nA, a step size of 1 μm, of each scan, camera and video setting were kept the same for all the specimens. For post processing of EBSD analysis, the TexSem Laboratories, orientation imaging microscopy (TSL OIM 6.1) software was used. The CSL (section 2.6.1 in chapter 2) boundary measurements were done as per Brandon's criteria $\Delta\theta = 15^\circ$ R-12 where $\Delta\theta$ is the angular deviation from the exact CSL boundary [100].

CHAPTER 4

ALLOY COMPOSITION AND MICROSTRUCTURE

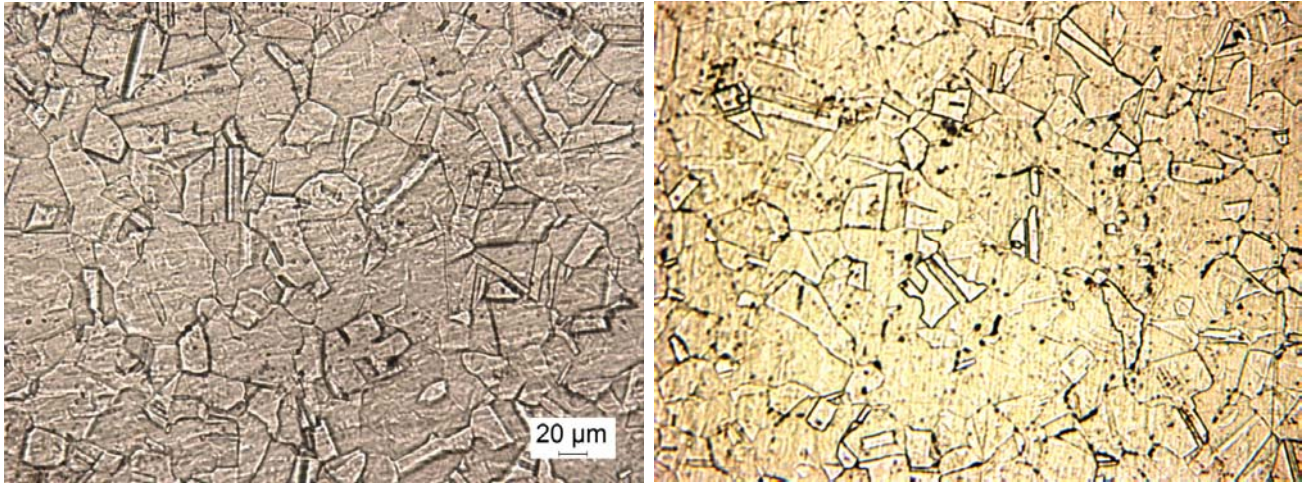
This chapter includes results on the investigations of the role of composition and microstructure (“step” “dual” and “ditch”) on corrosion behavior of austenitic SS in near boiling 6M HNO₃. Potentials were applied on Types 304L NAG1, 304L1 and 310L specimens exposed to in boiling 6M HNO₃ for a period of 48 h. The corrosion rates measured in such experiments were plotted as a function of applied potential. Threshold potential, above which IGC was observed, was established with the help of these plots. Below this potential, uniform and low rate of corrosion occurred. An equation derived from curve fitting of these data is proposed to be used for predicting the corrosion rates of a specific SS at any given operating potential. Corrosion behavior of Type 304L1, Type 304L NAG1 and Type 310L (all heat treated at 675 °C for 1h) were investigated and compared by Practice A, A262, ASTM, DL- EPR, Tafel polarization, potentiostatic experiments and morphological study. The differences in their corrosion behavior were attributed to the differences in their overall chemical composition. Type 304L1 and Type 304L NAG1 were subjected to various heat treatment in order to produce change in microstructure. The effect of microstructure on corrosion behavior of Type 304L1 and Type 304L NAG1 was investigated.

4.1 Results and Discussion

4.1.1 Degree of sensitization

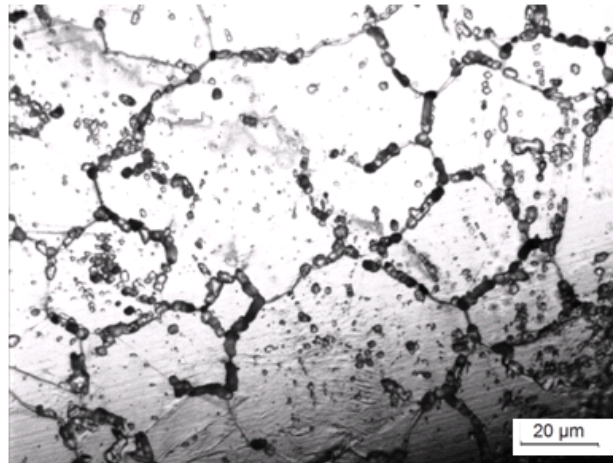
The microstructures of austenitic SS alloys after electroetching in the as-received condition and after different heat treatments are shown in Figs. 4.1-4.3. Type 304L1 showed “step” microstructure in the as-received condition (Fig. 4.1a), “dual” microstructure when heat-treated at 675 °C for 1 h (Fig. 4.1b) and “ditch” microstructure after heat treatment at 675 °C for 142 h (Fig. 4.1c). Type 304L NAG1 showed “step” microstructure in as-received condition (Fig. 4.2a), “dual” microstructure when heat treated at 675 °C for 1 h (Fig. 4.2b). A few specimens of 304L NAG1 were heat treated at 675 °C for 142 h in order to produce “ditch” microstructure. Type 304L NAG1 after heat treatment at 675 °C for 142 h retained “dual” microstructure (Fig. 4.2c). Therefore in order to produce “ditch” microstructure, a few specimens of Type 304L NAG1 were heat treated at 675 °C for a longer period. Microstructure of Type 304L NAG1 remained “dual” even after heat treatment at 675 °C for 171h (Fig. 4.2d). Microstructure of Type 310L in as-received condition is shown in Fig.4.3a and after heat-treatment at 675 °C for 1 h in Fig.4.3b.

DL-EPR tests have been performed to evaluate the degree of sensitization (DOS) and susceptibility to IGC of different types of SS [113-121]. It essentially measures the extent of Cr depletion induced by Cr_{23}C_6 precipitation at grain boundaries or by any other phase formations, e.g., σ phase [122-127]. Table 4.1 shows DOS for all the austenitic SS alloys in as-received condition as well as after different heat treatments. Among the three austenitic SS alloys, Type 304L1 showed the lowest DOS in as-received condition. However, when heat-treated at 675 °C for 1 h, Type 304L1 showed a higher value of DOS than Type 304L NAG1 and Type 310L.



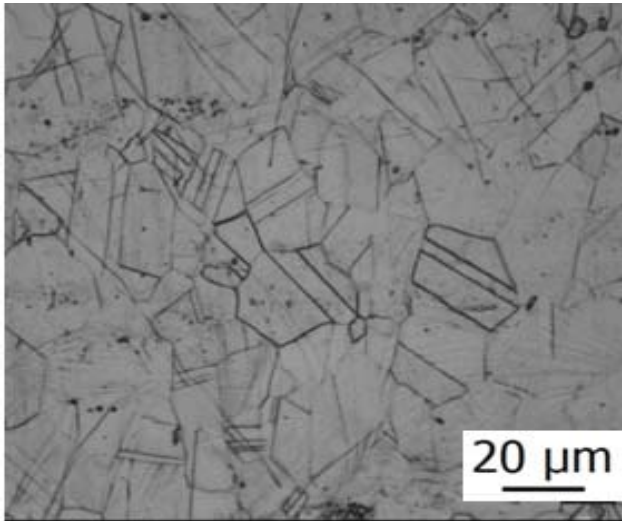
(a)

(b)

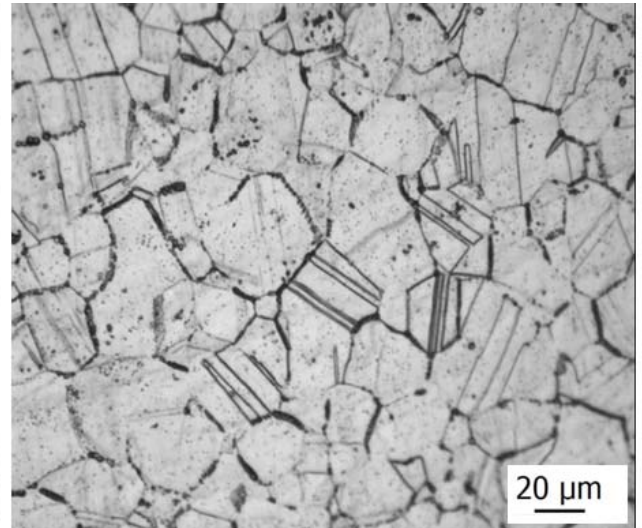


(c)

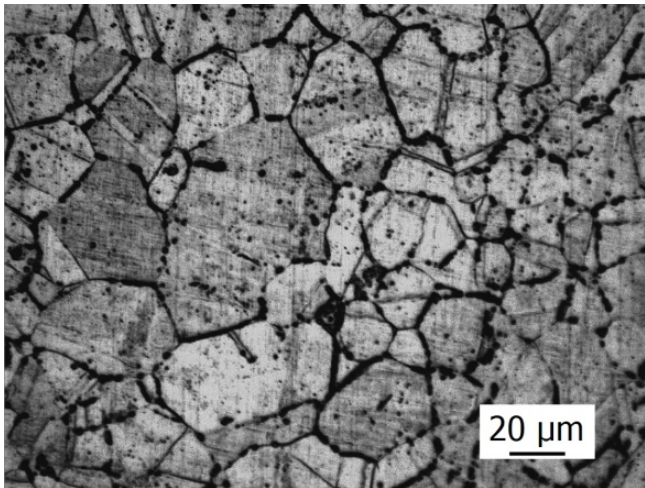
Fig.4.1 Microstructural characterization of Type 304L1 by optical microscope (a) as-received condition, (b) after heat-treatment at 675 °C for 1 h and (c) after heat-treatment at 675 °C for 142 h.



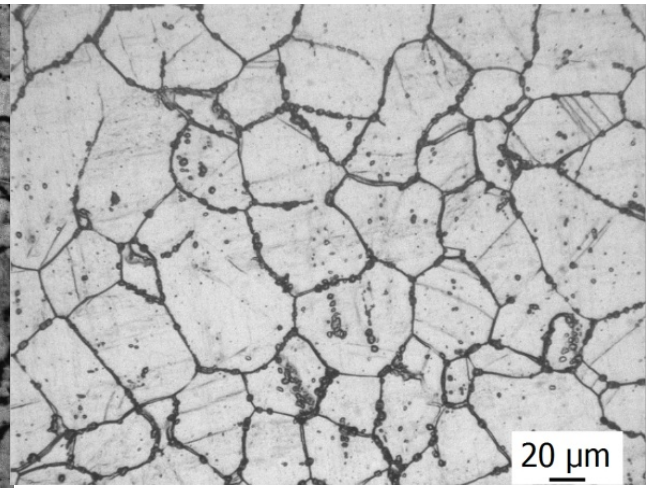
(a)



(b)



(c)



(d)

Fig. 4.2 Microstructural characterization of Type 304L NAG1 by optical microscope (a) as-received condition, (b) after heat treatment at 675 °C for 1 h, (c) after heat treatment at 675 °C for 142 h and (d) after heat treatment at 675 °C for 171 h.

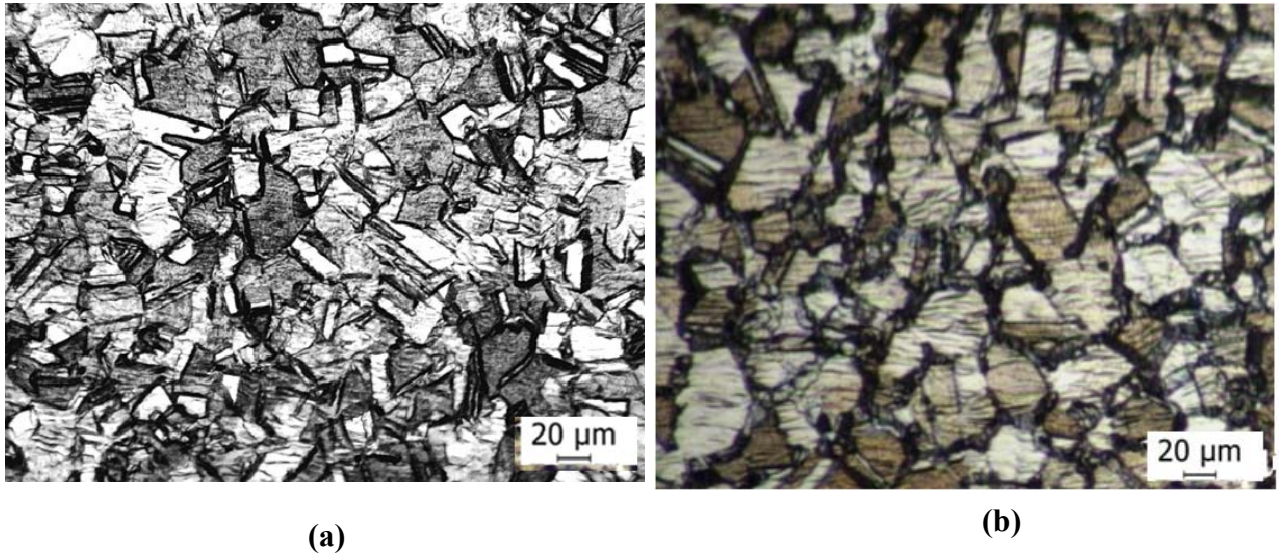


Fig. 4.3 Microstructural characterization of Type 310L by optical microscope (a) as-received condition and (b) after heat treatment at 675 °C for 1 h.

Type 304L1 specimen heat-treated at 675 °C for 142 h (“ditch” microstructure) gave the highest value of DOS among all the specimens. DOS for Type 310L in the as-received condition and after heat treatment at 675 °C for 1 h were same. This implies that Type 310L did not get sensitized by the heat treatment given to it. DOS values of Type 304L NAG1 specimens are (a) 0.14 for the as-received specimen (b) 0.50 for the specimen heat treated at 675 °C for 1h and (c) 0.17 for the specimen heat treated at 675 °C for 171h. These values indicated a very low value of DOS. Typically, a “ditch” microstructure is expected to have a DOS value of 5.0 or higher [103]. It has also been shown by systematic studies that it requires a DOS value above 5.0 to induce IGC in austenitic SS in practice C, A262, ASTM [103].

Table.4.1 Extent of sensitization for three Types of SS alloys in different heat-treated condition

Material	Heat treatment	Degree of sensitization (DOS) (%)	Microstructure
Type 304L 1	As-received	0.07	Step
	675 °C for 1h	0.7	Dual
	675 °C for 142 h	5.9	Ditch
Type 304L NAG1	As-received	0.11	Step
	675 °C for 1h	0.27	Dual
	675 °C for 171 h	0.17	Dual
Type 310L	As-received	0.38	Step
	675 °C for 1h	0.38	Dual

4.1.2 Potentiodynamic polarization behavior

Fig.4.4 shows the potentiodynamic polarization curves for the three austenitic SS alloys in near boiling 6M HNO₃. Anodic current density for Type 304L1 and Type 304L NAG1 was similar in the transpassive regime. The start of transpassive potential for these alloys was observed from Fig.4.4 to be 950–1000 mV_{SCE}. Anodic current density was lower for Type 310L than Type 304L1 and Type 304L NAG1 in the potential regime of 950–1000 mV_{SCE}. The E_{corr} was established using Fig.4.4. The i_{corr} was established by extrapolating the linear part of the cathodic current and establishing its intersection with E_{corr}. At E_{corr}, the corrosion rate (i_{corr}) for Type 304L1, 304L NAG1 and 310L were found to be 1.1 x 10⁻⁵, 9.7 x 10⁻⁶, and 5.7 x 10⁻⁶ Acm⁻² respectively. The cathodic current density was the highest for Type 304L1 and the lowest for Type 310L. The least rate of corrosion rate obtained in the case of Type 310L could be explained from higher contents of Cr and Ni in Type 310L compared to that in the other two alloys. Higher content of Cr is expected to lead to the formation of a

passive film containing a higher amount of chromium and hence more protective. For all the three austenitic SS alloys, the value of OCP is very close to transpassive potential (i.e. a potential where current density starts to increase) which shows low corrosion resistance for them at near boiling temperature in 6M HNO₃. Most electrochemical and chemical reactions proceed rapidly at higher temperatures and increasing the temperature aids in faster transition to transpassive state.

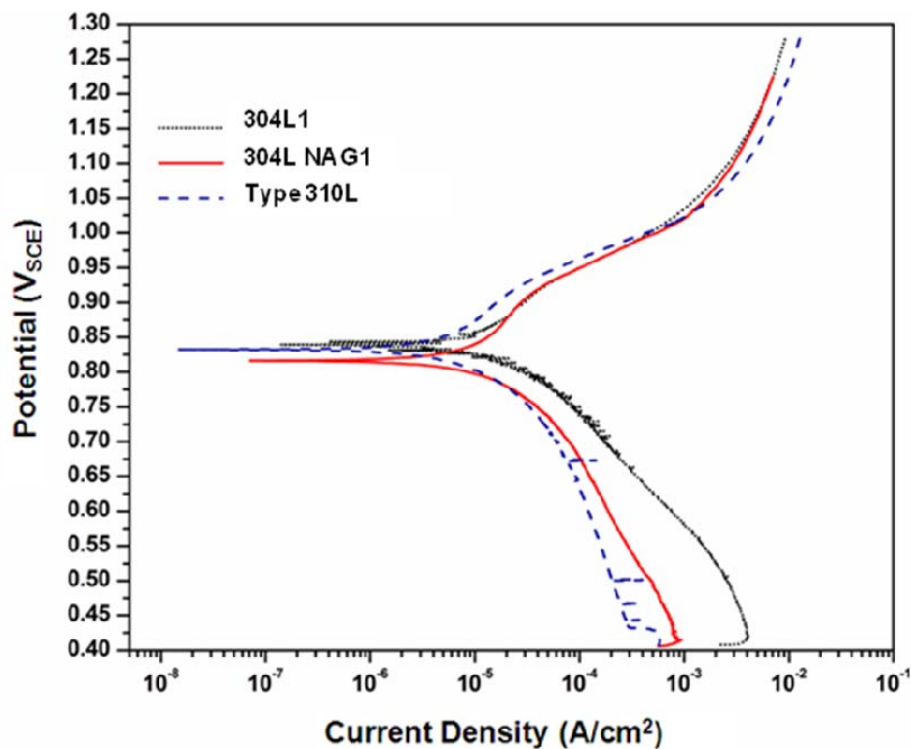


Fig.4.4 Polarization curves of austenitic SS alloys heat treated at 675 °C for 1 h in near boiling 6M HNO₃.

The polarization curves of Type 304L1 for “step” and “ditch” microstructure in near boiling 6M HNO₃ are shown in Fig.4.5. It shows nobler value of OCP for Type 304L1 having “step” microstructure than for “ditch” microstructure. More noble values of OCP (in the regime of “passivation” potentials) is indicative of faster growth of passive film and this depends on the nature of passive layer formed [5]. Fig.4.5 clearly indicated higher corrosion resistance of “step” microstructure than “ditch” microstructure at the chosen test parameters. Anodic current density for “ditch” microstructure was higher than that for “step”

microstructure. This indicated faster rate of dissolution of specimen having “ditch” microstructure. “ditch” microstructure represents a severe state of sensitization where at least one grain is completely covered by chromium carbide/chromium depletion region. Passive film formed over such a chromium-depleted region is weak and can easily be attacked in given test conditions.

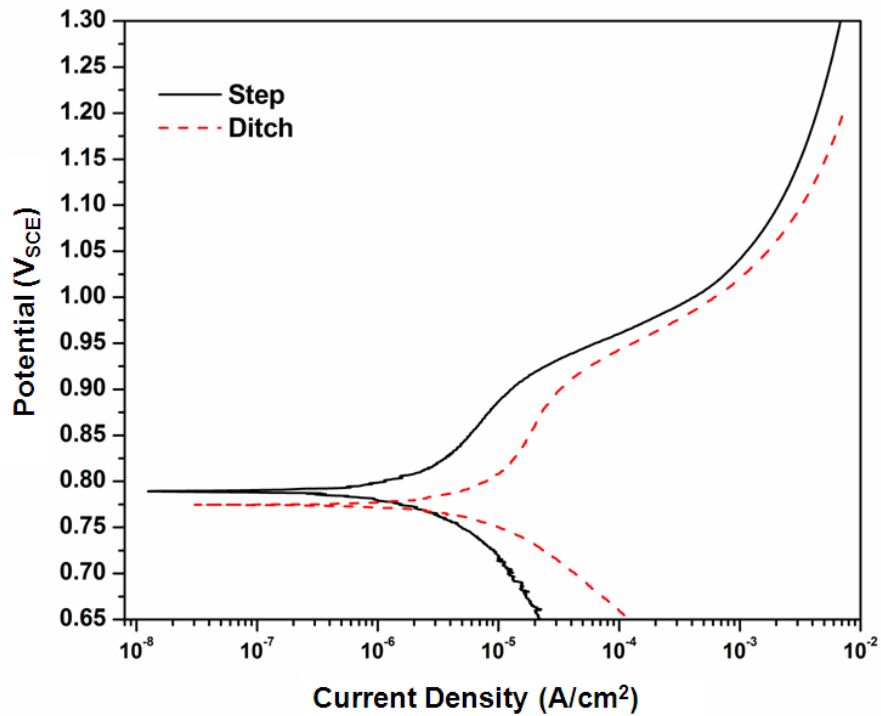


Fig 4.5 Polarization curves of Type 304L1 for “step” and “ditch” microstructure in near boiling 6M HNO₃.

Fig. 4.6 shows the potentiodynamic polarization curves for the Type 304L NAG1 in near boiling 6M HNO₃. For “step” as well as “dual” microstructure, the value of OCP was very close to transpassive potential (Fig. 4.6). Type 304L NAG1 having “dual” microstructure showed slightly lower value of transpassive potential compared to “step” microstructure.

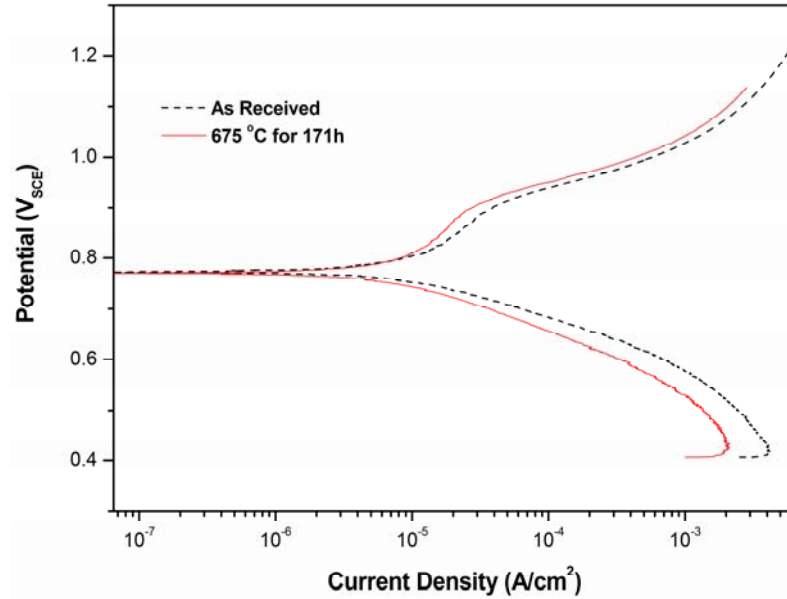


Fig. 4.6 Polarization curves of Type 304L NAG1 in near boiling 6M HNO₃.

4.1.3 Corrosion behavior of austenitic SS alloys in near boiling 6M HNO₃

Specimens of Type 304L1, Type 304L NAG1 and Type 310L heat treated at 675 °C for 1h were subjected to potentiostatic tests in near boiling 6M HNO₃ as described in section 3.3.3 of chapter 3. Corrosion rates (r) obtained from these tests data were plotted against applied potentials. Assuming an exponential dependence of corrosion rate on the applied potential, equation 4.1 was fitted to the data.

$$r = ae^{V/b} \quad (4.1)$$

where r is the corrosion rate (mm^{-1}) of SS upon exposure to near boiling 6M HNO₃ for a period of 48 h, V is the applied potential (V_{SCE}) and a and b are constants. Equation 1 can be rearranged to equation 4.2 which is a form of Tafel equation [1].

$$V = b \log \frac{r}{a} \quad (4.2)$$

The relationship between logarithm of corrosion rate (measured after 48 h exposures in near boiling 6M HNO₃) and applied potential was confirmed to be a linear function, as shown in Fig. 4.7. The constants calculated using equation 4.2 for the three SS alloys (heat-treated at 675 °C, for 1 h) used in this study (Fig.4.7) are shown in Table 4.2.

Table. 4.2 Constants calculated by fitting of equation 4.2 for the three SS alloys heat treated at 675 °C, for 1 h (Fig. 4.7)

Type of SS	a (mmy^{-1})	b (V_{SCE})
304L1	2.9×10^{-26}	0.0164
310L	9.9×10^{-22}	0.0202
304L NAG1	9.8×10^{-26}	0.0180

It is indicated from Fig.4.7 that at any given potential, Type 304L1 showed the highest corrosion rate and Type 310L showed the lowest corrosion rate. Type 304L NAG1 showed lower corrosion rates than Type 304L1. This matches well with the low corrosion rates of Type 304L NAG reported in boiling 65% HNO₃ (Practice C, A262, ASTM) test of 0.13-0.25 mmy^{-1} compared to $< 0.45 \text{ mmy}^{-1}$ for Type 304L. Results obtained from polarization experiment (Fig.4.4) indicated that Type 310L had the lowest anodic current density at the start of transpassive potentials (950–1000 mV_{SCE}). Fig.4.4 also showed that the cathodic current density for Type 310L was the lowest. These observations are in concordance with the results of potentiostatic experiments. It is to be noted that the potential at which a corrosion rate of 0.61 mmy^{-1} is observed was taken as the threshold potential in a previously reported study [35] as it is commonly accepted that severe IGC (grain dropping) takes place when corrosion rates are above 0.61 mmy^{-1} [16, 17, 21, 25, 29]. The threshold potential for Type 304L NAG1 after 675 °C, 1 h heat treatment (resulting in a “dual” microstructure) was

reported [35] to be $0.975 V_{SCE}$. From Fig. 4.7, it is indicated that the threshold potentials for Types 304L1, 304L NAG1 and 310L (each after heat treatment at $675\text{ }^{\circ}\text{C}$ for 1 h resulting in a “dual” microstructure) are 0.960 , 0.965 and $0.966 V_{SCE}$ respectively. Corrosion rates for SS below the threshold potential (i.e. up to $0.95 V_{SCE}$) are very low and are typical of corrosion rate of SS in the passivated condition below 0.51 mmy^{-1} .

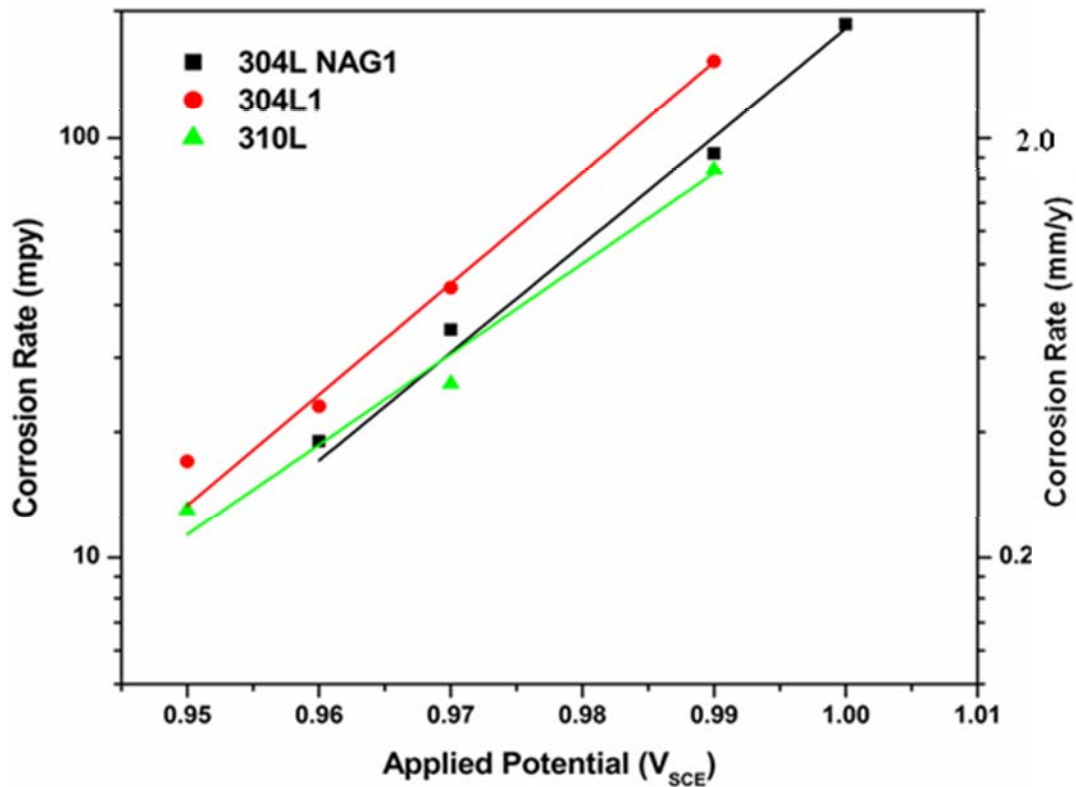


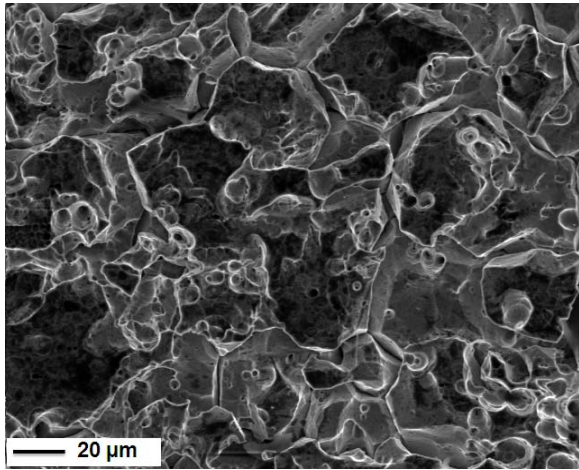
Fig. 4.7 Correlation between corrosion rate (r) and applied potential (V) for three Types of austenitic SS heat-treated at $675\text{ }^{\circ}\text{C}$ for 1 h exposed to near boiling 6M HNO_3 for 48 h.

These results indicated that potentiostatic application of potentials up to $0.95 V_{SCE}$ resulted in passivity being maintained on the SS specimens as only low rates of uniform corrosion could be observed on all the SS. This is not in agreement with potentiodynamic polarisation results where the current density increases from a much lower potential (Fig.4.4). This implies that there was a difference in the transpassive potential determined by the potentiodynamic and potentiostatic experiments. Similar difference of 200 mV in the pitting potentials for Type 304 SS has been reported in the chloride solution at room temperature

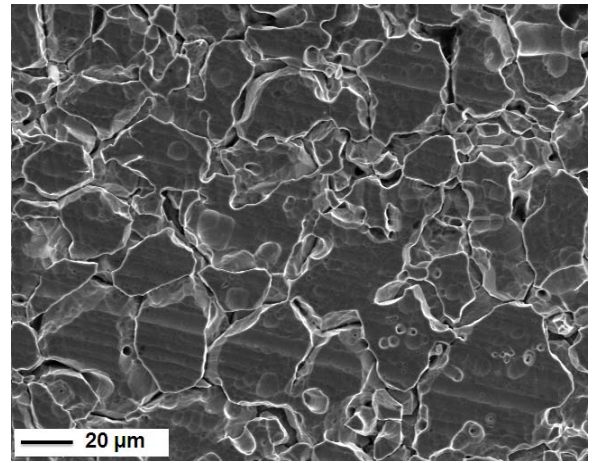
[127]. This difference in pitting potential was attributed to the pitting process not being disturbed by reactions at other potentials as the potential is maintained at a given (constant) value during the potentiostatic experiments. Therefore, the potentiodynamic polarisation curves (Fig.4.4) gave only a qualitative comparison of the corrosion tendency and could not be used to predict the corrosion rate of SS at a given applied/developed potential. The corrosion rate at an applied potential for a given duration of testing has to be determined by the potentiostatic technique. These threshold potentials would change slightly for a specific SS as also for the specific environment employed. In a given environment, e.g. near boiling 6M HNO₃, Fig.4.7 shows that Type 310L is the most resistant to onset of IGC in the transpassive potential regime followed by Type 304L NAG1 and 304L1. This is in line with the observation of lower current density for Type 310L in the potential regime of 950-1000 mV_{SCE} compared to that for Types 304L1 and 304L NAG1 as shown in Fig. 4.4.

Fig. 4.8 shows the morphology of corrosion attack on SS sensitized at 675 °C for 1 h exposed to near boiling 6M HNO₃ for 48 h at a potential of 0.99 V_{SCE}. It is evident from Fig. 4.8 that the nature of corrosion attack is intergranular. Maximum IGC was observed in Type 304L1 and the minimum in Type 310L.

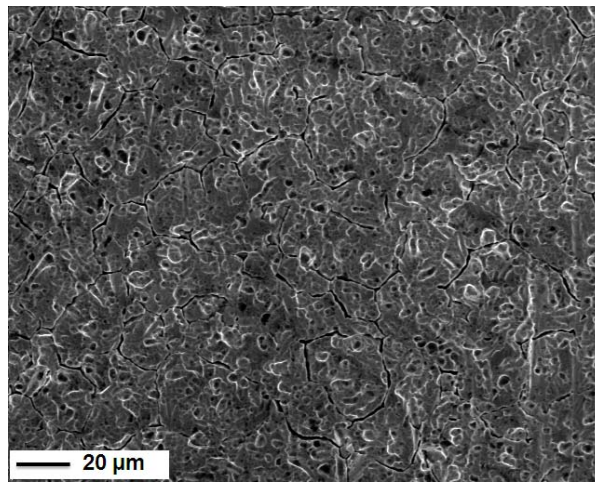
Fig.4.9 shows the morphology of corrosion attack after Type 304L1 (sensitized at 675 °C for 1 h) was exposed to near boiling 6M HNO₃ at potentials of 0.95 V_{SCE} and 0.99 V_{SCE} in two separate experiments. At 0.95 V_{SCE} (below the threshold potential) grain boundaries are slightly attacked (Fig. 4.9a) while at 0.99 V_{SCE} (above the threshold potential) severe IGC with dislodging of grains was observed (Fig. 4.9b). The corrosion rate at an applied potential of 0.96 V_{SCE} for Type 304L1 SS sensitized at 675 °C for 1 h was 0.58 mmy⁻¹.



(a)

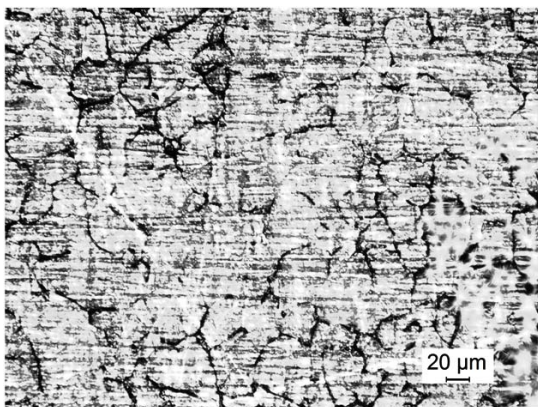


(b)

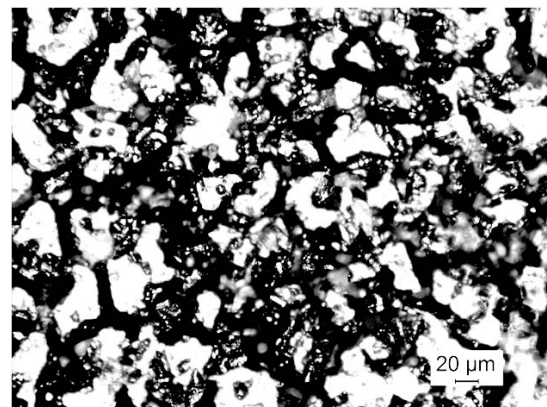


(c)

Fig. 4.8 IGC observed by SEM for (a) Type 304L1, (b) Type 304L NAG1 and (c) Type 310L each heat-treated at 675 °C for 1 h and exposed to near boiling 6M HNO₃ at 0.99 V_{SCE} for 48 h.



(a)

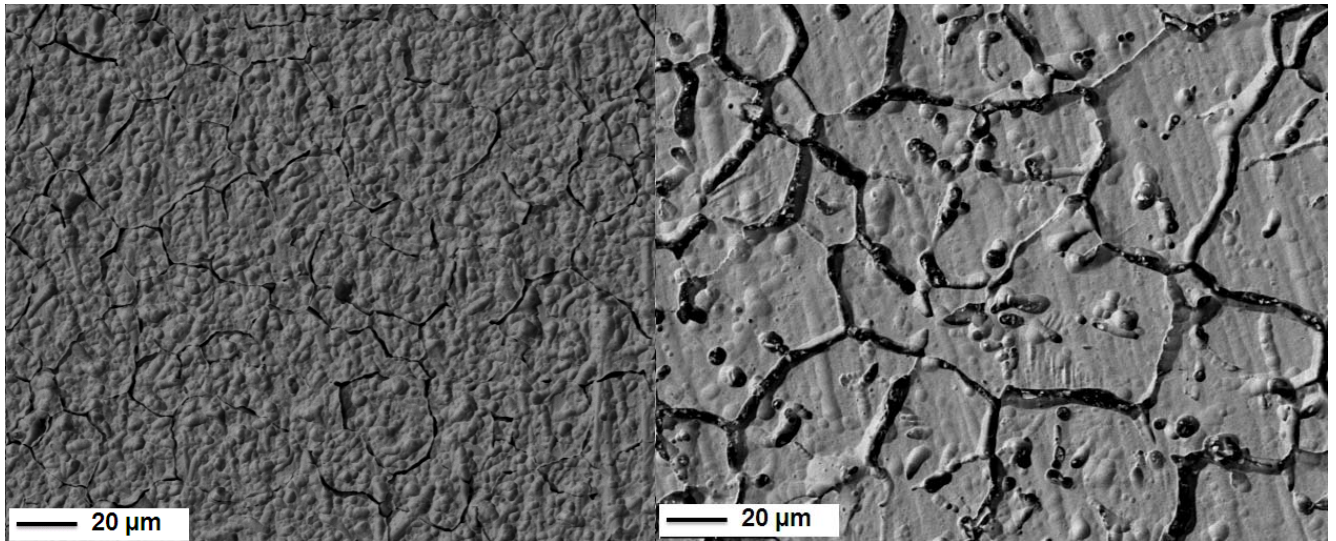


(b)

Fig. 4.9 IGC observed by optical microscope for Type 304L1 heat-treated at 675 °C for 1 h exposed to near boiling 6M HNO₃ for 48 h at (a) 0.95 V_{SCE} and (b) 0.99 V_{SCE}.

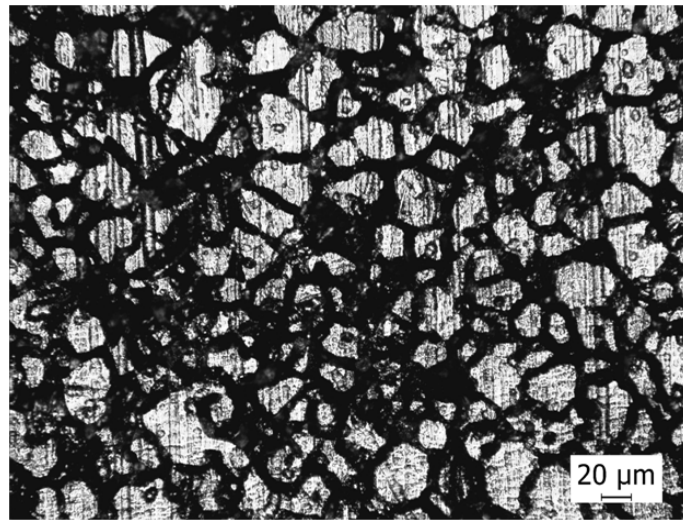
The mode of corrosion observed after Type 310L (heat-treated at 675 °C for 1 h) was exposed to near boiling 6M HNO₃ is shown in Fig.4.10a after application of applied potential of 0.960 V_{SCE} and in Fig. 4.10b-c after application of applied potential of 0.990 V_{SCE}. SEM images (Fig.4.10a-b) clearly indicate that with increase in applied potential, IGC became more severe and the optical micrograph (Fig.4.10c) clearly showed dislodging of grains at 0.990 V_{SCE} (this value is well above the threshold potential of 0.966 V_{SCE} for Type 310L). The IGC observed after Type 304L NAG1 (heat-treated at 675 °C for 1 h) was exposed to near boiling 6M HNO₃ is shown after application of applied potential of 0.960 V_{SCE} in Fig 4.11a and after application of applied potential of 0.990 V_{SCE} in Fig.4.11b and c. At 0.960 V_{SCE} (the potential is below the threshold potential of 0.966 V_{SCE}) beginning of attack at grain boundaries (with no grain dropping) was observed. Optical (Fig.4.11 b) as well as SEM micrograph (Fig. 4.11 c) clearly indicated that a potential of 0.990 V_{SCE}, which is well above the threshold potential, caused severe IGC with grain dropping. Specimens of Type 304L1 in as-received condition (“step” microstructure), heat-treated at 675 °C for 1 h (“dual” microstructure) and heat-treated at 675 °C for 142 h (“ditch” microstructure) were exposed to near boiling 6M HNO₃ at different applied potentials for a period of 48 h. The relationship between logarithm of corrosion rate and applied potential is confirmed to be a linear function, as shown in Fig. 4.12 for Type 304L1 having “step”, “dual” and “ditch” microstructures in near boiling 6M HNO₃. Type 304L1 with “step” microstructure and “dual” microstructure showed comparable corrosion rates at applied potentials of 0.950 – 0.975 V_{SCE}. However, beyond this potential range, Type 304L1 with “dual” microstructure showed higher corrosion rates. Type 304L1 with a “ditch” microstructure showed higher corrosion rates than those exhibited by “step” and “dual” microstructures at all the applied potentials. For all the three microstructures, corrosion rate increased exponentially with potential and the equation for

curve fitting is the same as equation 4.1. The constants a and b calculated for the three microstructures of Type 304L1 (Fig. 4.12) are shown in Table 4.3.



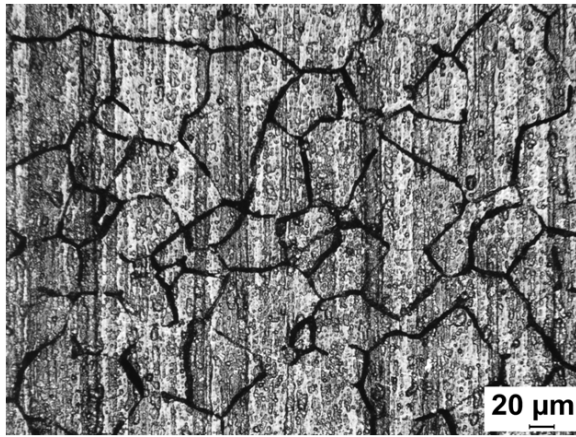
(a)

(b)

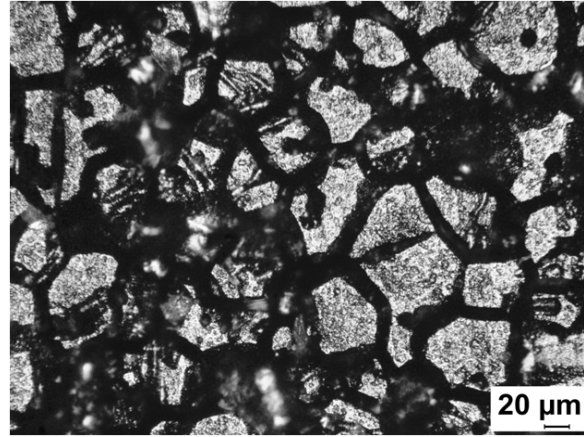


(c)

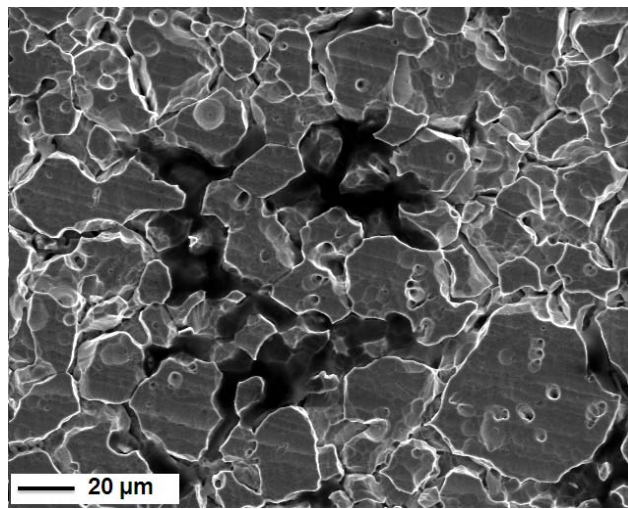
Fig. 4.10 IGC observed after Type 310L heat-treated at 675 °C for 1 h and exposed to near boiling 6M HNO₃ for 48 h at (a) 0.960 V_{SCE} under SEM, (b) 0.990 V_{SCE} under SEM and (c) 0.990 V_{SCE} under optical microscope.



(a)



(b)



(c)

Fig. 4.11 IGC observed after Type 304L NAG1 heat-treated at 675 °C for 1 h and exposed for 48 h to near boiling 6M HNO₃ at (a) 0.960 V_{SCE} under optical microscope, (b) 0.990 V_{SCE} under optical microscope and (c) 0.990 V_{SCE} under SEM.

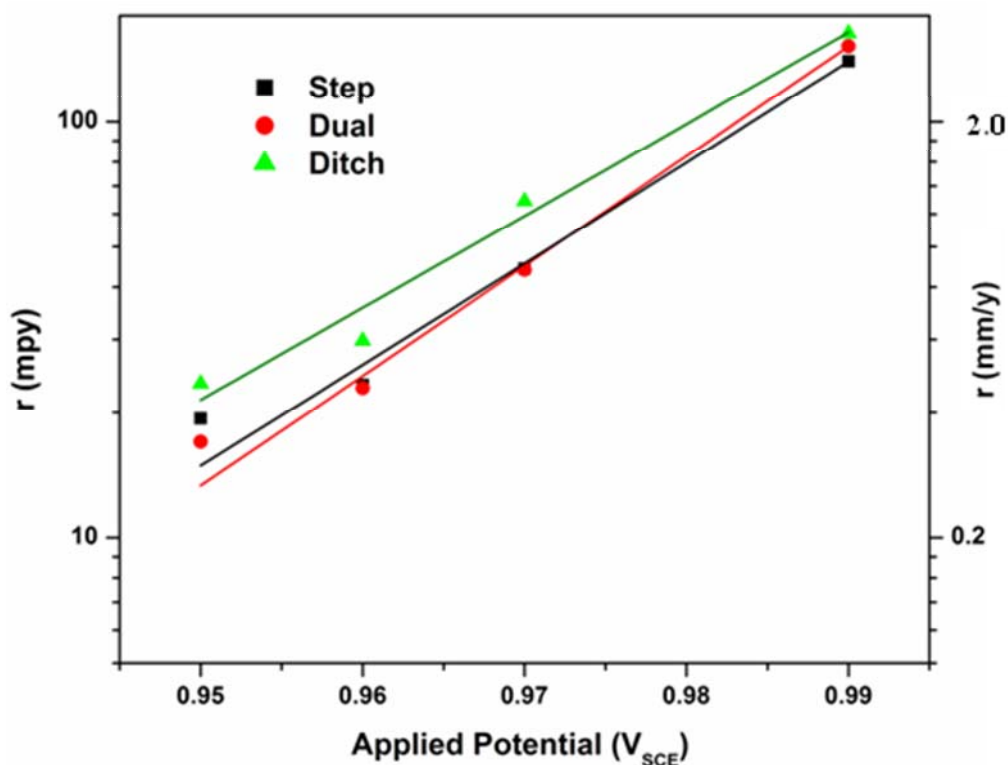


Fig.4.12 Correlation between corrosion rate (r) and applied potential (V) for “step”, “dual” and “ditch” microstructures of Type304 L1, exposed to near boiling 6M HNO_3 for 48 h.

Table. 4.3 Constants calculated by fitting of equation 4.2 for Type 304L1 having “step”, “dual” and “ditch” microstructure (Fig.4.12)

Microstructure	a (mmy^{-1})	b (V_{SCE})
Step	3.1×10^{-24}	0.1787
Dual	2.8×10^{-26}	0.0164
Ditch	5.7×10^{-22}	0.0197

The morphology of IGC in Type 304L1 with “step” “dual” and with and “ditch” microstructures are shown in Fig.4.13 It can be seen that the extent of grain drooping had increased in 48 h exposure of Type 304L1 SS when the microstructure of the material changed from “step” / “dual” to “ditch”. This is more evident from Fig. 4.12 as the corrosion rate at an applied potential of 0.970 V_{SCE} increased for the Type 304L1 SS with “step”/“dual”

microstructure from 1.12 mmy^{-1} to 1.64 mmy^{-1} for the “ditch” microstructure. At higher applied potentials, the difference in corrosion rates for the “step”/“dual” and “ditch” microstructures further increased. However, at lower potentials (where passivity remains intact and general corrosion is observed) there is hardly any difference in corrosion rates observed for these three microstructures. The main reason for enhanced IGC rates for Type 304L1 with a “ditch” microstructure could be due to more incorporation of oxidizing Cr^{6+} compared to that getting incorporated from Type 304L1 with “dual” or “step” microstructures. The Cr^{6+} and to a lesser extent Fe^{3+} raise the oxidizing power of the environment, hence cause more corrosion [35-37].

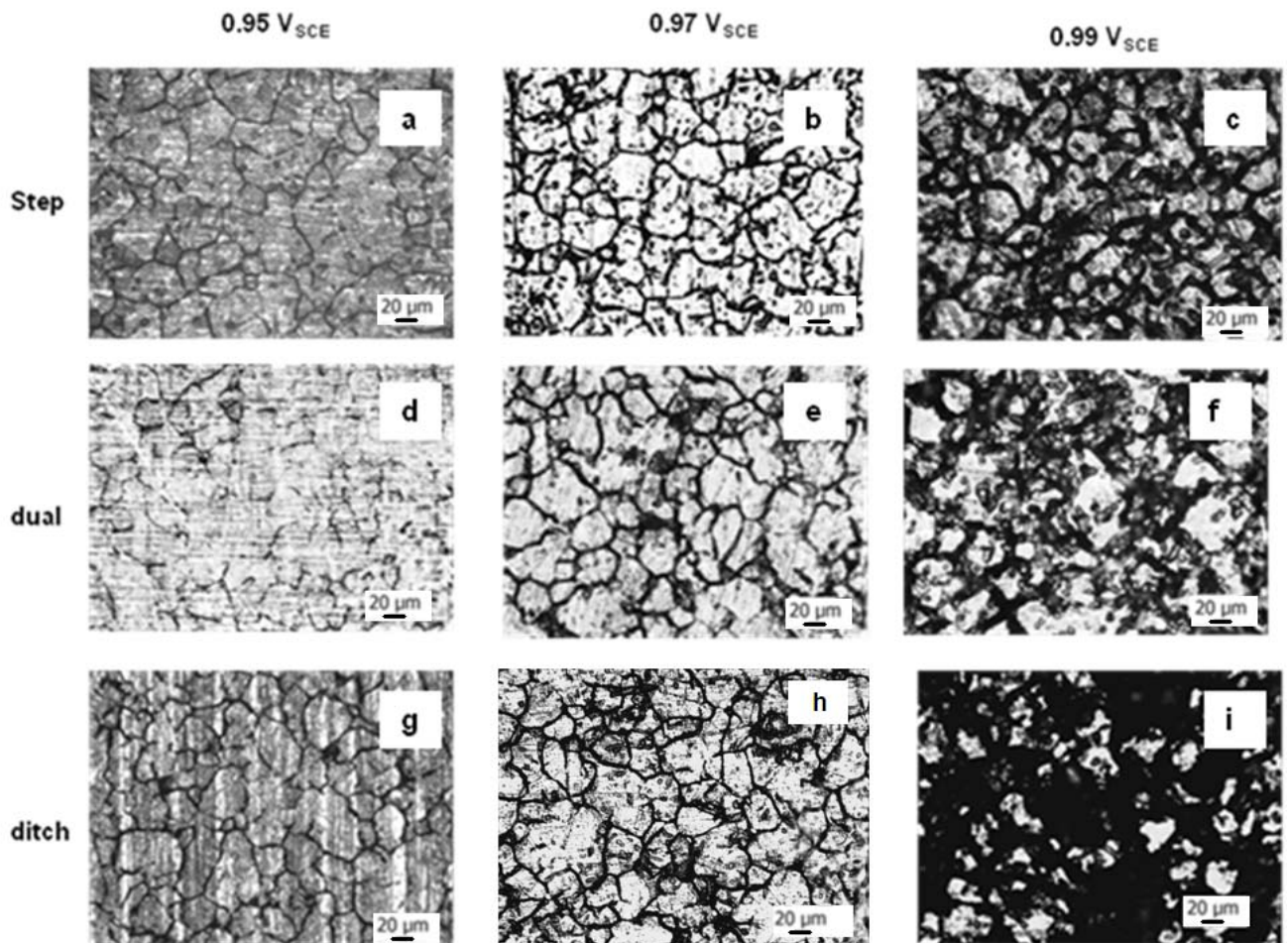


Fig. 4.13 IGC observed by optical microscope after exposure in near boiling 6M HNO_3 for 48 h in Type 304L1, having “step” microstructure at (a) $0.950 \text{ V}_{\text{SCE}}$, (b) $0.970 \text{ V}_{\text{SCE}}$ and (c) $0.990 \text{ V}_{\text{SCE}}$, having “dual” microstructure at (d) $0.950 \text{ V}_{\text{SCE}}$, (e) $0.970 \text{ V}_{\text{SCE}}$ and (f) $0.990 \text{ V}_{\text{SCE}}$ and having “ditch” microstructure at (g) $0.950 \text{ V}_{\text{SCE}}$, (h) $0.970 \text{ V}_{\text{SCE}}$ and (i) $0.990 \text{ V}_{\text{SCE}}$.

The relationship between logarithm of corrosion rate and applied potential for Type 304L NAG1 having “step” and “dual” microstructure is shown in Fig. 4.14 and constants calculated for the curve fitting using equation 4.1 corresponding to this figure are given in Table 4.4. From Fig. 4.14, it is indicated that the threshold potential for Type 304L NAG1 was (a) 0.967 for as received, (b) 0.966 V after heat treatment at 675 °C for 1 h and (c) 0.963 after heat treatment at 675 °C 171h. Corrosion rates for as-received and heat treated Type 304L NAG1 below the threshold potential (at 0.950-0.960 V_{SCE}) are very low and are typical of corrosion rate of SS in the passivated condition below 0.51 mmy⁻¹ (20 mpy). Type 304L NAG1 with “step” and “dual” microstructures showed comparable corrosion rates for entire range of applied potential. Various alloying elements are added to the steels to provide specific benefits in corrosion resistance, mechanical properties, or ease of fabrication. Section 2.3.1.2, chapter 2 describes how these alloying elements influence IGC of SS. In the following paragraph the results obtained from the present investigation are correlated with compositional and microstructural factors. At a given applied potential, corrosion rates measured after 48 h immersion tests in near boiling 6M HNO₃, were in the order of Type 310L < 304L NAG1 < 304L1 (Fig. 4.7). The carbon content of Type 304L1, Type 304L NAG1 and Type 310L are 0.024, 0.014 and 0.011 wt % respectively (Table 3.1). It is clear that Type 310 L with least content of carbon is the most resistant to IGC while Type 304L1 with highest content of carbon is least resistant to IGC. The role of carbon is easy to understand, since one of the major causes of susceptibility to IGC is the precipitation of chromium carbides [1, 2, 4-6]. Carbon up to 0.07 percent by weight is soluble during annealing at 1066 °C. It has less than 0.01 percent solubility by weight at ambient temperature. Rapid cooling from the annealing temperature results in super saturation of carbon in solution. Subsequent holding in the sensitization range enables this carbon to precipitate out as chromium rich carbides. IGC susceptibility in austenitic SS increases as the

carbon content increases [71]. Chromium content in Type 310L, 304L NAG1 and 304L1 are 24.31, 18.72 and 18.05 wt.% respectively. The highest content of chromium in Type 310L can be associated with its least corrosion rate at a given applied potential, in 48 h immersion tests in near boiling 6M HNO₃. The addition of chromium increase corrosion resistance properties. Normally the amount of chromium in austenitic SS varies from 11 % to 25 % by weight. This amount is generally not sufficient to prevent attack in the oxidizing medium. Fig 2.8 in chapter 2 shows corrosion behavior of austenitic SS with respect to Cr content in 65 wt % boiling HNO₃ [36].

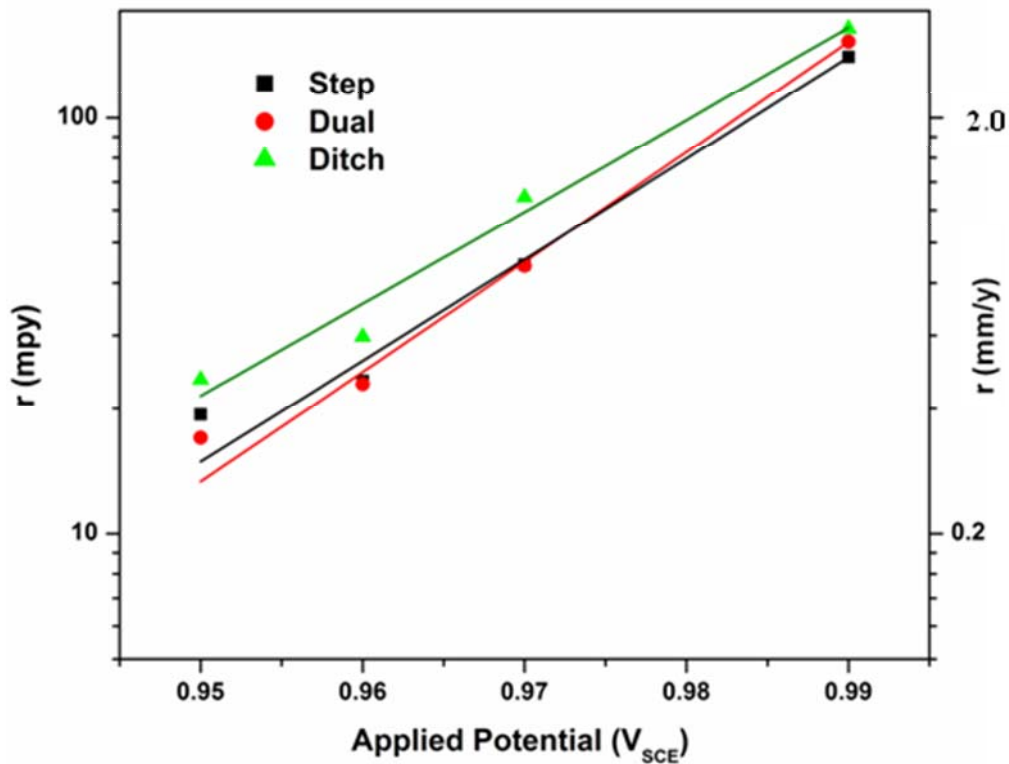


Fig. 4.14 Correlation between corrosion rate (r) and applied potential (V) for “step”, and “dual” microstructures of Type 304L NAG1, exposed to near boiling 6M HNO₃ for 48 h.

Table 4.4 Constants calculated by fitting of equation 4.2 for Type 304L NAG1 having “step” and “dual” microstructure (Fig.4.14)

Microstructure	a (mmy ⁻¹)	b (V _{SCE})
Step	1.5 x 10 ⁻²³	0.01735
Dual	3.9 x 10 ⁻²⁴	0.01692
Ditch	1.6 x 10 ⁻²²	0.01807

It is clear from Fig. 2.8 that high chromium content makes austenitic SS more corrosion resistant. The results shown in Fig. 4.7 also confirmed that higher chromium content improved corrosion behavior of austenitic SS in near boiling 6M HNO₃. The effect of Si content on IGC is more complex. Increase in IGC was observed up to 1 % Si content, after this limit IGC decreases when Si content increases IGC was not observed for Si values higher than 3 % in boiling HNO₃ containing oxidizing species (Fig. 2.10) [36]. The silicon content of Type 304L1, Type 304L NAG1 and Type 310L are 0.49, 0.31 and 0.09 wt % respectively (Table 3.1). It is clear that Si content is less than 1 wt % in all three grades of SS alloys and it is the lowest in Type 310L. Along with the highest content of Cr and the lowest content of C, lowest content of Si might be one of reasons for the least corrosion rate shown by Type 310 L at a given applied potential, in 48 h immersion tests in near boiling 6M HNO₃. Increasing the bulk nickel content decreases the solubility and increases the diffusivity of carbon. This effect is much more pronounced when nickel content is above 20 %. It is generally recommended that in 25/20 Cr-Ni steel, carbon content should be less than 0.02 % to guarantee resistance to IGC. For the same reason the carbon content in Type 310L is 0.011 wt % (Table 3.1). The corrosion rates were lower for Type 304L1 with “step” and “dual” microstructures than for the same material with a “ditch” microstructure over the entire range of applied transpassive potentials used in this study. This observation necessitates to discuss influence of precipitate morphology on the mechanism of attack. A continuous grain boundary precipitate is not

always necessary to get IGC because chromium diffusion (and depletion) could occur within the boundary itself. However, a continuous grain boundary precipitate would increase the chances of rapid attack. The morphology of the precipitate depends on prior thermal and mechanical history as well as sensitizing temperature. As described earlier in section 3.3, chapter 3 that in Practice A, A262, ASTM austenitic SS alloys were etched in 10 % oxalic acid at a current density of 1 A cm^{-2} for 90 s and the microstructures were classified as (1) “step” (no chromium carbide/chromium depletion regions at grain boundaries) (2) “dual” (discontinuous chromium carbide/chromium depletion regions at grain boundaries) and (3) “ditch” (at least one grain having complete encirclement with chromium carbide/chromium depletion regions) [22]. Such sensitized SS with “ditch” microstructure may be prone to IGC in boiling HNO_3 [16, 17, 22].

4.2 Summary

The following is a brief summary of the present investigations dealing with the role of composition and microstructure on corrosion behavior:

- Intergranular nature of corrosion of austenitic SS was clearly dictated by transpassive potential in HNO_3 .
- Corrosion rate measured after 48 h immersion tests in near boiling 6M HNO_3 increased exponentially with the increase in the applied potential for all the three austenitic SS alloys.
- At a given applied potential, corrosion rates measured after 48 h immersion tests in near boiling 6M HNO_3 , were in the order Type 310L < 304L NAG1 < 304L1. Polarization studies conducted on these SS alloys showed that at the start of the transpassive potential, current densities were in the order of Type 310L < 304L NAG1 < 304L1.

- The corrosion rates of Type 304L1 with “step” and “dual” microstructures, measured after immersion tests in near boiling 6M HNO₃ were comparable. The corrosion rates were lower for Type 304L1 with “step” and “dual” microstructures than for the same material with a “ditch” microstructure over the entire range of applied transpassive potentials used in this study. Polarization tests revealed that the current densities for Type 304L1 with “step” microstructure were lower compared to the same material with “ditch” microstructure in transpassive regime of potential.
- The correlation between corrosion rate and applied potentials revealed higher threshold potentials (corresponding to corrosion rate of 0.61 mmy⁻¹) for “step” and “dual” microstructures compared to “ditch” microstructure. Therefore grain dropping in Type 304L 1 with “step”/ “dual” microstructure started at a higher potential than for “ditch” microstructure. The morphology of corrosion attack after 48 h immersion tests in near boiling 6M HNO₃ also showed more grain droppings for “ditch” microstructure compared to “step”/ “dual” microstructure at a given potential.
- “Ditch” microstructure could not be produced in Type 304L NAG1 by chosen heat treatment. There was no significant difference in the corrosion rates between “step” and “dual” microstructures of Type 304L NAG1.
- It has been shown using morphology of corrosion attack after 48 h immersion tests in near boiling 6M HNO₃, that even non-sensitized SS (having “step” or “dual” microstructures) undergo severe IGC in transpassive regime of potential.
- It has been shown that there was a difference in the potential for onset of transpassivity when using potentiodynamic and potentiostatic techniques.
- Applicability of the methodology for establishing the relation between the electrochemical potential and the corrosion rate for any given system (grade of SS, microstructure of SS, operating parameters) has been demonstrated.

CHAPTER 5

Grain Size and Grain Boundary

Engineering

This chapter includes results on the investigations of the influence of grain size and grain boundary engineering on the corrosion behavior of Type 304L in near boiling 6M HNO₃. The grain sizes of Type 304L2 specimens were varied by annealing specimens at a chosen temperature for different time periods. These specimens with varying grain size were subjected to potentiostatic tests in near boiling 6M HNO₃ for a period of 48 h and their corrosion behavior was compared. Type 304L1 was strain-annealed using previously reported optimized parameters for thermomechanical processing. The Σ value (section 2.6.1) was evaluated using EBSD. The corrosion behavior of the as-received and the strain-annealed Type 304L1 were investigated in potentiostatic tests in near boiling 6M HNO₃.

5.1 Background

Conventionally corrosion resistance of materials is improved through bulk alloying. Alloying changes the bulk material chemistry. Grain size adjustments could be used to improve corrosion resistance without altering the bulk composition. In section 2.6.1 an introduction to grain boundary was given. The junction between adjacent grains is called grain boundary. Grain boundaries can be seen as non equilibrium defects in atomic arrangements arising from the misorientation of crystal lattices between adjacent grains [98]. In the grain boundary area the atomic bonds differ from those of regular crystal lattices. Grain boundaries exhibit different properties than the bulk crystals that they separate due to

difference in bond energy. Grain boundaries are high energy areas because most stable configuration of a crystalline material is its particular crystal lattice. Energy of grain boundaries can be reduced by its interaction with lattice defects [97]. Therefore impurities or solute atoms are segregated to the grain boundaries to form chemically different compound as compared to bulk. For example, formation of chromium carbide at the grain boundaries due to sensitization (section 2.3.1.1 chapter 2). In the EBSD grain boundaries are classified as either special or general. Grain boundaries containing a high density of coincidence sites are called coincidence site lattice (CSL) boundaries or special boundaries. For special boundary the value of Σ remains less than 29 [99], where Σ value is reciprocal density of coincident atomic lattice sites between two grains assuming interpenetration with one another [98]. Low value of Σ is indicative of high degree of coincidence between grains and thus a better fit. Therefore if Σ value is low, the interfacial energy becomes low and free volume in grain boundary region is less. When high purity nickel is exposed to 2N H₂SO₄ at 303 K grain boundaries with low value of Σ resist IGC [101]. Grain boundaries have distinct properties relative to the bulk material in terms of atomic coordination, reactivity and diffusion rates. Consequently, it is not unreasonable to expect surfaces with relatively high grain boundary density to exhibit different electrochemical behavior than surfaces with lower grain boundary densities. Many studies have suggested that corrosion rate decreases with decrease in grain size [129-131]. Kus et al. evaluated nanocrystalline specimens and conventional Al 5083 using HNO₃ weight loss test according to ASTM G 67 [129]. Nanocrystalline specimens showed lower loss in weight compared to conventional Al 5083 specimens. Nanocrystalline material showed no attack at the grain boundaries while conventional Al 5083 specimens showed attack at the grain boundaries. It is reported that pitting corrosion resistance of AA 1050 improves due to grain refinement in 0.1M Na₂SO₄+100 ppm Cl⁻ solution [130]. The pit forming mechanism of AA 1050 is related to formation of the local microgalvanic cell

between Al matrix (anode) and Si-containing impurities or mixed oxide containing Si (cathode). Ultrafine-grained AA 1050 had smaller Si-containing impurities compared to coarser grained AA 1050. Thus the area of cathode is reduced in ultrafine grained AA 1050 and as a result of this pitting resistance has improved. Improvement in stress corrosion cracking resistance of 7475 Al-alloy through grain refinement is reported in air and in 3.5 % NaCl + 0.3 % H₂O₂ solution [131].

Grain boundary engineering through grain refinement and various severe plastic deformation (SPD) techniques has been shown to be an effective way to improve mechanical properties such as strength and wear resistance [129, 130, 132-137]. Additionally, manipulation of grain boundary character has been used to enhance corrosion resistance of some materials. A classic example of this is improved IGC resistance of Alloy 600 tubing, used in nuclear power production, through development of an increased value of low Σ CSL boundaries [138]. It is indicated from Time–temperature–precipitation curves for austenitic SS that twin boundaries are resistant to carbide precipitation and corrosion. The reason for this is highly regular and coherent atomic structure as compared with those of other high angle grain boundaries [139]. Resistance of twin boundary to carbide precipitation is because of low boundary energy as reported by Trillo and Murr [140, 141]. This suggests that each grain boundary has its own sensitivity to sensitization depending on the nature and structure of the grain boundary. Low Σ grain boundaries are resistant to sensitization, i.e. precipitation of chromium rich carbides at the grain boundaries and therefore to Cr depletion formation [101, 139, 141]. Therefore low Σ grain boundaries tend to resist IGC [101, 140, 142]. The concept of grain boundary design and control was introduced by Watanabe [96]. This concept involves a favorable grain boundary character distribution (GBCD), including high frequency of CSL boundaries [96]. Later Palumbo developed this concept as grain boundary engineering (GBE) [143-145]. The feasibility of GBE has been demonstrated mainly by

thermomechanical treatments (section 2.6.2). Thermomechanical treatments can be divided into strain annealing and strain recrystallization processes based on process parameters, i.e. pre-strain and temperature [146-151]. Strain recrystallization process was used by Palumbo et al. to improve the IGC resistance in nickel based alloys [142, 143,145, 152]. King et al. have reported evolution of the GBCD in Cu by the strain annealing process [147, 149]. Shimada et al. have achieved IGC resistance in Type 304 austenitic SS by GBE [99].

In this chapter, influence of grain size and grain boundary engineering on corrosion of austenitic SS at transpassive potentials have been investigated. Type 304L2 was used to study the influence of grain size and Type 304L1 was used to study the influence of grain boundary engineering in near boiling 6M HNO₃. The grain size of Type 304L2 was varied by controlling annealing heat treatment. The GBE in Type 304L1 was done by thermomechanical processing and CSL frequencies were measured using EBSD. Potentiostatic tests were conducted in near boiling 6M HNO₃ to study the influence of grain growth and GBE on corrosion behavior.

5.2 Results and Discussion

5.2.1 Influence of Grain Size

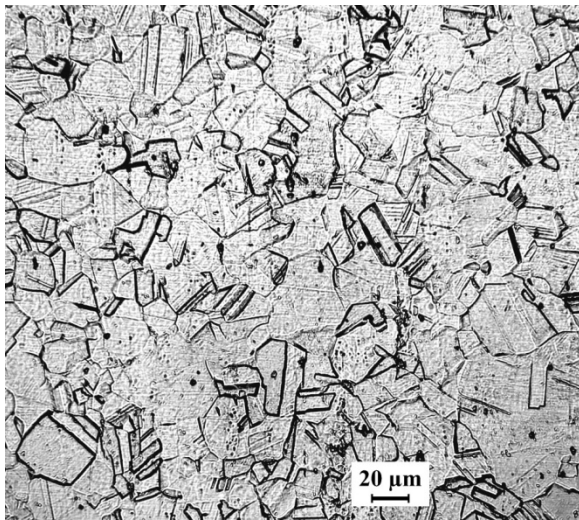
Microstructures of longitudinal surface of Type 304L2 after electroetching in 10 % oxalic acid in as-received condition and after various annealing heat treatments are shown in Fig.5.1. Type 304L2 in as-received condition showed “step” microstructure (Fig.5.1a). Microstructure of Type 304L2 after annealing heat treatment at 1050 °C for 45 min and 1050 °C for 2 h remained “step” (Fig. 5.1. b-c). The ASTM grain size number¹ of as-received Type 304L2 was 8 (average intercept length of 22.4 μm). Solution annealing of as-received Type 304L2 at 1050 °C for 45 min increased the grain size to ASTM grain size number 6

¹ ASTM grain size number, G , is defined as $N_{AE} = 2^{G-1}$, where N_{AE} is the number of grains per square inch at 100X magnification.

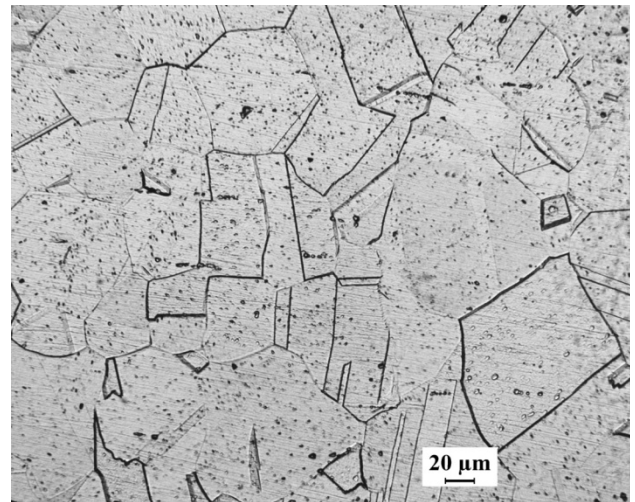
(average intercept length of 45 μm). The grain size increased to ASTM grain size number 4 (average intercept length of 90 μm), when solution annealing period was increased from 45 min to 2 h. The as-received and solution annealed specimens of Type 304L2 showed “dual” microstructure after heat treatment at 675 °C for 1h (Fig. 5.2 a-c).

The results of potentiostatic tests (section 3.3.3.3) conducted on Type 304L2 specimens having three grain sizes (each specimen was sensitized at 675 °C for 1h) are summarized in Fig.5.3. The Highest corrosion rate at each applied potential (except at 0.95 V_{SCE}) was shown by specimen having grain size number 8, the least grain size among all the specimens. Specimen with the largest grain size (ASTM grain size number 4) showed the least corrosion rate at each applied potential in separate potentiostatic tests. However specimen with the smallest grain size showed slightly lower corrosion rate compared to specimen having ASTM grain size number 6 at 0.95 V_{SCE} . Variation in grain size had more profound effect on corrosion rates at higher potentials (0.97 V_{SCE} and 0.99 V_{SCE}) compared to lower potentials (0.93 V_{SCE} and 0.95 V_{SCE}). The threshold potential for Type 304L1 heat treated at 675 °C for 1 h (resulting in a “dual” microstructure) was 0.960 V_{SCE} (section 4.1.3 chapter 4). It is mentioned in previous chapter that threshold potential is the potential at which a corrosion rate of 0.61 mm^{-1} (24 mpy) is observed [35]. Severe IGC (grain dropping) takes place when corrosion rates are above 0.61 mm^{-1} (24 mpy) [16, 17, 21, 25, 29]. It is clear that potentials 0.97 V_{SCE} and 0.99 V_{SCE} are above threshold potential and thus at these potentials Type 304L2 will show grain dropping. The grain dropping that starts at and above 0.96 V_{SCE} is expected to increase with increase in the applied potential. Therefore effect of grain size on corrosion rate above threshold potential is more pronounced compared to the corrosion rates below the threshold potential. The decrease in the rate of IGC with increase in grain size above the threshold potential (in transpassive regime) is consistent with observations available in literature [129].

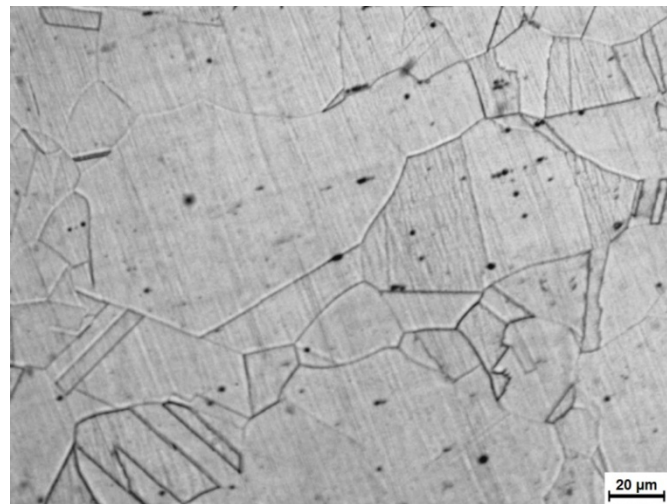
We have seen in the previous chapter that for constant grain size corrosion rate was not affected much if microstructure changes from “step” to “dual”. A drastic change in corrosion rate is observed only if the microstructure becomes “ditch” Microstructures of specimens of various grain sizes change from “step” (Fig. 5.1) to dual (Fig. 5.2) after sensitization heat treatment. Therefore if specimens were exposed to potentiostatic tests without sensitization similar corrosion rates would have been obtained.



(a)



(b)



(c)

Fig.5.1 Microstructures of longitudinal surface of Type 304L2 observed by optical microscope (a) in as-received condition, (b) After heat treatment at 1050 °C for 45 min and (c) After heat treatment at 1050 °C for 2 h.

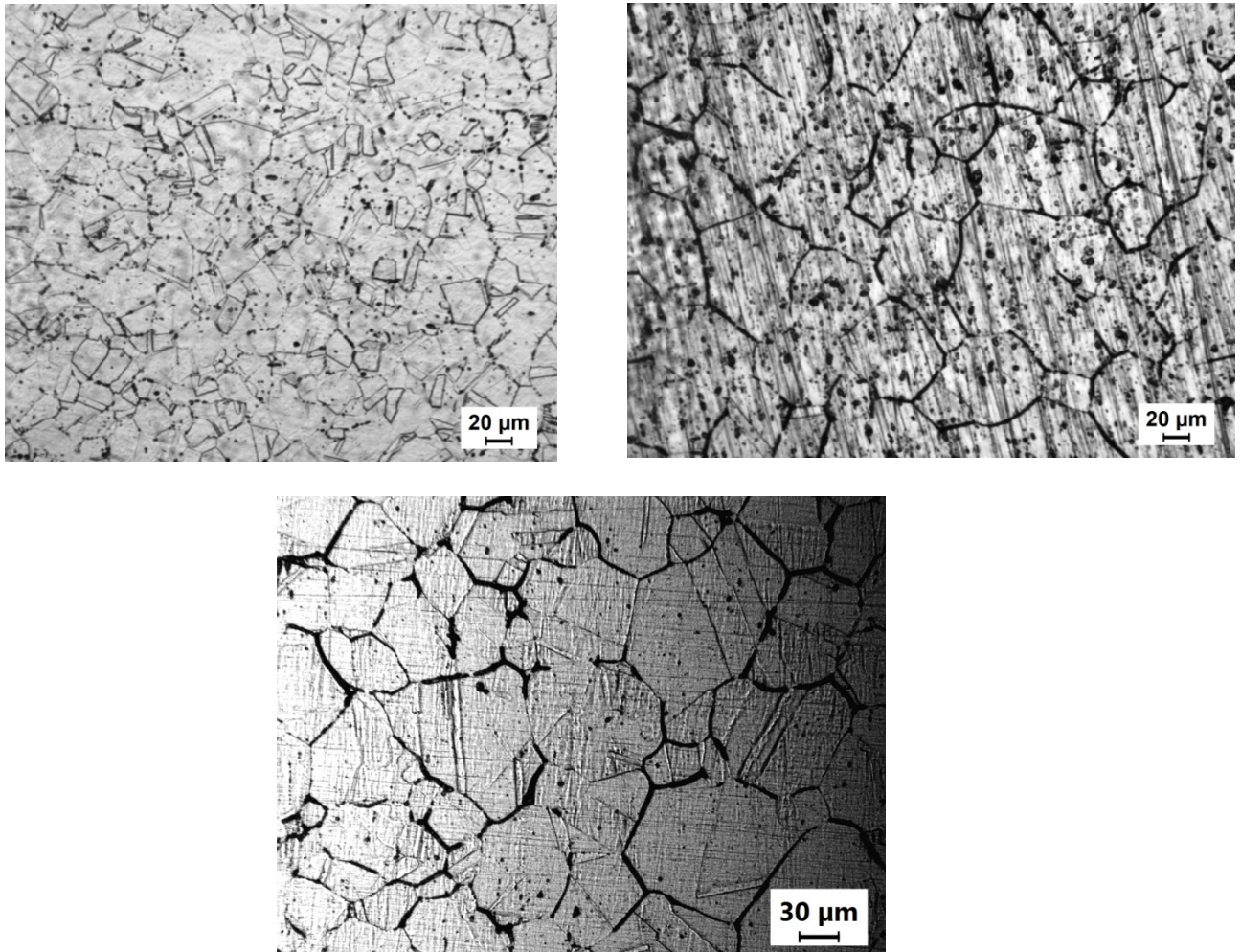


Fig. 5.2 Microstructures of longitudinal surface of Type 304L2 observed by optical microscope after (a) heat treatment at 675 °C for 1 h on as-received specimen, (b) heat treatment at 675 °C for 1 h on specimen annealed at 1050 °C for 45 min and (c) heat treatment at 675 °C for 1 h on specimen annealed at 1050 °C for 2 h.

Fine grain structures are expected to be more corrosion resistant only if grain boundary density dictates the oxide film conduction rate on surfaces with low to passive corrosion rates [153]. In the absence of passive film, when dissolution rates are high ($>10 \mu\text{A cm}^{-2}$), increased grain boundary densities will likely enhance overall surface reactivity [154]. Therefore, for higher corrosion rates, decrease in grain size results in increase in corrosion rates. It is mentioned in section 2.3.1.2 chapter 2 that IGC in SS reduces with smaller grain size. The reason for this is the presence of greater grain area, which may retard continuous formation of carbide at grain boundaries [6]. Since all the specimens subjected to potentiostatic tests had “dual” microstructure, i.e. no grain had continuous carbide, results can

not be interpreted in term of carbide precipitation. Specimens with smallest grain size possess the largest grain boundary area. It is mentioned in section 2.6.1 chapter 2 that grain boundaries possess excess free energy due to the presence of disorder. Therefore surface reactivity of specimen with least grain size is the highest and thus its tendency to IGC would be more compared to other two specimens. The other factor for the observation that specimens with smallest grain size showed highest tendency toward IGC might be corrosive environment used. It is known that in HNO_3 there might be rapid opening of small grains in the structure, so that fine grain steels are often corrode faster compared to coarse grained steels [6].

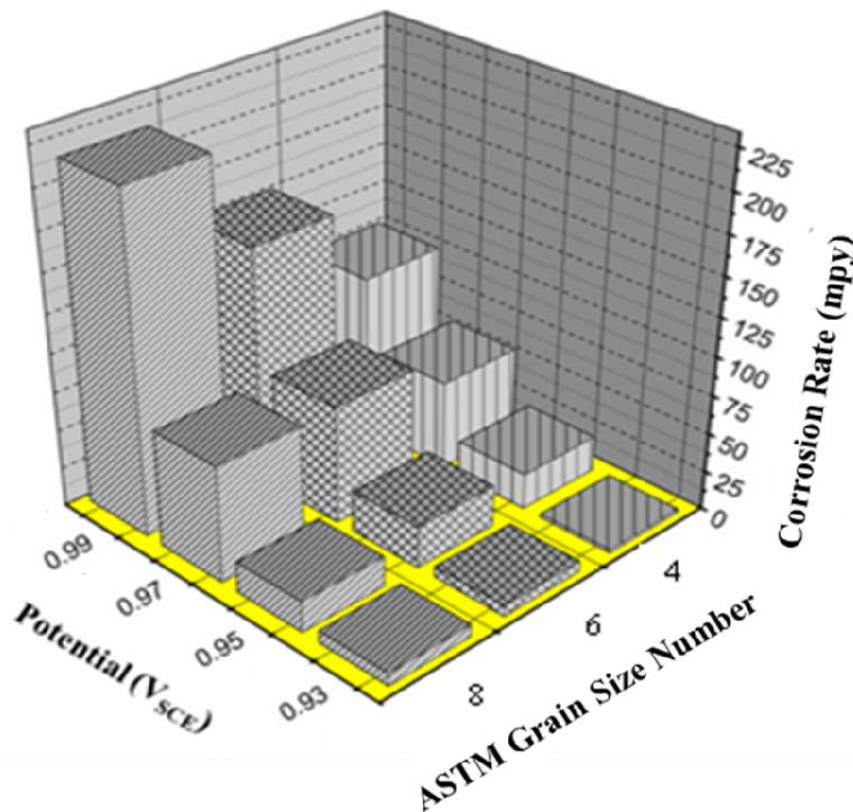


Fig. 5.3 Results of potentiostatic tests conducted on Type 304L2 specimens of different grain size in 6M near boiling HNO_3 for 48 h.

The morphologies of corrosion attack after potentiostatic tests in near boiling 6M HNO_3 are shown in Fig. 5.4 and Fig 5.5. When specimens were exposed to near boiling 6M HNO_3 at 0.93 V_{SCE} uniform corrosion occurred. The potential 0.93 V_{SCE} is much below the

threshold potential of $0.96 V_{SCE}$. Therefore at this potential corrosivity of near boiling 6M HNO_3 was not sufficient to produce grain droppings and specimen exhibited uniform corrosion. Fig. 5.4 shows uniform corrosion attack on Type 304L2 (with largest grain size) after it was subjected to potentiostatic test at $0.93 V_{SCE}$. Fig.5.5 shows clear IGC at $0.97 V_{SCE}$ and $0.99 V_{SCE}$. It is also evident from Fig. 5.5 that grain dropping becomes more severe with decrease in grain size and increase in potential. Specimen having smaller grains possess larger grain boundary area (active area) and therefore more prone to IGC. Therefore at a given potential specimen having finer grain showed more grain droppings compared to specimen having coarse grains. For the constant grain size more grains were dropped at $0.99 V_{SCE}$ compared to $0.97 V_{SCE}$. The reason for this is that grain droppings that start at $0.96 V_{SCE}$ (threshold potential) is expected to increase with increase in applied potential. If specimens were tested without sensitization heat treatment similar results would have been obtained. The reason for this is evident from foregoing discussion. Sensitization heat treatment did not produce continuous carbide precipitate at the grains boundaries (“ditch” microstructure). For the constant grain size no significant change in corrosion behavior is expected when the microstructure changes from “step” to “dual”.



Fig.5.4 Morphology of corrosion attack (observed by optical microscope) on longitudinal surface of Type 304L2 (ASTM grain size no 4) exposed to near boiling 6M HNO_3 at $0.93 V_{SCE}$.

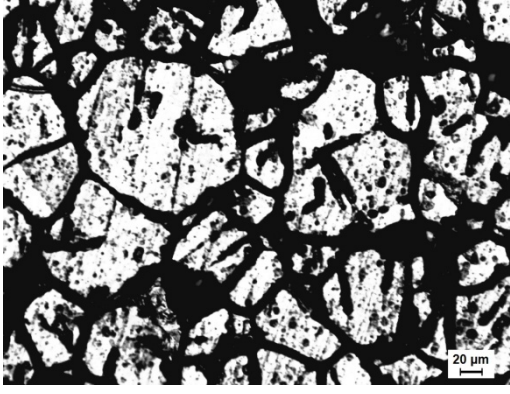
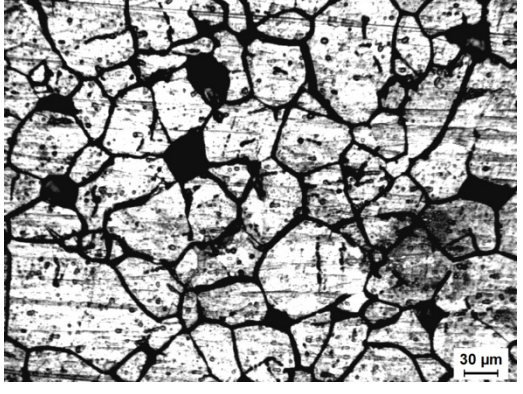
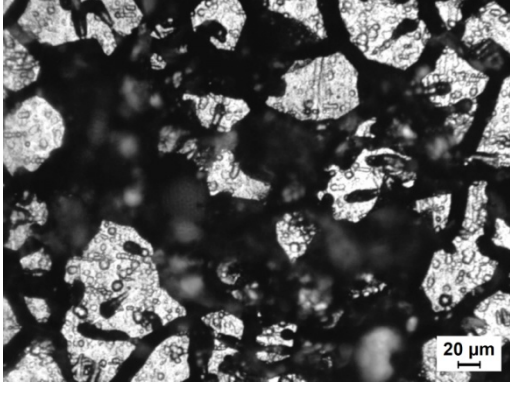
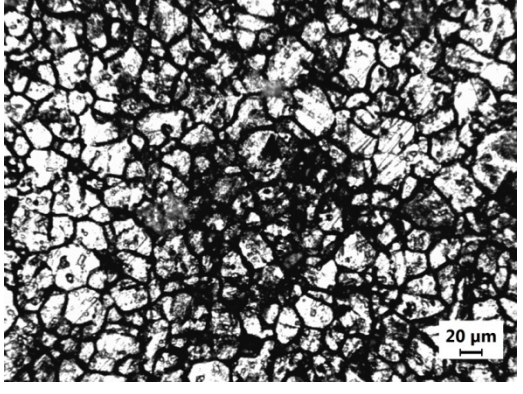
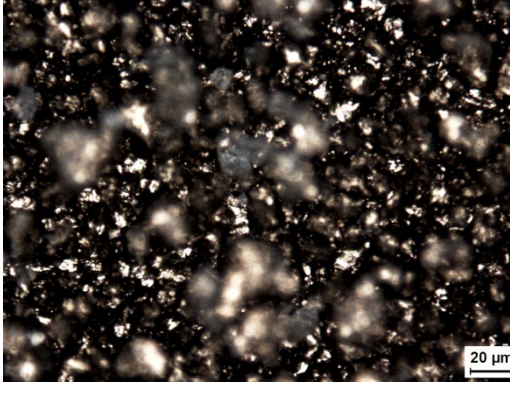
ASTM	Morphology of Corrosion Attack	
Grain Size Number	At 0.97 V _{SCE}	At 0.99 V _{SCE}
4		
6		
8		

Fig.5.5 Morphology of corrosion attack (observed by optical microscope) on Type 304L2 specimens (having varying grain size) exposed to near boiling 6M HNO₃ at 0.97 V_{SCE} and 0.99 V_{SCE}.

5.2.2 Influence of Grain Boundary Engineering

Optimum grain boundary character distribution (GBCD) is necessary to achieve IGC resistance by GBE. Optimum GBCD can be described as a uniform distribution of a high frequency of CSL boundaries (special grain boundaries) and consequent discontinuity of the random boundary network in the material. Special grain boundaries contain high density of coincidence sites and for them value of Σ remains less than 29 (section 5.1). During thermomechanical treatment, optimized parameters are used to achieve favorable GBCD. M. Shimada et al. [99] have optimized the parameters for thermomechanical treatment in order to achieve favorable GBCD in SS 304. In the present work same optimized parameters for thermomechanical processing (5 % reduction in specimen thickness by cold rolling followed by annealing at 927 °C for 72 h) were used.

The microstructure of Type 304L1 in as- received condition is shown in Fig. 4.1a in chapter 4. The microstructure is “step” and ASTM grain size number is 7 (32 μm) in as-received condition. Microstructure remained “step” in thermo mechanically processed (strain-annealed) specimens (Fig. 5.6). Strain-annealing caused grain growth from ASTM grain size number 7 to ASTM grain size number 4 (90 μm).

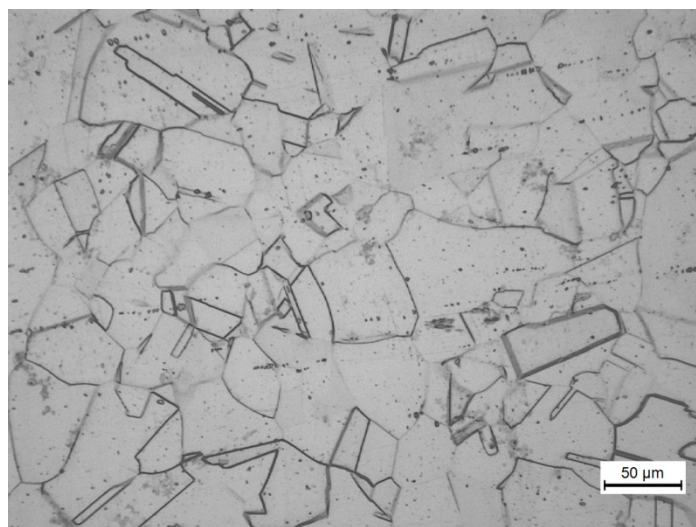


Fig. 5.6 Microstructure of Type 304L1 (observed by optical microscope) after 5 % reduction in specimen thickness by cold rolling followed by annealing at 927 °C for 72 h.

Fig. 5.7 shows image obtained by orientation imaging microscopy (OIM). OIM observations showed CSL frequency 43.8 % for as-received specimen and 52.9 % for strain-annealed specimen. The increase in CSL frequency is less compared to increase in CSL frequency using the same thermomechanical process for SS 304 used by Shimada et al [99]. Shimada et al [99] have reported 86.5% frequency of CSL boundaries using the same parameters for thermomechanical treatment on as- received Type 304 specimen having CSL frequency 63 %. Shimada et al. [99] have shown an excellent resistance to IGC in 304 SS during DL-EPR and ferric sulfate-sulfuric acid tests by achieving higher frequency of CSL and optimum GBCD using the same strain annealing- treatment. The evolution of the optimized GBCD during the strain annealing at 927 °C might be explained in the following way. The small pre-strain activates grain boundary migration. New grains are not generated during this process. Therefore grain growth accompanying twins are accelerated without any recrystallization. A migrating grain boundary interacts with lattice dislocations and other grain boundaries during grain growth. Because of these interactions, a low energy boundary cannot move a long distance. The reason for this is that the absorption rate of lattice dislocation by a low energy boundary is much lower than that of a random boundary [154]. Migration never occurs before completion of the absorption [155]. These interactions can brought down energy of grain boundary [156]. Low energy grain boundaries are stable and resistant to interactions with defects [156]. Therefore, a low energy boundary does not have tendency to move. Grain boundaries possessing high energy can migrate widely. Therefore a high energy boundary can interact with other boundaries or twin emissions to produce new low energy segments. Low energy boundary segments can survive for a long time. In the strain annealing at 927 °C, the small strain introduced by rolling promotes grain growth and subsequently preferentially initiates the high CSL frequency layer near the specimen surface. The CSL layer grows into the specimen interior inversely along the strain gradient.

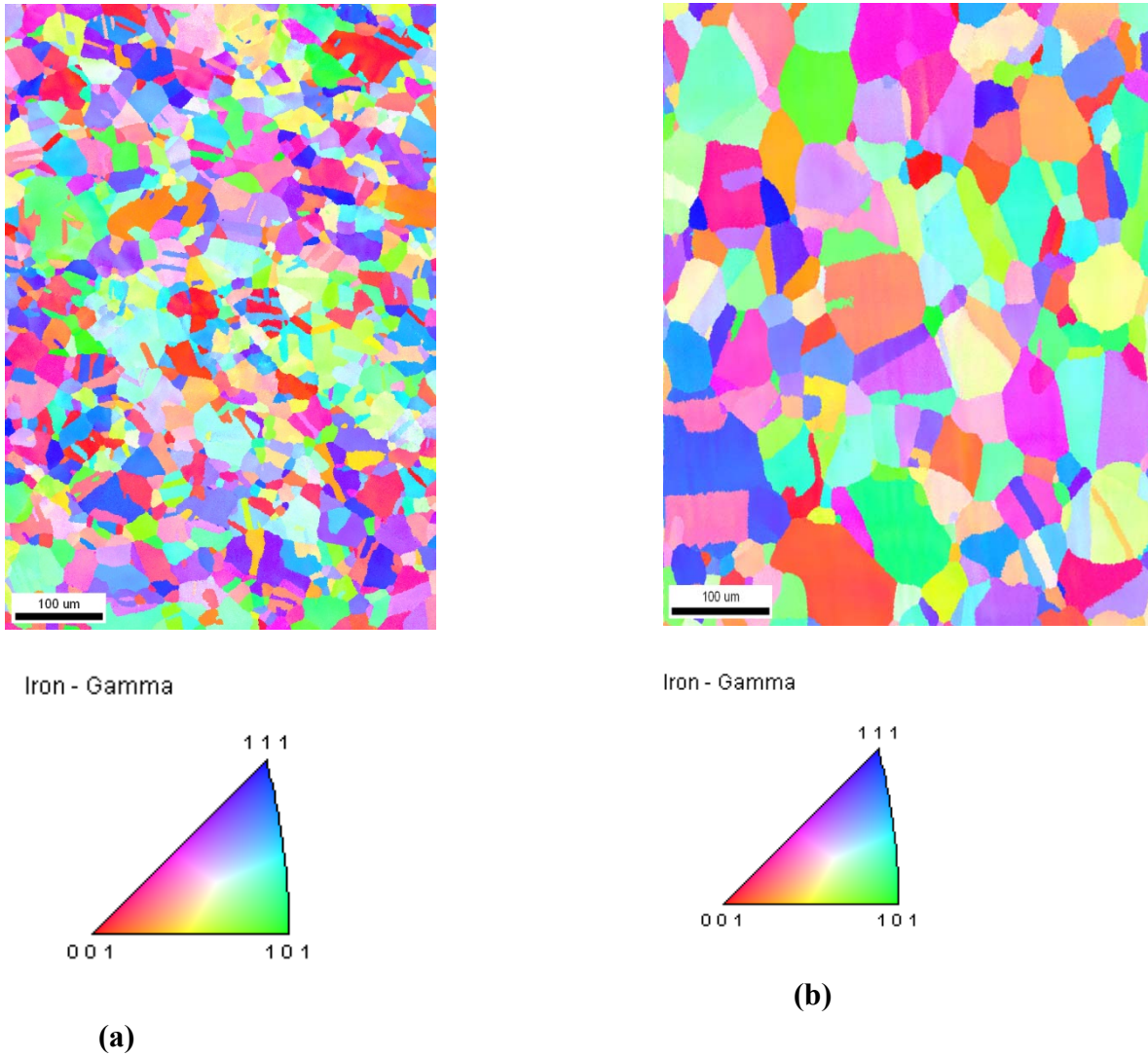


Fig.5.7 OIM images for (a) as-received Type 304L1 specimen (b) strain-annealed (5 % reduction in specimen thickness followed by annealing at 927 °C for 72 h) Type 304L1 specimen.

As-received and strain- annealed specimens were subjected to potentiostatic tests in near boiling 6M HNO₃ as described in section 3.3.3 of chapter 3. Results of these potentiostatic tests are summarized in Table 5.1. Strain-annealing brought down corrosion rate from 3.5 mmy⁻¹(140 mpy) to 2.2 mmy⁻¹ (88 mpy) at 0.99 V_{SCE}. Corrosion rate is expected to reduce to a value of 0.6 mmy⁻¹ (24 mpy) or below for resistance to IGC. The reason for this mentioned in chapter 4 is that grain dropping starts when corrosion rate is 0.6mmy⁻¹ (24 mpy) [16, 17, 21, 25, 29]. The improvement in corrosion resistance by strain-annealing is not sufficient to prevent IGC of Type 304L1 in near boiling 6M HNO₃. As we

have seen that increase in CSL frequency is marginal, the major cause of improvement in corrosion resistance may be grain growth during strain- annealing process. Significant grain growth was also observed in SS 304 after strain-annealing in Shimada et al. work [99]. The decrease in corrosion attack in strain-annealed specimen is also evident from the observation of morphology of attack in as-received Type 304L1 specimen (Fig. 4.13c in chapter 4) and strain-annealed Type 304L1 specimen (Fig. 5.8) after potentiostatic test at $0.99 V_{SCE}$.

Table 5.1 Corrosion rates of as-received Type 304L1 and strain-annealed Type 304 L1 specimens after exposer to near boiling 6M HNO₃ at 0.99 V_{SCE} for 48 h

Material	Corrosion Rate mmy^{-1} (mpy)
As-received Type 304L1	3.5 (140)
Strain-annealed Type 304L1	2.2 (88)

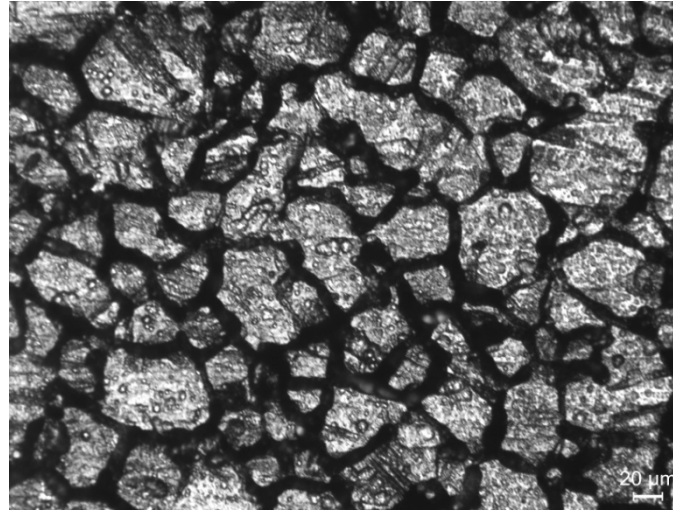


Fig. 5.8 Morphology of corrosion attack (observed by optical microscope) on strain-annealed Type 304L1 specimen exposed to 6M HNO₃ at $0.99 V_{SCE}$.

5.3 Summary

The following is the brief summary of the present investigations dealing with the role of grain size and GBE on corrosion behavior:

- The microstructure of Type 304L2 changes from “step” to “dual” after sensitization heat treatment at 675 °C for 1 h irrespective of grain size.
- Increasing grain size of Type 304L2 (in a lightly “dual” microstructure) from ASTM grain size number 8 to 4 resulted in a decrease in the corrosion rate at all the applied potential in potentiostatic test in near boiling 6M HNO₃.
- Effect of grain size variation on the corrosion rate was more pronounced at higher potentials (0.97 V_{SCE} and 0.99 V_{SCE}) compared to lower potential (0.95 V_{SCE} and 0.93 V_{SCE}). This is due to the fact that the potentials 0.97 V_{SCE} and 0.99 V_{SCE} are above the threshold potential of 0.96 V_{SCE}.
- Strain-annealing of Type 304L1 induced grain growth from ASTM grain size number 7 (average intercept length of 32 μm) to ASTM grain size number is 4 (average intercept length of 90 μm).
- OIM observation revealed that strain-annealing of Type 304L1 resulted in a marginal increase (from 43.8% to 52.9%) in CSL frequency. Using same strain-annealing process in SS 304 an increase in CSL frequency from 63 % to 86.5 % M is reported and excellent resistance to IGC is achieved [99].
- Strain-annealed Type 304L1 showed lower IGC compared to as-received Type 304L1 specimen in potentiostatic test at 0.99 V_{SCE}. However, the improvement achieved in corrosion resistance was not sufficient to prevent IGC at 0.99 V_{SCE}.
- Since increase in CSL frequency is marginal the decrease in corrosion rate after strain-annealing on Type 304L1 in potentiostatic test might be due to grain growth.

CHAPTER 6

Acid Concentration and Temperature

This chapter contains the results on the investigation of role of acid concentration and temperature on the corrosion behavior of SS. Type 304L1 (heat treated at 675 °C for 1h) specimens were subjected to potentiostatic tests in various concentrations of near boiling HNO₃, as described in section 3.3.3. The corrosion rates measured in these experiments were plotted as a function of the applied potential. Dependence of polarization behavior of Type 304L1 (heat treated at 675 °C for 1 h) on HNO₃ concentration was also investigated. Type 304L NAG1 (heat treated at 675 °C for 1 h) specimens were subjected to potentiostatic tests in 6M HNO₃ at various temperatures. The logarithm of corrosion rates measured in these experiments was plotted as a function of inverse of the temperature. Activation energy of corrosion of Type 304L NAG1 (heat treated at 675 °C for 1h) in 6M HNO₃ at 0.99 V_{SCE} was calculated using this plot.

6.1 Background

Several incidences of failures of components made of Type 304L have been reported in spent nuclear fuel reprocessing plants when they were used in HNO₃ medium beyond 8 N concentration, and temperatures beyond 80 °C. These failures were caused by transpassive corrosion [5, 23]. Operating potential may increase up to transpassive potential due to increase in concentration and/or operating temperature of the HNO₃ coupled with increase in concentration of oxidising ions in HNO₃ [35-39]. Therefore, there is a definite limit on concentration of HNO₃, temperature of HNO₃ and concentration of oxidizing ions in the

HNO₃ that can be allowed for a given SS, to avoid IGC [21, 35-38]. Thus it was worthwhile to study the influence of HNO₃ concentration and temperature on corrosion behavior.

Materials concentration but at a very high corrosive concentration they show a rapid increase in corrosion rate [1]. For example, lead shows this effect in sulfuric acid. The reason for this behavior is that lead is protected by lead sulfate film in low concentration of sulfuric acid which dissolves at high concentration of sulfuric acid [1]. Corrosion behavior in acids that are soluble in all concentration of water is different. Initially the corrosion rate increases with the increase exhibiting passive behavior are negligibly affected by changes in corrosive environment [1]. Some materials show similar behavior up to moderate corrosive in corrosive concentration due to increase in concentration of hydrogen ions as hydrogen ions are the active species [1]. However on further increase of acid concentration, corrosion rate reaches a maximum and then decreases. This is due to reduction of ionization at high concentration of acid. It is reported that increasing solution temperature increased the susceptibility to both pitting and active dissolution in HNO₃ containing chloride ions [90]. Increasing temperature has increased anodic kinetics more rapidly than cathodic kinetics [90].

In this chapter, influence of HNO₃ concentration on corrosion behavior of Type 304L1 was investigated. Type 304L1 was used after a heat treatment of 675 °C for 1 h. HNO₃ of three concentrations 3M, 6M and 9M were used. Influence of solution temperature on corrosion behavior of Type 304L NAG1 was also investigated. Using Arrhenius plot, activation energy of corrosion of Type 304L NAG1 in 6M HNO₃ at 0.99 V_{SCE} potential was calculated.

6.2 Results and Discussion

6.2.1 Effect of Acid Concentration

The electrochemical polarization behavior of Type 304L1 SS in 3M, 6M and 9M HNO₃ solutions at 95 °C is shown in Fig. 6.1. It is observed from Fig. 6.1 that as the

concentration of HNO_3 is increased, the E_{corr} increased towards the transition to transpassivity. The E_{corr} increased from $0.742 V_{\text{SCE}}$ to $0.826 V_{\text{SCE}}$ when the concentration was increased from 3M to 9M. However, value of E_{corr} ($0.839 V_{\text{SCE}}$) was slightly higher in 6M HNO_3 compared to that in 9M HNO_3 .

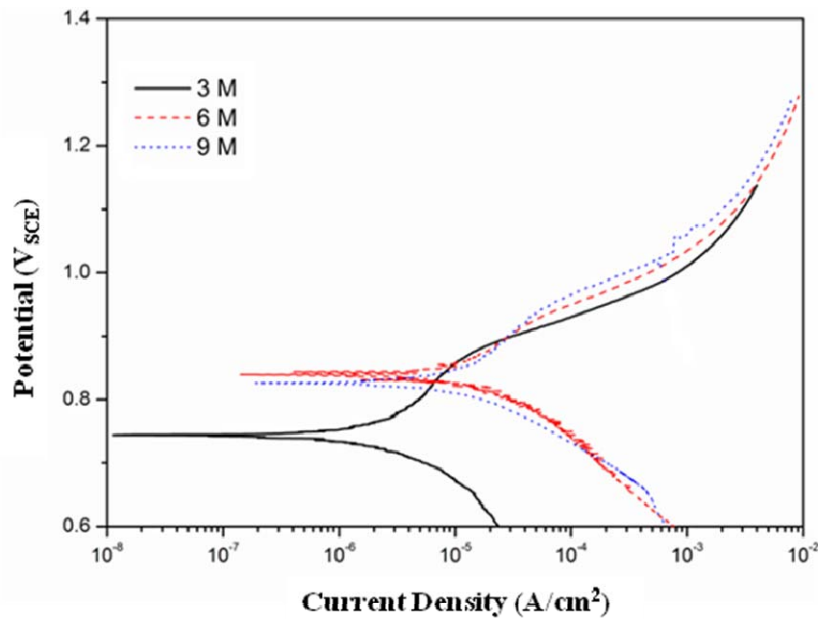


Fig. 6.1 Polarization curves of Type 304L1 in near boiling HNO_3 .

The relationship between corrosion rates of Type 304L1 measured after 48 h exposure to near boiling HNO_3 of various concentrations and applied potentials is shown in Fig. 6.2. The corrosion rate increased at each potential with decreasing concentration of HNO_3 . The threshold potential for Type 304L1 in 3M, 6M and 9M HNO_3 were $0.92 V_{\text{SCE}}$, $0.96 V_{\text{SCE}}$ and $0.98 V_{\text{SCE}}$ respectively. The polarization curves (Fig. 6.1) show anodic current densities that are in the order of $3\text{M} > 6\text{M} > 9\text{M}$ above threshold potentials. This observation is supported by the result obtained from potentiostatic immersion tests (Fig. 6.2). It is described in chapter 4 that below threshold potential corrosion rate remains low and uniform corrosion occurs and above threshold potential IGC with grain dropping was observed. When Type 304L1 was exposed to 3M HNO_3 for 48 h at $0.90 V_{\text{SCE}}$ a corrosion rate of 0.28 mmy^{-1} (10.9Mpy) was observed. The morphological study showed uniform corrosion after this exposure (Fig. 6.3).

Uniform corrosion was observed at 0.90 V_{SCE} in 3M HNO₃ because this potential is below threshold potential (0.92 V_{SCE}).

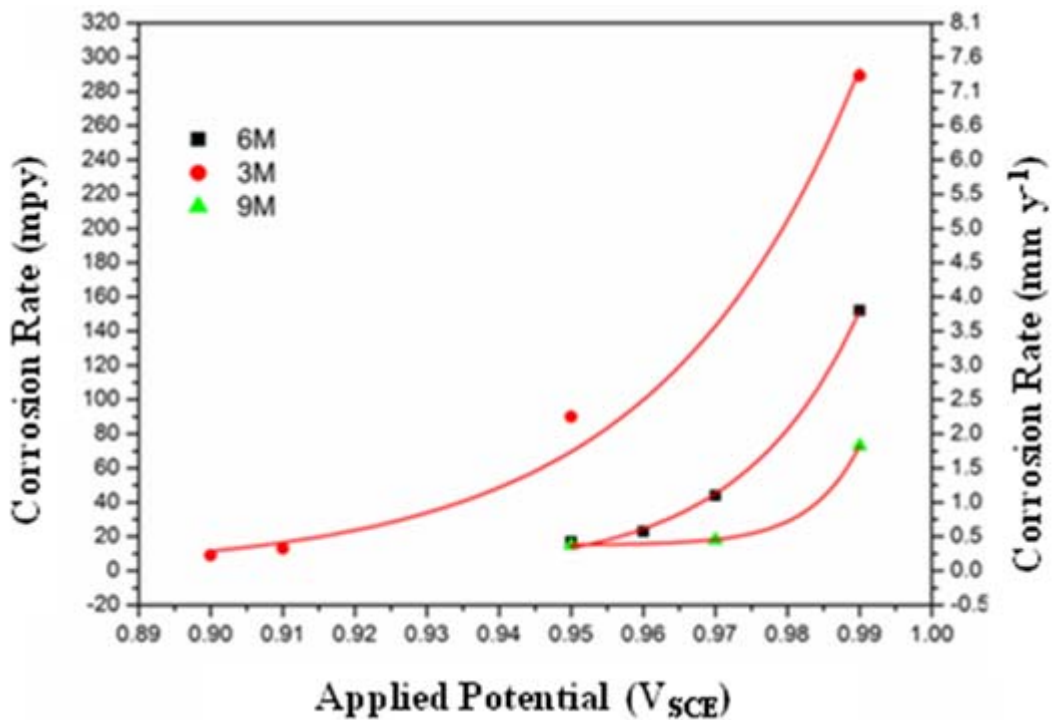


Fig. 6.2 Corrosion rate of Type 304L1 as a function of applied potential at different concentrations of near boiling HNO₃.

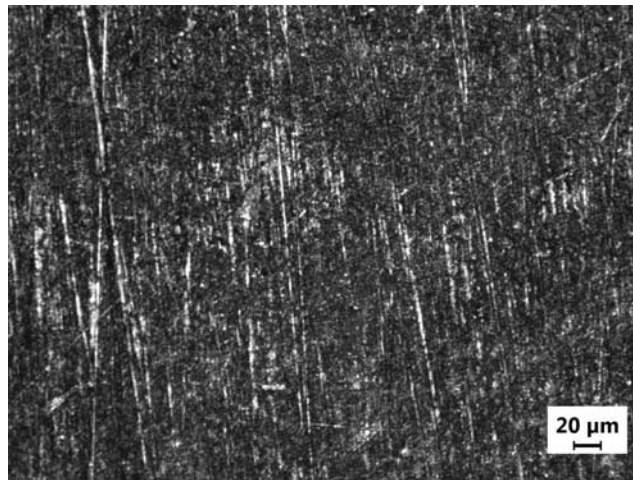


Fig. 6.3 Uniform corrosion of Type 304L1 (observed under optical microscope) exposed to near boiling 3M HNO₃ at 0.90 V_{SCE}.

A comparison of morphology of corrosion attack in 3M and 9M HNO₃ at 0.95 V_{SCE} and 0.99 V_{SCE} is shown in Fig. 6.4. The morphology of corrosion attack at 0.95 V_{SCE} and 0.99 V_{SCE} in 6M HNO₃ is shown in Fig. 4.9. At 0.95 V_{SCE} corrosion rates were 0.43 Mmy⁻¹ (17

mpy) and 0.38 mmy^{-1} (15 mpy) in 6M and 9M HNO_3 respectively. Grain boundaries were slightly attacked in 6M and 9M HNO_3 at $0.95 V_{\text{SCE}}$ (Fig. 4.9a and Fig. 6.4a). Corrosion rate increased to 2.28 mmy^{-1} (90 mpy) at $0.95 V_{\text{SCE}}$ when acid concentration was decreased to 3M. The morphology of attack was characterized by severe grain droppings at $0.95 V_{\text{SCE}}$ in 3M HNO_3 (Fig. 6.4b). At $0.99 V_{\text{SCE}}$ corrosion rates were 7.3 mmy^{-1} (289 mpy), 3.8 mmy^{-1} (152 mpy) and 1.85 mmy^{-1} (73 mpy) in 3M, 6M and 9M HNO_3 respectively. The morphology of attack was characterized by grain droppings at $0.99 V_{\text{SCE}}$ in all the three concentrations of HNO_3 but the extent of grain dropping increased with decrease in acid concentration (Fig. 4.9b and Fig.6.4c and d).

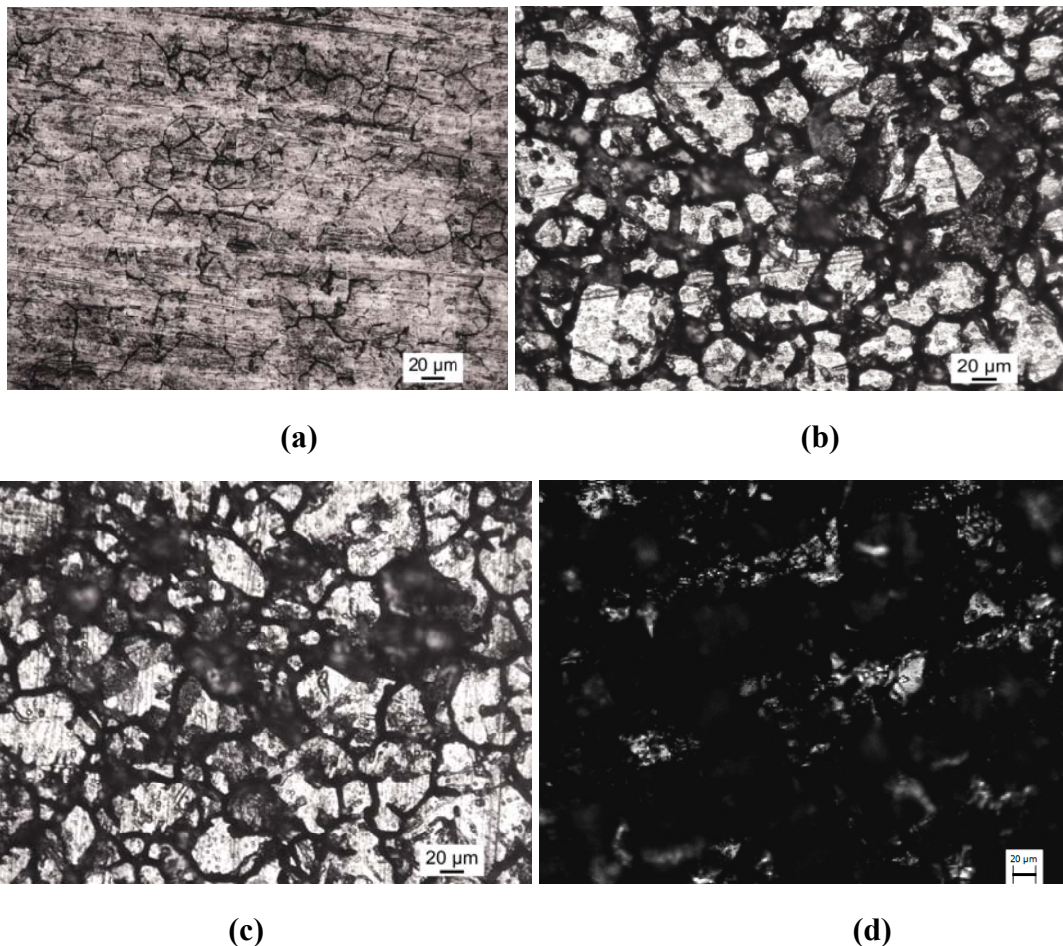


Fig.6.4 Morphology of corrosion attack (observed by optical microscope) of Type 304L1 at $0.95 V_{\text{SCE}}$ in (a) 9M (b) 3M and at $0.99 V_{\text{SCE}}$ (c) 9M and (d) near boiling 3M HNO_3 .

6.2.2 Effect of Test Temperature on Corrosion of Type 304L NAG1

The effect of temperature on corrosion behavior of Type 304L NAG1 (heat treated at 675 °C for 1 h) was investigated in 6M HNO₃ at an applied potential of 0.99 V_{SCE}. The relationship between corrosion rate and solution temperature at 0.99 V_{SCE} is shown in Fig.6.5. The corrosion rates increased from 0.11mm⁻¹ (4.5 mpy) to a value of 2.11 mm⁻¹ (83 mpy) on increasing the solution temperature from 55 to 95 °C.

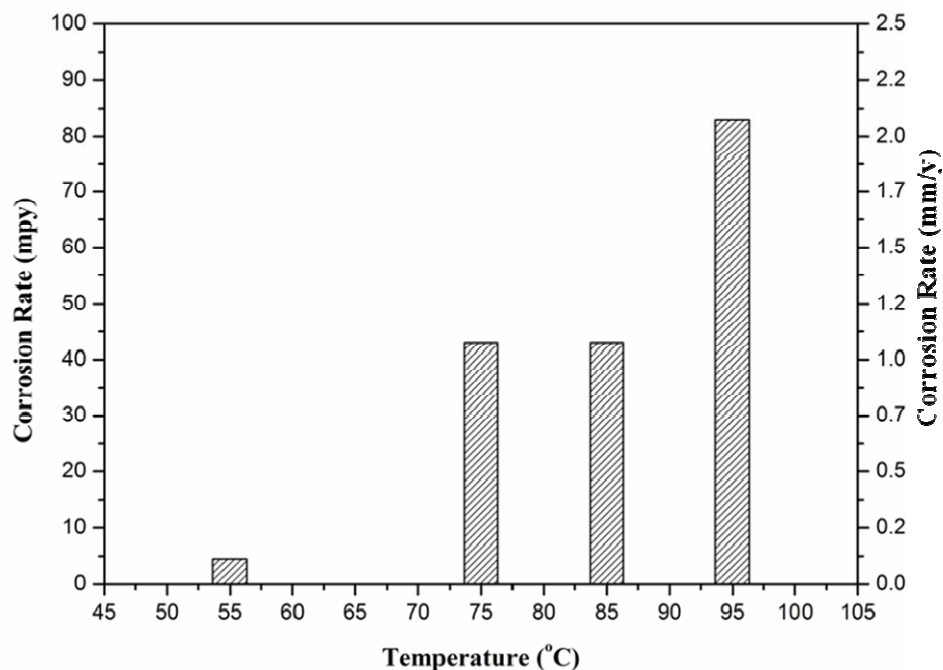


Fig.6.5 Relationship between corrosion rate and solution temperature for Type 304L NAG1 at 0.99 V_{SCE} in 6M HNO₃.

The value of activation energy was evaluated using equation 6.1 by plotting log r vs. 1/T.

$$\text{Log } r = -\frac{E_a}{2.303 RT} + A \quad (6.1)$$

where E_a is activation energy, A is pre-exponential factor, R is universal gas constant, r is corrosion rate and T is absolute temperature.

The value of activation energy calculated using equation 6.1 by plotting log r vs 1/T was 72.56 kJ⁻¹. Covino et al., evaluated activation energy for corrosion of Type 304 in

HNO₃/HF solutions ranging from 0.8 M to 3.5 M HNO₃ and 0.5 M to 2.6M HF at 30, 50, 70 and 90 °C [157]. They observed a minimum for activation energy at 1.3M HNO₃. Activation energy for dissolution of Type 304 ranged from 20.9 to 41.8 kJM⁻¹ in solutions with HNO₃ of concentration higher than 1.3M. Activation energy for dissolution of Type 304 ranged from 37.6 to 58.57 kJM⁻¹ in solutions with HNO₃ of concentration lower than 1.3M. Concentration of hydrofluoric acid did not have any significant effect on activation energy for dissolution of Type 304. Activation energy for corrosion of Type 304L NAG1 was higher compared to Type 304. This can be due to: (1) corrosion systems in the present investigation and in study by Covino et al. [157] are not the same and (2) Type 304L NAG1 is an improved grade over Type 304 thus exhibits superior corrosion resistance compared to Type 304 SS in HNO₃.

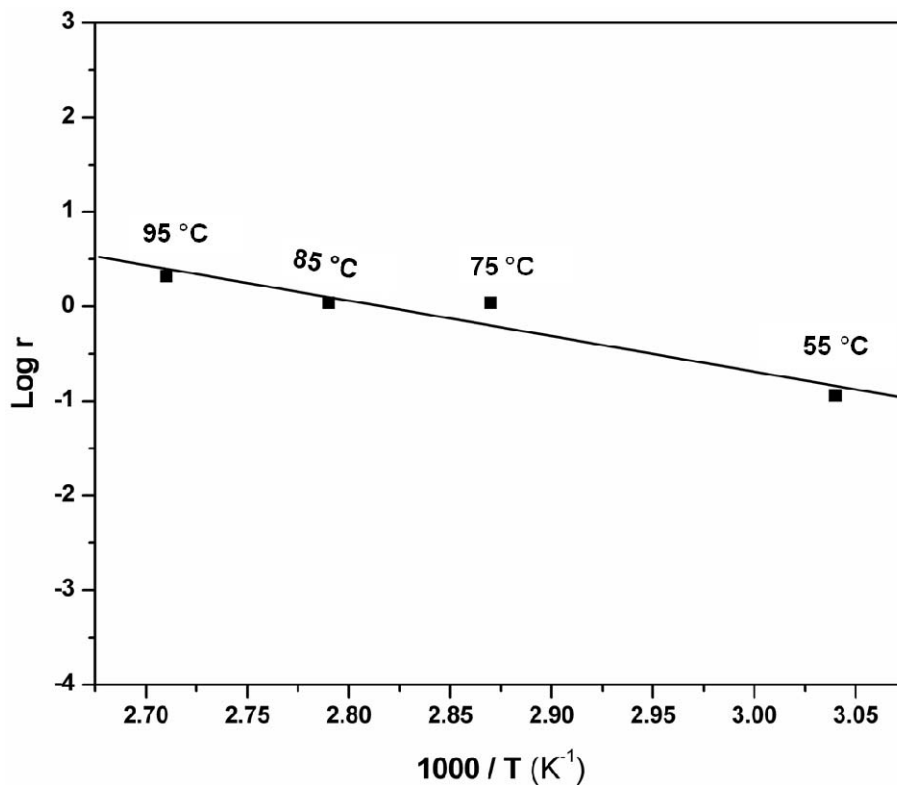


Fig.6.6 Arrhenius plot of log r vs. 1 / T.

6.3 Summary

The following is the brief summary of the present investigations on the role of acid concentration and solution temperature on corrosion behavior:

- Type 304L1 even in non sensitized condition showed severe IGC at transpassive potentials in HNO₃ of all the three concentrations (3M, 6M and 9M).
- Polarization studies showed an increase in E_{corr} when acid concentration was increased from 3M HNO₃ to 6M HNO₃. However the E_{corr} in 9M HNO₃ was slightly lower compared to the value obtained for 6M HNO₃.
- Threshold potential of Type 304L1 in various concentrations of HNO₃ were in the order: 3M < 6M < 9M.
- The activation energy for corrosion of Type 304L NAG1 in 6M HNO₃ at 0.99 V_{SCE} was 72.56 kJ⁻¹.

CHAPTER 7

END GRAIN CORROSION

This chapter contains the results on the investigations of the mechanism of “End Grain Corrosion” of Type 304L NAG2 in boiling 9M HNO₃ containing Cr⁶⁺ ions. Influence of Cr⁶⁺ concentration on the susceptibility to “End Grain Corrosion” was studied on as-received Type 304L NAG2. The as-received specimens were subjected to specific heat treatments to induce intergranular segregation of phosphorus or sulfur. These heat treated specimens were subjected to “End Grain Corrosion” test to investigate their susceptibility to “End Grain Corrosion”. The morphology of corrosion attack was confirmed by optical microscopy and SEM. A clear effect on “End Grain Corrosion” was found for heat treatment reported to induce phosphorus or sulfur segregation. Finally, specific annealing heat treatment was developed that removes the phosphorus segregation, without affecting the grain size or sensitization.

7.1 Background

A brief introduction to “End Grain Corrosion” was given in chapter 2. Many studies dealing with IGC in relation to reprocessing plants are available [13, 14, 17, 24, 158]. “End Grain Corrosion” is also known as tunnel penetration [84]. Like IGC, “End Grain Corrosion” is considered as a major mode of degradation of austenitic SS in highly oxidizing HNO₃ [84]. Probably the most important example of “End Grain Corrosion” is austenitic SS in HNO₃. It should be mentioned here that it is not peculiar to austenitic SS in HNO₃. Exfoliation corrosion of high-strength aluminum alloys comes closest to “End Grain Corrosion” in terms of morphology. It is mostly observed in high humidity and salt containing environments

[159]. Rolled or extruded aluminum alloys products in which grains are elongated and flattened are susceptible to exfoliation corrosion [159].

Presence of non-metallic elements in SS enhances “End Grain Corrosion” [31]. In the case of plate, which is usually manufactured by continuous casting, non-metallic constituents such as phosphorus and silicon tend to gather toward the core of an ingot [84] and are then drawn out along the hot working direction forming segregated bands. For niobium stabilized SS, such as 18Cr–13Ni–1Nb, the dissolution of NbC precipitate and MnS inclusion stringers orientated with the rolling direction contribute significantly to enhance “End Grain Corrosion”. Takeuchi and Whillock studied “End Grain Corrosion” of 18Cr–10Ni austenitic SS in simulated dissolver liquor [84]. They found from the distribution of end grain pits, maximum penetration rate into the end grain, even under non boiling condition, was 8.8 mmy^{-1} . Chandra et al. have shown that the possible reasons for the directional nature of “End-Grain Attack” are the manganese sulfide inclusions aligned along the hot-working direction and/or segregation of chromium along the flow lines during the fabrication stage itself [30]. They have also shown that controlled solution annealing, laser surface remelting, and weld overlay can be used to avoid/minimize end-grain corrosion [30]. Kain et al. have compared Type 304L and Type 304L NAG susceptibility to “End Grain Corrosion” in $9\text{M HNO}_3 + 1\text{g Cr}^{6+} \text{ L}^{-1}$ [24]. They have reported a much less susceptibility to “End Grain Corrosion” of Type 304L NAG compared to Type 304L [24]. Available literature in this area is scarce to provide a comprehensive understanding of mechanism of “End Grain Corrosion” and prediction of its likely occurrence.

In this chapter, “End Grain Corrosion” of Type 304L NAG2 in HNO_3 containing Cr^{6+} ions was investigated. Influence of Cr^{6+} concentration on “End Grain Corrosion” was studied. Also separate specimens were subjected to different heat treatment to induce selective segregation of phosphorus and sulfur. The susceptibility to “End Grain Corrosion” was

established in the tests using boiling HNO₃ containing oxidizing Cr⁶⁺ ions (test procedure detailed in section 3.4.2.). A clear effect on “End Grain Corrosion” was found for heat treatment reported to induce phosphorus segregation and sulfur segregation. Finally, salvaging heat treatment has been developed that equilibrate the phosphorus segregation.

7.2 Results and Discussion

7.2.1 End Grain Corrosion at Different Concentrations of Cr⁶⁺

Type 304L NAG2 was in “non-sensitized” condition and showed “step” microstructure” (Fig.7.1) after electroetching in 10% oxalic acid. Fig.7.2 shows corrosion rate of the as-received Type 304L NAG2 specimens as a function of time for different concentrations of Cr⁶⁺ in boiling 9M HNO₃. It is clear that the corrosion rate increased with increase in Cr⁶⁺ concentration. Specimen exposed to 9M HNO₃ containing 1.5 g L⁻¹ Cr⁶⁺ showed the highest corrosion rate while specimen exposed to 9M HNO₃ containing 1g L⁻¹ Cr⁶⁺ showed the least corrosion rate. Trend of increase in corrosion rate with time was observed for all the three specimens. The corrosion rate for specimen exposed to 9M HNO₃ containing 1.5 g L⁻¹ Cr⁶⁺ in the 19th period was 23 mmy⁻¹ (909 mpy). The corrosion rate of the specimen exposed to 9M HNO₃ containing 1.25 g L⁻¹ Cr⁶⁺ in 19th period was 17.4 mmy⁻¹ (688 mpy). Specimen exposed to 9M HNO₃ containing 1g L⁻¹ Cr⁶⁺ in showed a corrosion rate of 8.4 mmy⁻¹ (332 mpy) after the same exposure period (57 h).

The corrosion attack as seen in the longitudinal direction of the specimen was typical “End Grain Corrosion” as seen in Fig. 7.3. The depth of “End Grain Corrosion” in the specimen exposed to boiling 9M HNO₃ containing 1.5 g L⁻¹ Cr⁶⁺ after 19th period was 475 μm. The depth of the “End Grain Corrosion” in specimen exposed to boiling 9M HNO₃ containing 1.25 g L⁻¹ Cr⁶⁺ after 20th period was 100 μm.

Fig.7.4 shows potential variation with time of Type 304L NAG2 in boiling 9M HNO₃ containing different concentrations of Cr⁶⁺. It is clear that the potential developed when specimens were exposed to boiling 9M HNO₃ containing different concentrations of Cr⁶⁺ ions is increased with increase in Cr⁶⁺ concentration. The higher potential developed on the specimen exposed to boiling 9M HNO₃ containing 1.5 g L⁻¹ Cr⁶⁺ may be the reason for higher corrosion rate and very deep “End Grain Corrosion” attack observed in this specimens.

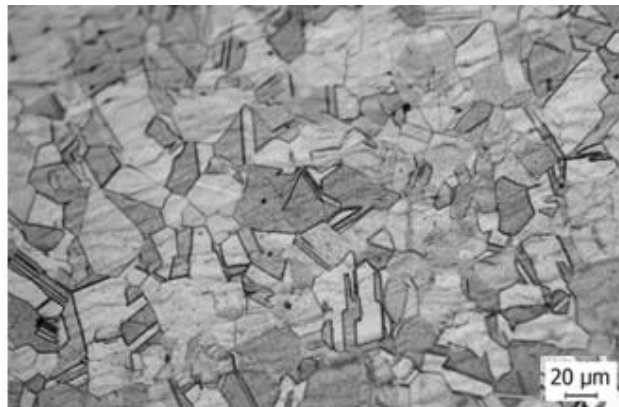


Fig. 7.1 Microstructure of Type 304L NAG2 observed by optical microscope in as received condition.

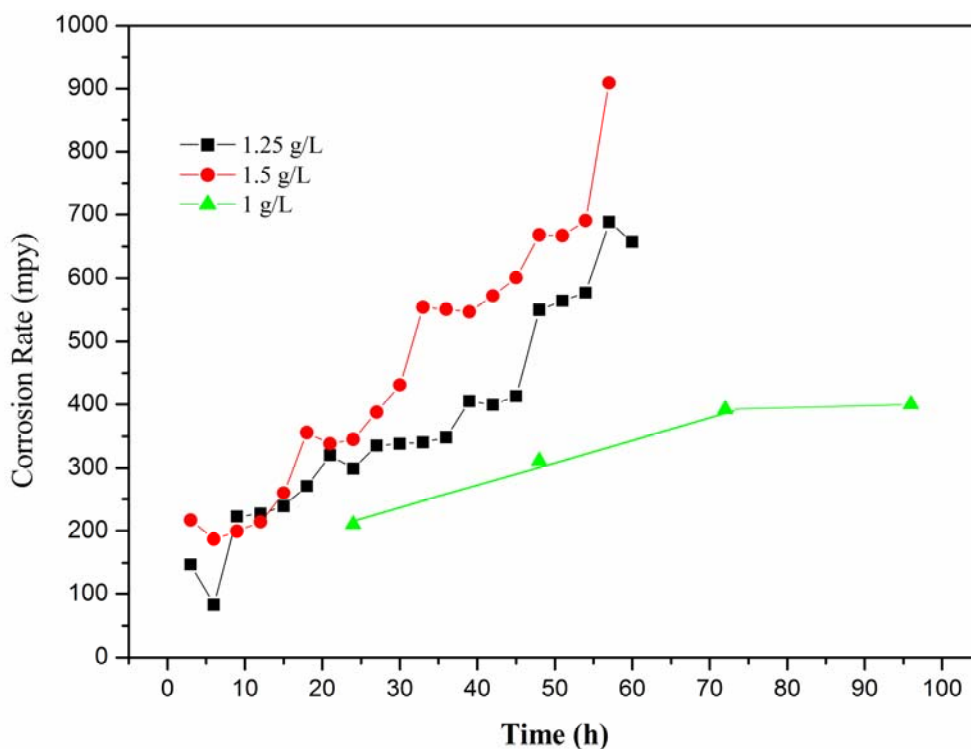


Fig. 7.2 Corrosion rate of Type 304L NAG2 as a function of time at different concentrations of Cr⁶⁺ in boiling 9M HNO₃.

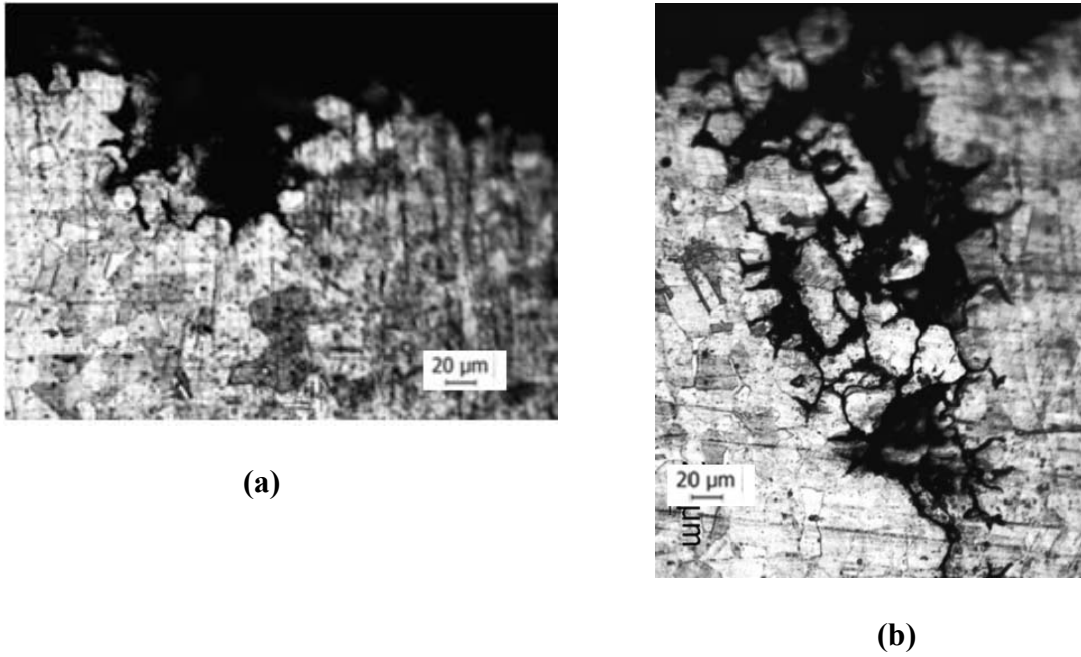


Fig.7.3 Corrosion attack as seen in the longitudinal direction of Type 304L NAG2 specimen by optical microscope exposed to 9M HNO₃ containing (a) 1.25 g L⁻¹ Cr⁶⁺ and (b) 1.5 g L⁻¹ Cr⁶⁺.

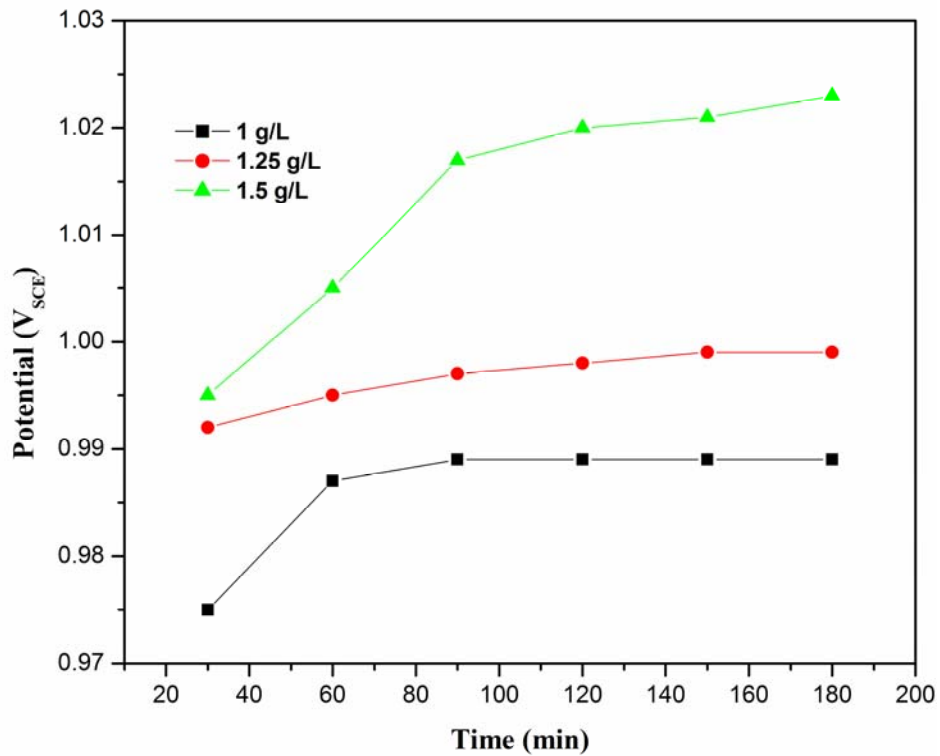


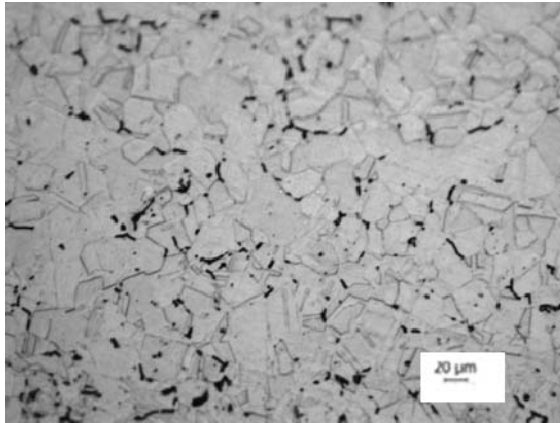
Fig.7.4 Potential variation with time of Type 304L NAG2 in boiling 9M HNO₃ containing different concentrations of Cr⁶⁺.

7.2.2 Influence of Intergranular Elemental Segregation on End Grain Corrosion

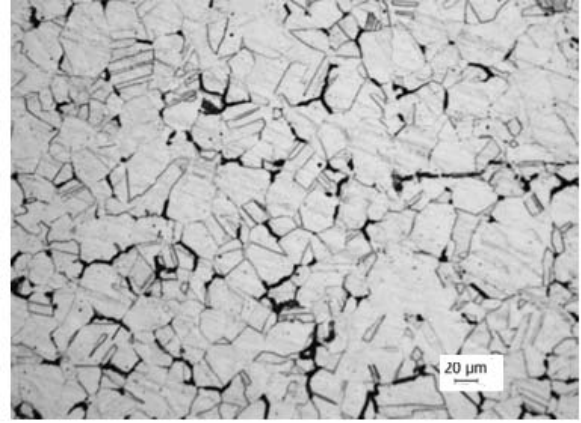
7.2.2.1 Degree of Sensitization

The microstructure of the as-received specimen was “step” (Fig. 7.1). “step” microstructure became “dual” microstructure after heat treatment at 650 °C for 3 h (Fig.7.5a). A “dual” microstructure was also revealed when the as-received material was heat treated at 650 °C for 100 h (Fig.7.5b). Heat treatment at 950 °C for 90 min on specimen previously heat treated at 650 °C for 100 h converted “dual” microstructure to “step” microstructure without any change in grain size (Fig. 7.5 c). Specimen heat treated at 990 °C for 5 minute showed “step” microstructure (Fig. 7.5 d).

Table 7.1 lists the values of degree of sensitization (DOS) for the as-received and heat treated specimens evaluated from DL-EPR test. The as-received specimen showed very low value of DOS which corresponds to “step” microstructure. A slight increase in DOS value was observed after the heat treatment of 650 °C for 3 h. Microstructure after DL-EPR test of specimen heat treated at 650 °C for 3 h was marginally “dual”. When the duration of heat treatment was increased from 3 h to 100 h at 650 °C the DOS value increased from 0.18 to 1.4. It is confirmed by the microstructure seen after DL- EPR test that DOS value 1.4 corresponds to “dual” microstructure. An annealing heat treatment at 950 °C for 90 min on specimen previously heat treated at 650 °C for 100 h lowered the DOS from 1.4 to 0.06. The DOS value of specimen heat treated at 990 °C for 5 min was 0.13. It is evident from the above discussion that the as-received as well as the heat treated specimen show low DOS values which correspond to either “step” or “dual” microstructure. In other words none of the heat treatments resulted in severe sensitization to cause “ditch” microstructure.



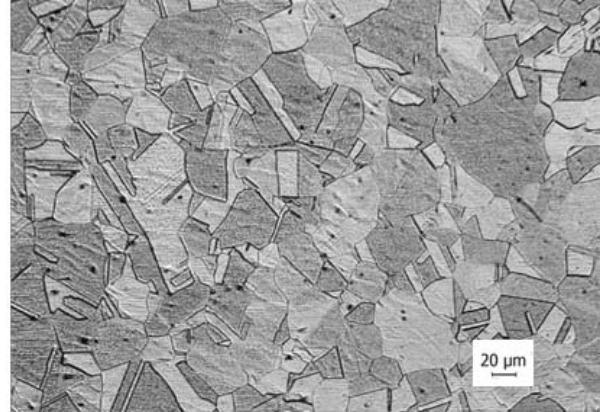
(a)



(b)



(c)



(d)

Fig.7.5 Microstructures of the transverse section of the Type 304L NAG2 observed by optical microscope after the following heat treatments (a) 650 °C for 3 h, (b) 650 °C for 100 h, (c) 650 °C for 100 h then 950 °C for 90 min and (d) 990 °C for 5 min.

Table 7.1 Summary of the degree of sensitization (DOS) of Type 304L NAG2 in as-received condition and after heat treatments evaluated from DL-EPR test

Heat Treatment Type	DOS (%)	Mirostructural attack seen After DL-EPR
As-received	0.11	Step
650 °C for 3h	0.18	Dual
650 °C for 100 h	1.4	Dual
990 °C for 5 min	0.13	Step
650 °C for 100 h then 950 °C for 90 min	0.06	Step

7.2.2.2 Results of “End Grain Corrosion”

To assess the influence of intergranular elemental segregation on “End Grain Corrosion”, the as-received as well as the heat treated specimens were subjected to “End Grain Corrosion” test. Specimens were immersed in boiling 9M HNO₃+1 g L⁻¹ Cr⁶⁺ for four periods of 24 h duration each (section 3.4.2 of chapter 3). The results of these tests are shown in Fig. 7.6. Specimen heat treated at 650 °C for 100 h exhibited a corrosion rate of 11.09 mmy⁻¹ (437 mpy) in the first period which increased to 27.5 mmy⁻¹ (1083 mpy) in the second period. Because of such a high corrosion rate specimen heat treated at 650 °C for 100 h was not subjected to “End Grain Corrosion” test beyond second period. When the specimen previously heat treated at 650 °C for 100 h was annealed at 950 °C for 90 min and subjected to “End Grain Corrosion” test a drastic decrease in the corrosion rate was observed. In fact this specimen showed least average corrosion rate of 3.2 mmy⁻¹ (126 mpy) among all the specimens.

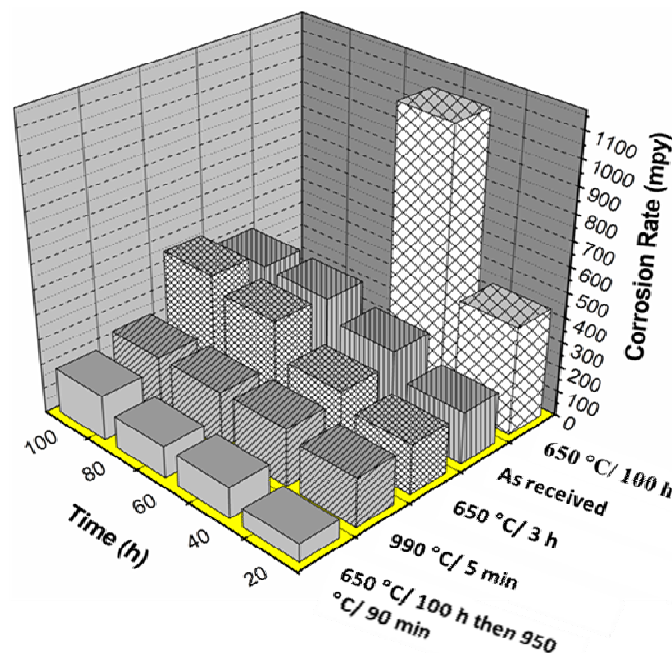


Fig.7. 6 Corrosion rate measured as a function of discrete periods using the “End Grain Corrosion” test in boiling 9M HNO₃ + 1 g L⁻¹ Cr⁶⁺ solution.

The morphology of the corrosion attack starting from the cross section of the tube, examined after the “End Grain Corrosion” test is shown in Fig.7.7 for all the specimens. It is clear that the corrosion attack was visible only at a few locations from the cross-sectional surfaces that propagated in longitudinal direction through intergranular mode of corrosion. Therefore, clearly it is an example of “End Grain Corrosion”. From Fig. 7.7, it is evident that the maximum extent of “End Grain Corrosion” (depth of corrosion attack) was in the specimen heat treated at 650 °C for 100 h (Fig. 7.7c). Depth of “End Grain Corrosion” was much lower in specimen heat treated at 650 °C for 3 h compared to specimen heat treated at 650 °C for 100 h (Fig. 7.7 b). It is to be noted that the specimen heat treated at 650 °C for 100 h and specimen heat treated at 650 °C for 3 h showed “dual” microstructure in practice A ASTM A 262. Type 304L with “dual” microstructure is not prone to IGC in practice C ASTM A 262 [22]. This practice detects susceptibility to IGC associated with chromium carbide precipitate and with sigma-like phase precipitate [22]. Specimen heat treated at 650 °C for 100 h (showed highest value of DOS) was also subjected to practice C ASTM A 262. The average corrosion rate in practice C ASTM A 262 was 0.15 mmy^{-1} (6 mpy). This shows that the specimen is not prone to IGC due to Cr depletion in practice C ASTM A 262. Thus the “End Grain Corrosion” in these specimens can not be explained due to “dual” microstructure or in other words due to Cr depletion. It has been reported that the heat treatment (at 650 °C for 100 h) resulted in the maximum segregation of phosphorus in austenitic SS [111]. Therefore “End Grain Corrosion” in this specimen is due to the segregation of phosphorus that is induced by the stated heat treatment. In the “End Grain Corrosion” test specimen heat treated at 650 °C for 100 h and then annealed at 950 °C for 90 min showed the least corrosion rate. Also the depth of “End Grain Corrosion” was least for this specimen (Fig 7.7 d). The heat treatment at 950 °C for 90 min is taken to equilibrate segregation without sensitization or grain growth of the material [30]. Therefore “End Grain

Corrosion” is minimal in the specimen that received this heat treatment. Fig. 7.7 also showed very deep “End Grain Corrosion” in specimen heat treated at 990 °C for 5 min. It is shown that heat treatment at 990 °C for 5 min resulted in intergranular segregation of S in austenitic SS [112]. Very severe “End Grain Corrosion” in specimen heat treated at 990 °C for 5 min might be due to segregation of sulfur along the grain boundaries. Corrosion rate for this specimen in “End Grain Corrosion” test was lower compared to as-received specimen. As received specimen showed IGC starting from OD as well as ID side of the tube and propagating along thickness of the tube (Fig 7.8. a-b). In the specimen heat treated at 990 °C for 5 min from OD and ID side of the tube IGC was not severe (Fig. 7.8 c shows IGC from OD side of the tube). The higher corrosion rate in as-received specimen compared to specimen heat treated at 990 °C for 5 min might be due to higher IGC from OD and ID side of the tube.

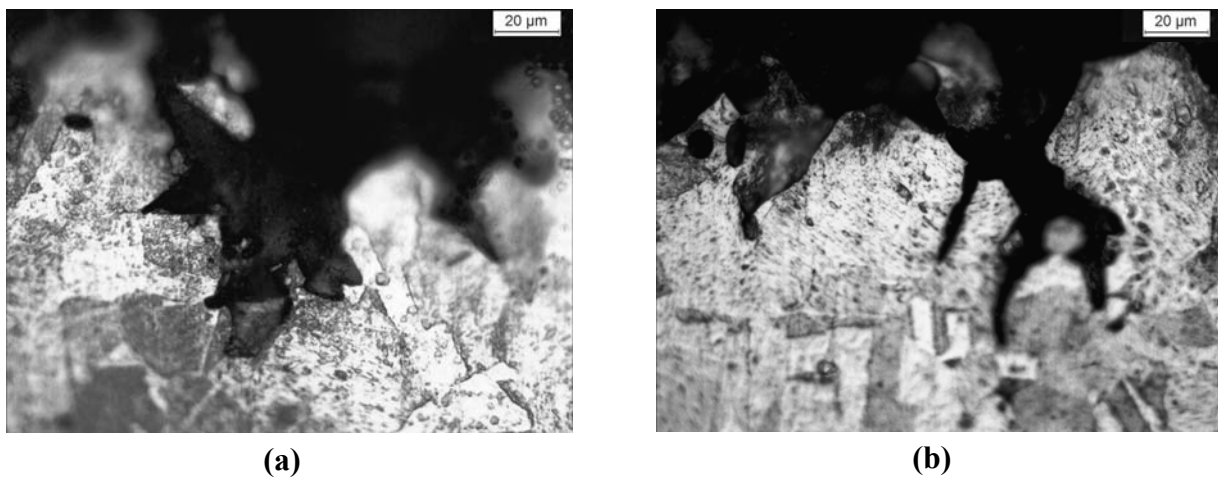
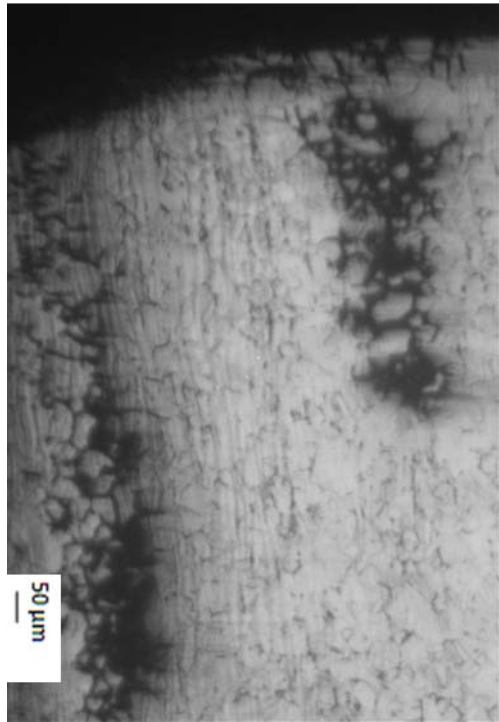
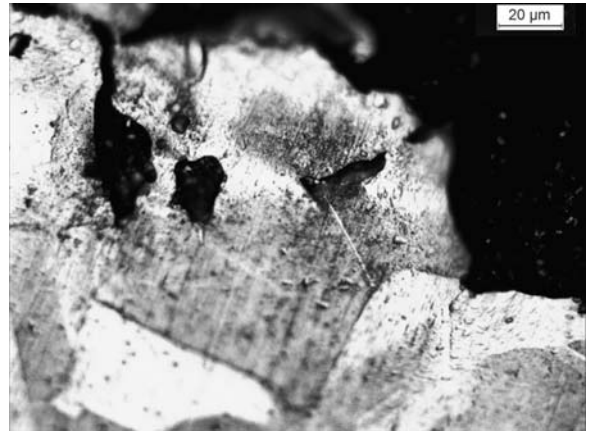


Fig.7. 7 Morphology of corrosion attack observed by optical microscope in (a) As received, (b) 650 °C for 3h, (c) 650 °C for 100 h, (d) 650 °C for 100 h then annealed at 950 °C for 90 min and (e) 990 °C for 5 min, after “End Grain Corrosion” test in boiling 9M HNO₃ + 1 g L⁻¹ Cr⁶⁺ solution.



(c)



(d)



(e)

Fig.7. 7 Continued

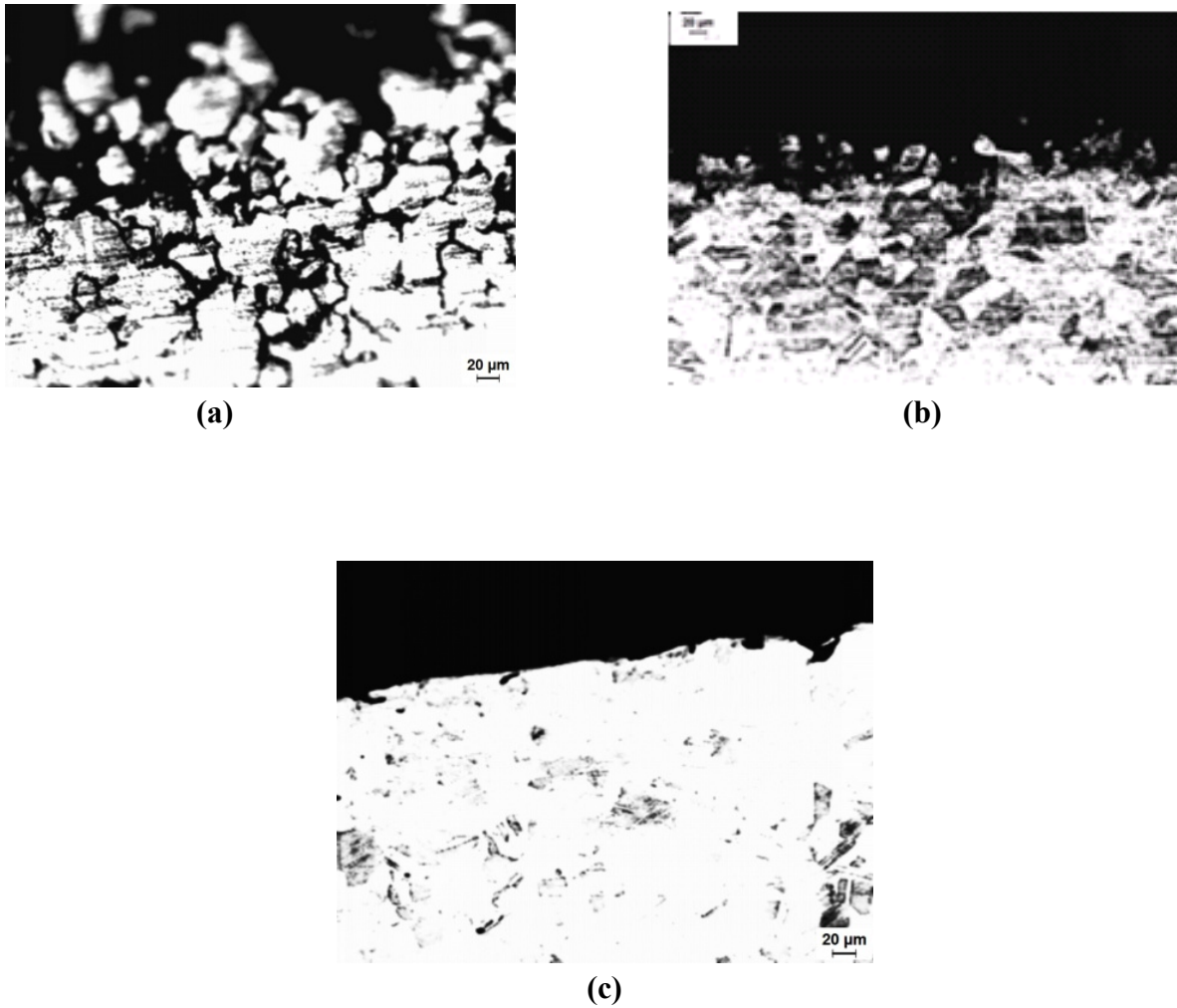
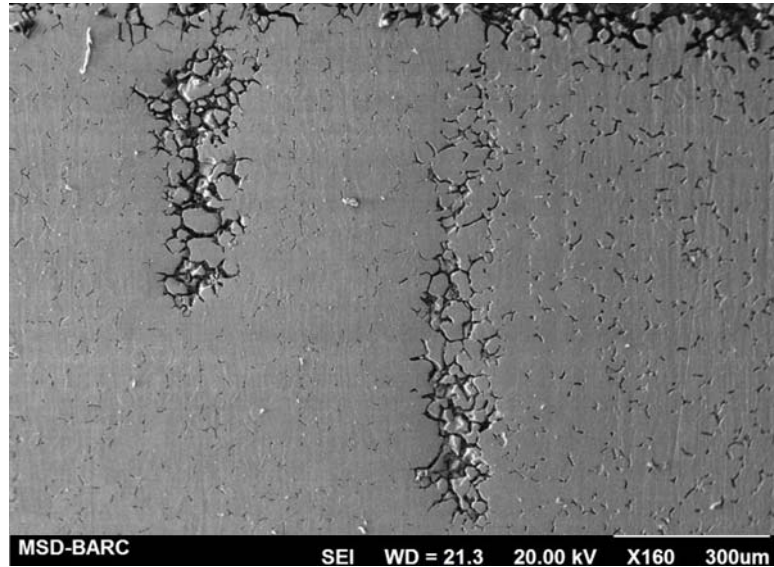
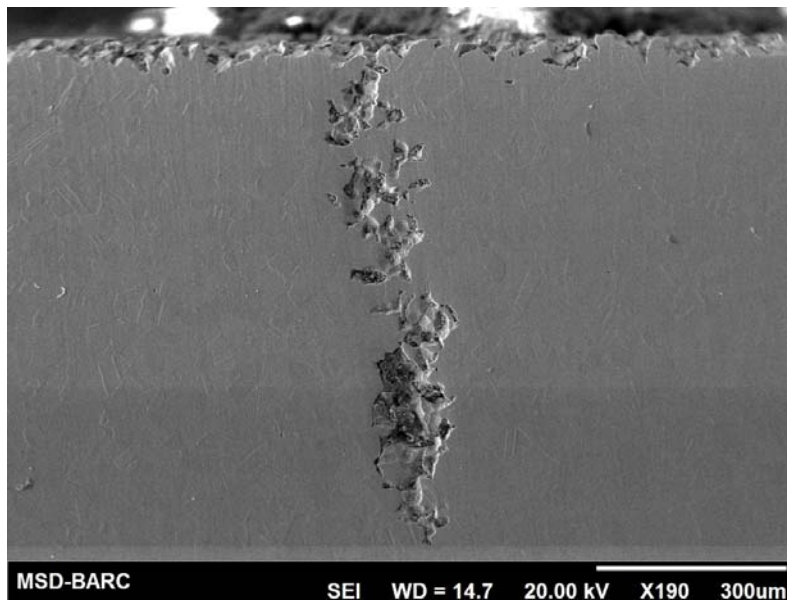


Fig.7. 8 IGC observed by optical microscope after the “End Grain Corrosion” test (a) in as-received specimen from OD side of the tube, (b) in as-received specimen from ID side of the tube and (c) in specimen heat treated at 990 °C for 5 min from OD side of the tube.

The morphology of corrosion attack after “End Grain Corrosion” test was confirmed by SEM examination and is shown in Fig. 7.9. Corrosion attack in the specimen heat treated at 650 °C for 100 h and in the specimen heat treated at 990 °C for 5 min are typical examples of “End Grain Corrosion”. The “End Grain Corrosion” is not directly shown in this study to be affected by segregation of phosphorus or sulfur but heat treatments that are reported to lead to S or P segregation have been shown to lead to “End Grain Corrosion”.



(a)



(b)

Fig. 7.9 Morphology of “End Grain Corrosion” observed by SEM after (a) specimen heat treated at 650 °C for 100 h was exposed to 9M HNO₃ containing 1 g Cr⁶⁺ for four periods of 24 h. and (b) specimen heat treated at 990 °C for 5 min was exposed to 9M HNO₃ containing 1 g L⁻¹Cr⁶⁺ for four periods of 24 h.

The segregation of phosphorus or sulfur is likely to take place more along the flow lines / shear bands aligned along the working direction. This would induce the corrosion attack to propagate preferentially along those regions from the exposed cross sectional surfaces that have the segregation of phosphorus. Once the accelerated corrosion starts at these locations, further propagation occurs by intergranular corrosion as the grain boundaries

(even the non-sensitized) are high energy boundaries and the highly corrosive solution developed in these “pits” (due to accumulation of Cr^{6+} , the corrosion product in an oxidizing solution) would cause fast dissolution of any material as the operating electrochemical potential is in transpassive regime [160]. The heat treatment at 950 °C for 90 minutes did result in freedom from “End Grain Corrosion” and it did not cause sensitization in SS either . Therefore all the SS that are prone to “End Grain Corrosion” (as determined by the test stated in this study) can be subjected to this heat treatment to equilibrate segregation of phosphorus and make it resistant to “End Grain Corrosion”. Salvaging heat treatment at 950 °C for 90 min did result in freedom from “End Grain Corrosion” without altering grain size of the material and without inducing any sensitization to material.

7.3 Summary

The following is the brief summary of the present investigations dealing with the role of Cr^{6+} concentration present in HNO_3 and intergranular segregation of sulfur and phosphorus:

- Increase in Cr^{6+} concentration in 9M HNO_3 increased Type 304L NAG2 susceptibility to “End Grain Corrosion”.
- This increase in susceptibility to “End Grain Corrosion” of Type 304L NAG2 is attributed to increase in electrochemical potential with increase in Cr^{6+} concentrations.
- Any heat treatment used in this work did not result in extensive sensitization and Type 304L NAG2 remained resistant to intergranular corrosion in practice A and C, A 262, ASTM.
- Significant increase in “End Grain Corrosion” in specimen heat treated at 650 °C for 100 h was observed which is taken to be due to high segregation of phosphorus to the grain boundary.

- After inducing a high susceptibility to “End Grain Corrosion” by heat treatment at 650 °C for 100 h, a salvaging heat treatment at 950 °C for 90 min lowered the susceptibility to “End Grain Corrosion”. This was taken to be due to the equilibration of segregation of phosphorus.
- Heat treatment at 990 °C for 5 min resulted in a high increase in “End Grain Corrosion”.
- This increase in susceptibility to “End Grain Corrosion” after the heat treatment at 990 °C for 5 min is attributed to segregation of sulfur to the grain boundaries.

CHAPTER 8

CONCLUSIONS

8.1 Conclusions

The studies described in this thesis have centered around the corrosion behavior of austenitic SS alloys in HNO_3 at transpassive potentials. The austenitic SS alloys chosen for the study are important due to their use in the spent nuclear fuel reprocessing plants. The major objective has been to understand influence of various material parameters like alloy chemical composition, microstructure, grain size and grain boundary character, and process parameters such as acid concentration and its temperature on the corrosion behavior. For parameters like alloy chemical composition, microstructure and acid concentration, a “safe/limiting” OCP was established to keep the structural material safe from attack in plants. The conclusions derived from the results discussed in chapters 4-7 are mentioned below:

- Applicability of the methodology for establishing the relation between the electrochemical potential and the corrosion rate for the chosen system (grade of SS, microstructure of SS, operating parameters) has been demonstrated.
- A difference in the potential for onset of transpassivity when using potentiodynamic and potentiostatic techniques was observed.
- The potentiostatic immersion corrosion tests revealed that SS even in solution annealed condition are susceptible to IGC at transpassive potentials. In operating plants OCP may reach to transpassive potential regime due to combined effect of concentration of acid, its high temperature and the presence of oxidizing ions. In such a situation, IGC would start even in a solution annealed SS. Therefore, SS can not be used for such applications. It was observed that when the developed potential (OCP)

is just at the transition to transpassivity, different alloys like Types 304L1, 304L NAG1, and 310L with different microstructures (“step”, “dual”, “ditch”) would behave differently as the transpassive potentials for each would be slightly different.

- At transpassive potentials austenitic SS alloy namely Types 310L , 304L NAG1 and 304L1 followed corrosion rate in the order: type 310L < 304L NAG1 < 304L1. The limiting potential for Type 304L1, 304L NAG1 and 310L were 0.960, 0.965 and 0.966 V_{SCE} respectively. These alloys can be used safely below their respective limiting potential in HNO_3 . These results can be applied to HAZ of weldment as well because these alloys were given heat treatment to simulate worst microstructure in the HAZ of weldments prior to corrosion test.
- The corrosion rates for Type 304L1 and Type 304L NAG1 with “step” and “dual” microstructures were comparable at each applied potential. The corrosion rates were lower for Type 304L1 with “step” and “dual” microstructures than for the same material with a “ditch” microstructure over the entire range of applied transpassive potentials used in this study. “ditch” microstructure was not produced for Type 304L NAG1 after heat treatment at 675 °C for extended period of 171 h. From this it can be important observation, that Type 304L NAG1 is a better choice as constructional material for reprocessing plants over Type 304L1 although it is of higher cost.
- Increasing grain size of the Type 304L2 did not show any significant effect on the sensitization. The corrosion rate was lower for Type 304L2 with coarse grain compared to fine grain. Strain-annealing of Type 304L1 induced grain growth and an increase in CSL frequency. The corrosion rate for strain-annealed Type 304L1 was lower compared to as-received Type 304L1. From this an important observation is that SS with coarser grain would perform better compared to SS with fine grain in HNO_3 at transpassive potentials.

- Type 304L1 showed higher corrosion rates with decrease in HNO₃ concentration at transpassive potentials. The value of limiting potential was lower for HNO₃ of lower concentration compared to HNO₃ of higher concentrations. Increase in temperature of HNO₃ increased the corrosion rate of Type 304L NAG1. The activation energy for corrosion of Type 304L NAG1 in 6M HNO₃ at 0.99 V_{SCE} was 72.56 kJ M⁻¹.
- Type 304L NAG2 susceptibility to “End Grain Corrosion” was increased with increase in Cr⁶⁺ concentration in HNO₃. Increase in potential with increase in Cr⁶⁺ concentration was the cause for increase in severity of “End Grain Corrosion”. The heat treatments known to induce intergranular segregation of phosphorus and sulfur caused significant increase in the severity of “End Grain Corrosion” in boiling solution of 9M HNO₃+1g L⁻¹ Cr⁶⁺. These heat treatments did not affect Type 304L NAG2 susceptibility to IGC in 65% boiling HNO₃. It can be inferred from this that Type 304L NAG2 can be used safely for those applications where HNO₃ concentration reaches up to 65% at boiling temperature. Type 304L NAG2 may suffer from “End Grain Corrosion” if used in those applications where HNO₃ used become highly oxidizing due to the presence of oxidizing ions. From the present detailed investigations it can be concluded that all the SS alloys that are prone to “End Grain Corrosion” can be subjected to salvaging heat treatment (at 950 °C for 90 minutes) to equilibrate segregation of phosphorus and make it resistant to “End Grain Corrosion”.

CHAPTER 9

SCOPE FOR FUTURE WORK

It can be stated that through this thesis research work the stated objectives and the initial curiosities on the subject could be addressed. Nevertheless, further scope and research possibilities do exist. Some of the thoughts on the scope of future research are mentioned below:

- **Development of solid state electrode**

Saturated calomel electrode was used as reference electrode in the present work. This electrode is not stable at temperatures above 85°C and hence can not be inserted directly into the near boiling HNO₃ solution for measurements. This limitation necessitates use of acid bridges and intermediate acid and KCl solutions for providing continuous electrical path for potential measurements. Direct potential measurement can provide more accurate readings and simple experimental set up. A solid state electrode suitable to be used in boiling HNO₃ solution can be developed for this purpose.

- **Online monitoring in actual reprocessing plant**

Feasibility of constructing a bypass loop which can be isolated if need be in the actual plant should be studied. If such a set up is possible, then with the help of solid state electrode potential - corrosion rate relationship for the candidate materials can be established in the actual process conditions. The results obtained from this can be used for the development of plant specific online corrosion monitoring system. Such a system can be used for monitoring the plant as well as for separate monitoring of components most prone to IGC like evaporators. The components more prone to IGC due to unfavorable area ratio can be

monitored separately. These measures are expected to result in reduced failures and thus reduced solid waste generation.

- **Determination of intergranular segregation of phosphorus and Sulfur**

In the present work it is shown that heat treatments known to induce phosphorus segregation and sulfur segregation increase the extent of “End Grain Corrosion” attack. This increase in severity of “End Grain Corrosion” was possibly due to intergranular segregation of phosphorus and sulfur. Determination and quantification of intergranular segregation of these elements can be another important area of research.

- **Optimization of thermomechanical process for Type 304L1 to achieve high CSL frequency**

The strain-annealing of Type 304L1 resulted in increase in CSL frequency and grain growth. The influence of strain-annealing was not sufficient to prevent IGC at transpassive potentials. Therefore there is sufficient scope and challenge to optimize thermomechanical process for Type 304L1 to achieve higher CSL frequency and thus prevent its IGC at transpassive potentials.

- **Sensitization in Type 310L SS**

In the present work Type 310L did not show any change in DOS after receiving sensitization heat treatment. The main purpose in this study was to subject Type 310L to the same sensitization heat treatment (675 °C for 1 h) and compare its IGC behavior with that of the Type 304L1 and Type 304L NAG1. Development of sensitization in Type 310L SS may be the subject of another in-depth study.

REFERENCES

- [1] M. G. Fontana, Corrosion Engineering, third ed., Tata McGraw-Hill Publishing Company Limited, New York, 2005.
- [2] D.A. Jones, Principles and Prevention of Corrosion, second ed., MacMillan Publishing Co., 1992.
- [3] J. F. Grubb, T. DeBold, J. D. Fritz, Corrosion of Wrought Stainless Steels, in: S. D. Cramer, B. S. Covino (Eds), Corrosion: Materials, Vol 13B, ASM Handbook (tenth edition), ASM International, Ohio, 2005, p. 54-77.
- [4] K. H. Lo., C.H. Shek, J.K.L. Lai, Mater. Sci. Eng. R., 65 (2009) 39.
- [5] A. J. Sedriks, Corrosion of stainless steels, second ed., John Wiley and Sons, New York, NY, 1996.
- [6] V. Cihal, Intergranular Corrosion of Stainless Steels and Alloys, Materials Science Monograph No. 18, Elsevier, New York, 1984, p.196.
- [7] “ASTM Designation A 380” “Standard recommended practice for cleaning and descaling stainless steels parts, equipments and system”, , Annual book of ASTM Standards, ASTM International, West Conshohocken, PA 19428-2959, United States, 2006.
- [8] “ASTM Designation: A967 – 05” Standard specification for chemical passivation treatments for stainless steel parts, Annual book of ASTM standards, ASTM International, West Conshohocken, Pennsylvania 19428-2959, United States, 2005 .
- [9] V. Kain, Corrosion Resistant Materials, in: S. Banerjee,A. K. Tyagi (Eds), Functional Materials: Preparation, Processing and Applications, Elsevier, 2011. ISBN: 9780123851420.
- [10] A. Hannani, F. Kermiche, A. Pourbaix, K. Belmorke, T.I. Met. Finish., 75 (1997) 7.
- [11] V. Kain, P. K. De, Trans. Ind. Inst. Met., 56 (2003) 31.

- [12] H.S. Ahluwalia, M. Davies, Te-Lin Yau, Corrosion by Nitric Acid, in: S. D. Cramer, B. S. Covino (Eds), Corrosion: Environments and Industries, Vol 13C, ASM Handbook, tenth edition, ASM International, Ohio, 2006, p 668-673.
- [13] J. S. Armijo, Corrosion, 21 (1965) 235.
- [14] K. Osozawa, K. Bohnenkamp, H. J. Engell, Corros. Sci., 6 (1966) 421.
- [15] R. L. Cowan, C. S. Tedmon, Intergranular corrosion of iron-nickel-chromium alloys, in : M. G. Fontana, R. W. Staehle (Eds.), Advances in corrosion science and technology, Plenum Press, New York, 1973, p. 293-395.
- [16] V. Kain, R. C. Prasad, P. K. De, Corrosion, 58 (2002) 15.
- [17] M. H. Brown, Corrosion, 30 (1974) 1.
- [18] K. T. Aust, Trans. Metall. Soc. AIME, 245 (1969) 2117.
- [19] U. K. Mudali, C. B. Rao, B. Raj, Corros. Sci., 48 (2006) 783.
- [20] J.D. Fritz, Effects of Metallurgical Variables on the Corrosion of Stainless Steels, in: S. D. Cramer, B. S. Covino (Eds), Corrosion: Fundamentals, Testing, and Protection, Vol 13A, ASM Handbook, tenth edition, ASM International, Ohio, 2003, p 266–274.
- [21] V. Kain, R. C. Prasad, P. K. De, H. S. Gadiyar, J. Test. Eval., 23 (1995) 50.
- [22] “ASTM Designation A 262 – 02a”: Standard practice for detecting susceptibility to intergranular attack in austenitic stainless steels, Annual book of ASTM standards, ASTM International, West Conshohocken, PA 19428-2959, United States, 2002.
- [23] R. D. Shaw, Brit. Corros. J., 25 (1990) 97.
- [24] V. Kain, S. S. Shinde, H. S. Gadiyar, ASM J. Mater. Eng. Perform., 3(1994) 699.
- [25] V. Kain, P. K. De, Int. J. Nucl. Ener. Sci. Technol. 1 (2005) 220.
- [26] J. S. Armijo, Corrosion, 24 (1968) 24.
- [27] A. Joshi, D. F. Stein, Corrosion, 28 (1972) 321.
- [28] C. L. Briant, Metall. Trans. A, 18A (1987) 691.

- [29] V. Kain, P. Sengupta, P. K. De, S. Banerjee, *Metall. Mater. Trans. A.*, 36 (2005)1075.
- [30] K. Chandra, V. Kain, P. Ganesh, *ASM J. Mater. Eng. Perform.*, 17 (2008) 115.
- [31] V. Kain, S. S. Chouthai, H. S. Gadiyar, *Brit. Corros. J.*, 27 (1992) 59.
- [32] G. L. Song, C.N. Cao, H. C. Lin, *Corros. Sci.*, 36 (1994) 165.
- [33] N. Hara, K. Sugimoto, *J. Electrochem. Soc.*, 126 (1979) 1328.
- [34] N. Hara, K. Sugimoto, *J. Electrochem. Soc.* 138 (1991) 1594.
- [35] S. Bhise, V. Kain, *Corros. Eng. Sci. Techn.*, 47(2011) 61.
- [36] P. Fauvet, F. Balbaud, R. Robin, Q. -T. Tran, A. Mugnier and D. Espinoux, *J. Nucl. Mater.*, 375 (2008) 52.
- [37] M. A. Striecher, *J. Electrochem. Soc.*, 106 (1959)161.
- [38] V. Kain, K. Chandra, M. K. Kumar, S. Rhode, R. Gupta, in : *Proceedings of Eurocorr, Moscow: European federation of corrosion, PA (2010), Paper no. 9133.*
- [39] S. Ningshen, U. K. Mudali, S. Ramya, B. Raj, *Corros. Sci.*, 53 (2011) 64.
- [40] B. Raj, H. S. Kamath, R. Natarajan, P. R. Vasudeva Rao, *Prog. Nucl. Energy*, 47(2005) 369.
- [41] P.K. Dey, N. K. Bansal, *Nucl. Eng. Des.*, 236 (2006) 723.
- [42] C. K. Gupta, *Chemical Metallurgy; principles and practices*, Ed: C. K. Gupta, Wiley-VCH, 2003.
- [43] Baldev Raj, U. Kamachi Mudali, *Prog. Nucl. Energy.*, 48 (2006) 283.
- [44] U. Kamachi Mudali, R. K. Dayal, J. B. Gnanmoorthy, *J. Nucl. Mater.*, 203 (1993) 73.
- [45] S. Ningshen, U. Kamachi Mudali, G. Amarendra, Baldev Raj, *Corros. Sci.*, 51 (2009) 322.
- [46] H. Nagano, H. Kajimura, *Corros. Sci.*, 38 (1996) 781.
- [47] A. Ravi Shankar, V.R. Raju, M. Narayana Rao, U. Kamachi Mudali, H.S. Khatak, Baldev Raj, *Corros. Sci.*, 49 (2007) 3527.

- [48] Te-Lin Yau, Richard C. Sutherlin, ATI Wah Chang, Corrosion of zirconium and zirconium alloys, in: S. D. Cramer, B. S. Covino (Eds), Corrosion: Materials, Vol 13B, ASM Handbook, tenth edition, ASM International, Ohio, 2005, p 300-323.
- [49] Jonathan Beddoes, J. Gardon Parr, "Introduction to Stainless steels", 3rd Edition, 1999, ASM International.
- [50] Nilamadhab Padhi, Role of passivity and surface modification on the corrosion behavior of AISI 304L stainless steel in nitric acid medium, Ph.D. thesis, Homi Bhabha National Institute, Mumbai, India, 2010.
- [51] D. Peckner, I. M Bernstein, "The Handbook of Stainless Steels", McGraw- Hill 1977.
- [52] H. S. Khatak, Baldev Raj, Corrosion of austenitic stainless steel Mechanism, Mitigation and Monitoring, Eds: H. S. Khatak, Baldev Raj, Narosa Publishing House, 2002.
- [53] R. I. L. Guthrie, J. J. Jonas, Steel processing technology, in: Steven R. Lampman, Theodore B. Zorc (Eds), Properties and selection: Irons Steels and high performance alloy, Vol 1, ASM Handbook, tenth edition, ASM International, Ohio, 1993, p 269.
- [54] P. Marcus, Corrosion mechanism in theory and practice, Ed: Philippe Marcus, Marcel Dekker Inc, 2002.
- [55] H. Saito, T. Shibata, G. Okamoto, Corros. Sci., 19 (1979) 693.
- [56] H. H. Uhlig, Corros. Sci., 19 (1979) 777.
- [57] G. Okamoto, T. Shibata, Corros. Sci., 10 (1970) 371.
- [58] U. Kamachi Mudali, Baldev Raj, high nitrogen steels and stainless steels; Manufacturing, Properties and applications, Eds: U. K. Mudali, Baldev Raj, Narosa Publishing House, 2002.
- [59] K. Sugimoto, Y. Sawada, Corros. Sci., 17 (1979) 425.
- [60] K. Hasimoto, K. Asami, K. Teramoto, Corros. Sci., 19 (1970) 3.
- [61] E. McCafferty, Corros. Sci., 50 (2008) 3622.

- [62] D. D. MacDonald, ECS Transactions, 2 (2007) 73.
- [63] E. Mc Cafferty, J. Electrochem. Soc., 154 (2007) C571.
- [64] E. McCafferty, Corros. Sci., 44 (2002) 1393.
- [65] E. McCafferty, J. Electrochem. Soc., 149 (2002) B333.
- [66] E. McCafferty, Corros. Sci., 42 (2000) 1993.
- [67] R. B. Diegle, J. E. Slater, Corrosion, 32 (1976) 155.
- [68] F. Balbaud, G. Sanchez, P. Fauvet, G. Santarini, G. Picard, Corros. Sci., 42 (2000) 1685.
- [69] J. Y. Jeng, B.E. Quayle, P. J. Modern, W. M. Steen, B. D. Bastow, Corros. Sci., 35 (1993) 1289.
- [70] Corrosion of Stainless Steel Weldments, Corrosion: Fundamentals, Testing, and Protection, Vol 13A, ASM Handbook, ASM International, 2003, p 301–316.
- [71] M. Henthorne, “Intergranular Corrosion in Iron and Nickel Base Alloys” in: “Localized Corrosion-Cause of Metal Failure”, ASTM special technical publication 516, ASTM, Philadelphia, Pa. 19103, P 66.
- [72] R. Stickler, A. Vinckier, Corros. Sci., 3(1963)1.
- [73] K. Aemi, S. shimodaire: Corros. Sci., 18 (1978) 151.
- [74] C.S. Tedmon, D. A. Vermilyea, D. E. Broecker, Corrosion. 27 (1871) 104.
- [75] H. D. Solomon, Corrosion, 36 (1980) 356.
- [76] H. D. Solomon, D. C. Lord, Corrosion, 36 (1980) 395.
- [77] W. L. Clark, G. M. Gordon, Corrosion, 29 (1973) 1.
- [78] S. Pednekar, S. Smialowska, Corrosion, 36 (1980) 565.
- [79] V. Kain, K. Chandra, K. N. Adhe, P.K.Dey, J. Nucl. Mater., 334 (2004) 115.
- [80] D.A. Vormilyen, C.S. Tedmon, D.E. Brocker, Corrosion, 31 (1975) 140.
- [81] T. yamamota et al., J. Nucl. Sci. Technol., 35 (1998) 353.

- [82] T. nagai, M. takeuchi, S.takeda, J. Nucl. Sci. Technol., 35 (1998) 502.
- [83] A.B.McIntosh, T.E.Evans: Peaceful uses of atomic energy, 17, 1956.
- [84] M. Takeuchi, G. O. H. Whillock, J. Nucl. Sci. Technol., 41 (2004) 702.
- [85] S. Ningshen, U. Kamachi Mudali, P. Mukherjee, A. Sarkar, P. Barat, N. Padhy, Baldev Raj, Corros. Sci., 50 (2008) 2124.
- [86] S. Girija, V. R. Raju, U. Kamachi Mudali, Baldev Raj, Corros. Eng. Sci. Technol., 38 (2003) 309.
- [87] S. Girija, U. Kamachi Mudali, H. S. Khatak, Baldev Raj, Corros. Sci., 49 (2007) 1665.
- [88] J. Asher, R. F. A. Carney, T. W. Conlon, N. J. M. Wilkins, Corros. Sci., 24 (1984) 411.
- [89] M. C. Petit, D. Desjardins, M. Puiggali, A. E. Kheloui, C. Clement, Corros. Sci., 32 (1991) 1315.
- [90] D. G. Kolman, D. K. Ford, D. P. Butt, T. O. Nelson, Corros. Sci., 39 (1997) 2067.
- [91] J. Kruger, Passivity, in: S. D. Cramer, B. S. Covino (Eds),Corrosion: Fundamentals, Testing, and Protection, Vol 13A, ASM Handbook, tenth edition, ASM International , Ohio, 2003, p 61– 67.
- [92] C. Kato, K. Kiuchi, K. Sugimoto, Corros. Eng., 52 (2003) 69.
- [93] F. Balbaud, G. Sanchez, G. Santarini, G. Picard, Eur. J. Inorg. Chem., (1999) 277.
- [94] F. Balbaud, G. Sanchez, G. Santarini, G. Picard, Eur. J. Inorg. Chem. (2000) 665.
- [95] H. Coriou, J. Hure', G. Plante, Electrochim. Acta, 5 (1961) 105.
- [96] Watanabe T., Res Mechanica, 11 (1984) 47.
- [97] P. Lejcek et al., Acta Mater., 51 (2003) 3951.
- [98] Jeffery A. Zelinsky, An evaluation of grain boundary engineering technology and processing scale-up, M.Tech. thesis, Massachusetts Institute of Technology, Cambridge, Massachusetts, United States, 2005.
- [99] M. Shimada et al., Acta Mater., 50 (2002) 2331.

- [100] D. G. Brandon, *Acta Metall*, 14(1966)1479.
- [101] G. Palumbo, K. T. Aust, *Acta Metall. Mater.*, 38 (1990) 2343.
- [102] ASTM A240/A240M⁻¹1a, “Standard Specification for Chromium and Chromium Nickel Stainless Steel Plate, Sheet and Strip for Pressure Vessels and for General Applications” (West Conshohocken, PA: ASTM International, 2011).
- [103] A. P. Majidi, M. A. Streicher, *Corrosion*, 40 (1984) 584.
- [104] “ISO 12732:2006”, Corrosion of metals and alloys - Electrochemical potentiokinetic reactivation measurement using the double loop method (based on Cihal's method), International standard organisation, Geneva, Switzerland, 2006.
- [105] K. Chandra, V. Kain, R. Tewari, *Corros. Sci.*, 67 (2013) 118.
- [106] K. Chandra, V. Kain, V.S. Raja, R. Tewari, G.K. Dey, *Corros. Sci.*, 54 (2012) 278.
- [107] V. Cihal, T. Shoji, V. Kain, Y. Watanabe, R. Stefec, *EPR – A Comprehensive review*, FRRRI Publication, Tohoku University, Japan, 2004, ISBN - 4-9901953-0-2.
- [108] V. Kain, R. C. Prasad, P.K. De, *High Temp. Mater. Proc.*, 16 (1997) 183.
- [109] M. Momeni, M. H. Moayed, A. Davoodi, *Corros., Sci.*, 52 (2010) 2653.
- [110] Z. Ahmad, *Principle of corrosion engineering and corrosion control*, Ed: Zaki Ahmad, Elsevier, 2006.
- [111] C. L. Briant, E. L. Hall, *Corrosion*, 43 (1987) 525.
- [112] M. Tvrdy et al., *Scripta Metall Mater.*, 19 (1985) 5.
- [113] H. Shaikh, N. Sivaibharasi, B. Sasi, T. Anita, R. Amirthalingam, B.P.C. Rao, T. Jayakumar, H.S. Khatak, Baldev Raj., *Corros Sci*, 48 (2006)1462.
- [114] Shu-Xin Li, Lei Li, Shu-Rong Yu, R. Akid, Hong-Bo Xia, *Corros. Sci.* 53 (2011) 99.
- [115] M.V. Utrilla, A. Urena, E. Otero, C.J. Munez, *Corrosion*, 62 (2006) 85.
- [116] F. Martin, C. Garcia, P. de Tiedra, Y. Blanco, M.L. Aparicio, *Corrosion*, 64 (2008) 70.

- [117] C. Garcia, M.P. de Tiedra, Y. Blanco, O. Martin, F. Martin, *Corros. Sci.*, 50 (2008) 2390.
- [118] C. García, F. Martín, P. de Tiedra, Y. Blanco, J.M. Ruíz-Roman, M. Aparicio, *Corros. Sci.* 50 (2008) 687.
- [119] G.H. Aydogdu, M.K. Aydinol, *Corros. Sci.* 48 (2006) 3564.
- [120] C. García, F. Martín, Y. Blanco, M.L. Aparicio, *Corros. Sci.* 52 (2010) 3725 .
- [121] N. Ebrahimi, M. Momeni, M.H. Moayed, A. Davoodi, *Corros. Sci.* 53 (2011) 637.
- [122] S.C. Bali, V. Kain, V. S. Raja, *Corrosion*, 65 (2009) 726.
- [123] P. Gogola, T. Kunikova, M. Domankova, P. Sevc, S. Tuleja, L. Caplovic, M. Vach, J. Janovec, *Corrosion*, 65 (2009) 355.
- [124] B. Hashemi, A. Davoodi, M. Momeni, M.H. Moayed, *Corrosion*, 69 (2013) 230.
- [125] K.H. Lo, C.T. Kwok, W.K. Chan, *Corros. Sci.*, 53 (2011) 3697.
- [126] K.S. de Asis, F.V.V. de Sousa, M. Miranda, I.C.P. Margarit-Mattos, V. Vivier, O.R. Mattos, *Corros. Sci.*, 59 (2012) 71.
- [127] V. Kain, Y. Watanabe, *J. Nucl. Mater.* 302 (2002) 49.
- [128] V. Kain, G. C. Palit, S. S. Chouthai, H. S. Gadiyar, *J. Electrochem. Soc. Ind.*, 38 (1989) 505.
- [129] E. Kus, Z. Lee, S. Nutt, F. Mansfeld, *Corrosion*, 62 (2006)152.
- [130] M. K. Chung, Y. S. Choi, J.G. Kim, Y. M. Kim, J. C. Lee, *Mater. Sci. Eng. A* 366 (2004).
- [131] T. C. Tsai, T. H. Chuang, *Mater. Sci. Eng., A* 225 (1997)135.
- [132] R.J. Hellmig, M. Janecek, B. Hadzima, O.V. Gendelman, M. Shapiro, X. Molodova, A. Springer, Y. Estrin, *Mater. T.*, 49 (2008) 31.
- [133] V. Randle, *Mater. Sci. Trch Ser.*, 26 (2009) 253.
- [134] R.Z. Valiev, T.G. Langdon, *Prog. Mater. Sci.*, 51 (2006) 881.

- [135] H.W. Zhang, Z.K. Hei, G. Liu, J. Lu, K. Lu, *Acta Mater.*, 51 (2003) 1871.
- [136] H.Q. Sun, Y.-N. Shi, M.-X. Zhang, K. Lu, *Acta Mater.*, 55 (2007) 975.
- [137] A. Yamashita, Z. Horita, T.G. Langdon, *Mater. Sci. Eng. A.*, 300 (2001)142.
- [138] P. Lin, G. Palumbo, U. Erb, K.T. Aust, *Scripta Metall. Mater.*, 33 (1995)1387.
- [139] V. Cihal, I. Kacova. *Corros. Sci.*, 10 (1970) 875.
- [140] E. A. Trillo, L. E. Murr. *J. Mater. Sci.*, 33 (1998) 1263.
- [141] E. A. Trillo, L. E. Murr, *Acta. Mater.*, 47 (1999) 235.
- [142] E. M. Lehockey, G. Palumbo, P. Lin , *Brennenstuhl AM. Scripta mater.*, 36 (1997) 1211.
- [143] G Palumbo, E. M. Lehockey, P. Lin , *J. O. M*, 40 (1998) 50.
- [144] C. Cheung , U. Erb, G. Palumbo, *Mater. Sci. Eng.*, A185 (1994) 39.
- [145] E. M. Lehockey, G. Palumbo, P. Lin, *Metall. Mater. Trans.A.*, 29A (1998) 3069.
- [146] C. B. Thomson, V. Randle, *J. Mater. Sci*, 32(1997)1909.
- [147] W. E. King, A. J. Schwartz., *Scripta mater*, 38 (1998) 449.
- [148] V. Thaveerungsriporn, P. Sinsrok, D. Thong-Aram, *Scripta mater.*, 44 (2001) 67.
- [149] A. J. Schwartz, W. E. King, *J.O.M.*, 50 (1998) 50.
- [150] M. Kumar, W. E. King, A. J. Schwartz. *Acta Mater.*, 48 (2000) 2081.
- [151] V. Randle. *Acta mater.*, 47 (1999) 4187.
- [152] P. Lin, G. Palumbo, K. T. Aust., *Scripta mater.*, 36 (1997) 1145.
- [153] K. D. Ralston, N. Birbilis,C.H.J. Davies, *Scripta Mater.*, 63 (2010) 120.
- [154] P. H. Pumphrey, H. Gleiter, *Philos. Mag.*, 30 (1974) 593.
- [155] H. Kokawa, T. Watanabe, S. Karashima. *Philos Mag A*, 44 (1981)1239.
- [156] H. Kokawa, T. Watanabe, S. Karashima . *Scripta Metall. Mater.*, 17 (1983) 1155.
- [157] B. S. Covino, Jr., J. V. Scalera, T. J. Driscoll, J. P. Carter, *Metall. Trans. A*, 17A (1986) 137.

[158] M. A. Streicher, J. Electrochem. Soc., 106 (1959) 16.

[159] S. J. Ketcham, I. S. Shaffer, Exfoliation Corrosion of Aluminum Alloys, in: "Localized Corrosion-Cause of Metal Failure", ASTM special technical publication 516, ASTM, Philadelphia, Pa. 19103, PP 3.

[160] Y. Watanabe, R.G. Ballinger, O.K. Harling, G.E. Kohs, Corrosion, 51 (1995) 651.